




2023

Characterization of the Function and Regulation of the HMPV Phosphoprotein

Rachel Thompson

University of Kentucky, rethompson2@live.com

Author ORCID Identifier:

 <https://orcid.org/0009-0008-5584-3845>

Digital Object Identifier: <https://doi.org/10.13023/etd.2023.195>

[Right click to open a feedback form in a new tab to let us know how this document benefits you.](#)

Recommended Citation

Thompson, Rachel, "Characterization of the Function and Regulation of the HMPV Phosphoprotein" (2023). *Theses and Dissertations--Molecular and Cellular Biochemistry*. 64.
https://uknowledge.uky.edu/biochem_etds/64

This Doctoral Dissertation is brought to you for free and open access by the Molecular and Cellular Biochemistry at UKnowledge. It has been accepted for inclusion in Theses and Dissertations--Molecular and Cellular Biochemistry by an authorized administrator of UKnowledge. For more information, please contact UKnowledge@lsv.uky.edu.

STUDENT AGREEMENT:

I represent that my thesis or dissertation and abstract are my original work. Proper attribution has been given to all outside sources. I understand that I am solely responsible for obtaining any needed copyright permissions. I have obtained needed written permission statement(s) from the owner(s) of each third-party copyrighted matter to be included in my work, allowing electronic distribution (if such use is not permitted by the fair use doctrine) which will be submitted to UKnowledge as Additional File.

I hereby grant to The University of Kentucky and its agents the irrevocable, non-exclusive, and royalty-free license to archive and make accessible my work in whole or in part in all forms of media, now or hereafter known. I agree that the document mentioned above may be made available immediately for worldwide access unless an embargo applies.

I retain all other ownership rights to the copyright of my work. I also retain the right to use in future works (such as articles or books) all or part of my work. I understand that I am free to register the copyright to my work.

REVIEW, APPROVAL AND ACCEPTANCE

The document mentioned above has been reviewed and accepted by the student's advisor, on behalf of the advisory committee, and by the Director of Graduate Studies (DGS), on behalf of the program; we verify that this is the final, approved version of the student's thesis including all changes required by the advisory committee. The undersigned agree to abide by the statements above.

Rachel Thompson, Student

Dr. Rebecca Dutch, Major Professor

Dr. Trevor Creamer, Director of Graduate Studies

CHARACTERIZATION OF THE FUNCTION AND REGULATION OF THE HMPV
PHOSPHOPROTEIN

DISSERTATION

A dissertation submitted in partial fulfillment of the
requirements for the degree of Doctor of Philosophy in the
College of Medicine
at the University of Kentucky

By
Rachel Erin Thompson
Lexington, Kentucky
Director: Dr. Rebecca Dutch, Professor of Molecular and Cellular Biochemistry
Lexington, Kentucky
2023

Copyright © Rachel Thompson 2023

ABSTRACT OF DISSERTATION

CHARACTERIZATION OF THE FUNCTION AND REGULATION OF THE HMPV PHOSPHOPROTEIN

Human metapneumovirus (HMPV) is a non-segmented, negative strand RNA virus (NNSV) that frequently causes respiratory tract infections in infants, the elderly, and the immunocompromised. Despite the initial identification of HMPV in 2001, there are currently no FDA approved antivirals or vaccines available. Therefore, understanding the mechanism of HMPV replication is critical for the identification of novel therapeutic targets. A key feature in the replication cycle of HMPV and other NNSVs is the formation of membrane-less, liquid-like replication and transcription centers in the cytosol termed inclusion bodies (IBs). Recent work on NNSV IBs suggests they display characteristics of biomolecular condensates formed through a liquid-to-liquid phase transition. Intrinsically disordered proteins are common drivers of biomolecular condensate formation, and post-translational modifications have been shown to regulate condensate properties. The HMPV phosphoprotein (P) and nucleoprotein (N) are the minimal viral proteins necessary to form IB-like structures and are both required for the viral polymerase to synthesize RNA during infection. HMPV P is a necessary co-factor for the viral polymerase, has regions of intrinsic disorder, and has several known and predicted phosphorylation sites. I hypothesized that 1) the HMPV P intrinsically disordered domains facilitate IB formation and 2) changes to P phosphorylation state regulates the properties of IBs and the function of P as a polymerase co-factor.

Upon deletion of regions of HMPV P, we found that the C-terminal intrinsically disordered domain (CTD) must be present to facilitate IB formation with HMPV N, while either the N-terminal intrinsically disordered domain or the central oligomerization domain were dispensable. Alanine substitution at a single tyrosine residue in the CTD was a minimal mutation which abrogated IB formation and reduced co-immunoprecipitation with HMPV N, identifying this residue as a key interaction site for N and as a facilitator of IB formation. Phospho-dead and

phosphomimetic mutations to C-terminal phosphorylation sites revealed a potential role for phosphorylation in regulating RNA synthesis and P binding partners within IBs. Phosphorylation mutations which reduced RNA synthesis in a reporter assay produced comparable results in a recombinant viral rescue system, measured as an inability to produce infectious viral particles with genomes containing these single P mutations. This work highlights the critical role HMPV P plays in facilitating a key step of the viral life cycle and reveals the potential role for phosphorylation in regulating the function of this significant viral protein.

KEYWORDS: Inclusion Bodies, Human Metapneumovirus, Phosphoprotein, Phosphorylation, Phase Separation, Viral Replication

Rachel Erin Thompson

(Name of Student)

03/09/2023

Date

CHARACTERIZATION OF THE FUNCTION AND REGULATION OF THE HMPV
PHOSPHOPROTEIN

By
Rachel Erin Thompson

Dr. Rebecca Dutch

Director of Dissertation

Dr. Trevor Creamer

Director of Graduate Studies

03/09/2023

Date

ACKNOWLEDGMENTS

It is difficult to put into words the gratitude I have for all the people that have helped me during my time in this program. First, I must thank my mentor, Dr. Becky Dutch, for her guidance, support, and understanding though what has been one of the most challenging and rewarding experiences of my life. She is an incredible scientist, speaker, and leader, and her passion and enthusiasm for science is truly infectious. During my time in her lab, she pushed me to challenge myself when I feared failure and encouraged me to rest when I was overwhelmed. She gave me the creative space to explore and test my own ideas and helped me develop and strengthen skills I didn't think I was capable of. I am incredibly fortunate and grateful she gave me this opportunity to complete my PhD work under her mentorship.

I am thankful to past lab members Drs. Nicolás Cifuentes-Muñoz, Stacy Webb, Farah el Najjar, Cheng-Yu Wu, Liz Zamora-Reyes, Chelsea Barrett, Tyler Kinder, Jean Branttie, and Kerri Beth Boggs, and to my current lab members Kearstin Edmonds, Hadley Neal, and Chase Heim. I don't have enough room to describe the thousands of ways you all have helped and supported me all these years, but I know I would not be the person or scientist I am today without each of you. I will always have fond memories of our coffee time conversations, conference adventures, escape room attempts, reality TV show discussions, and Secret Santa exchanges. I want to give special thanks to Dr. Nicolás Cifuentes-Muñoz, who trained me in most of our lab's techniques and helped me conceptualize my dissertation work. I am also incredibly thankful to Kearstin Edmonds and Hadley Neal for their support, friendship, and contributions to this project. Kearstin graciously and diligently completed the FRAP experiments for me, and she has given me valuable advice that's helped me improve the soft skills I will need to succeed in my future career. Hadley created the mCherry-P mutants, and she has been an incredible source of support and understanding as I've reached the end of this process. The Dutch Lab is one of a kind, and I am lucky to have been part of such an amazing and talented group of scientists.

I'm thankful to my committee members, Drs. Trevor Creamer, Jessica Blackburn, and Beth Garvy. Their multidisciplinary expertise and insight helped me learn to view my project from perspectives I had not previously considered. Thank you to Dr. Anthony Sinai for acting as my outside examiner, and to all the faculty, students, and office staff for all the ways, big or small, that you have contributed to my amazing experience in this department. There are so many things done behind the scenes to keep this department running, and whenever anyone needs assistance, there is always someone who is willing to help. I want to thank Dr. Rachel Fearn for the minireplicon system, Dr. Makoto Takeda for the HMPV rescue system, and Dr. Trevor Creamer, Martin Chow, and the University of Kentucky Protein Core for their help purifying the P nanobody. This project would not have been possible without their technical contributions. Additionally, I want to acknowledge Caroline Smith for her providing her protocols and advice for using nanobodies. I also

want to thank her for being an incredible roommate and friend as we've gone through this program together.

Finally, thank you to my parents, Pat and Marta, and my sisters and best friends, Natalie and Casey, for always being my biggest supporters. Whether it was weekend trips back to Louisville for a home-cooked meal or playing video games together at the end of a hard day, you all have helped and supported me through this journey from beginning to end. I have had moments of self-doubt where I wondered if I would ever actually get to the end of this process, but with you it was never a question of "if", it was a question of "when." I would not have accomplished this without you.

TABLE OF CONTENTS

| | |
|--|-----|
| ACKNOWLEDGMENTS | iii |
| LIST OF FIGURES | vii |
| CHAPTER 1. BACKGROUND AND INTRODUCTION..... | 1 |
| 1.1 <i>Mononegavirales</i> | 1 |
| 1.2 <i>Pathogenesis and Epidemiology of Pneumoviruses</i> | 2 |
| 1.2.1 Clinical Features and Transmission..... | 3 |
| 1.2.2 Global Impact | 4 |
| 1.2.3 Treatment Options | 5 |
| 1.3 <i>The Viral Life Cycle</i> | 7 |
| 1.3.1 Entry | 8 |
| 1.3.2 Replication..... | 9 |
| 1.3.3 Assembly and Spread..... | 10 |
| 1.4 <i>Inclusion Bodies are Virus-Induced Biomolecular Condensates</i> | 11 |
| 1.4.1 Properties of Inclusion Bodies | 12 |
| 1.4.2 LLPS and Biomolecular Condensates | 12 |
| 1.4.3 Regulation of Biomolecular Condensates..... | 14 |
| 1.4.4 Inclusion Bodies as a Replication Strategy..... | 15 |
| 1.5 <i>Inclusion Bodies of Pneumoviruses</i> | 16 |
| 1.5.1 Host Proteins Found in Inclusion Bodies | 17 |
| 1.5.2 The Phosphoprotein and the Nucleoprotein | 17 |
| 1.6 <i>Dissertation Summary</i> | 19 |
| CHAPTER 2. METHODS..... | 31 |
| 2.1 <i>Materials and Standard Protocols</i> | 31 |
| 2.1.1 Cell Lines..... | 31 |
| 2.1.2 Transfections | 31 |
| 2.1.3 Plasmids, Antibodies, and Reagents | 32 |
| 2.1.4 Mutagenesis and P Domain Constructs..... | 33 |
| 2.2 <i>Methods to Analyze Inclusion Bodies</i> | 33 |
| 2.2.1 Inclusion Body Formation Assay..... | 33 |
| 2.2.2 FRAP Acquisition..... | 34 |
| 2.2.3 FRAP Analysis..... | 34 |
| 2.3 <i>Methods to Analyze HMPV P Interactions</i> | 35 |
| 2.3.1 Minireplicon Assay | 35 |

| | |
|---|----|
| 2.3.2 Western Blots | 36 |
| 2.3.3 Nanobody and DynaBead Coupling..... | 36 |
| 2.3.4 Co-immunoprecipitation | 36 |
| 2.3.5 Recombinant Virus Mutagenesis | 37 |
| 2.3.6 Recombinant Virus Rescue | 38 |
| CHAPTER 3. RESULTS | 39 |
| 3.1 <i>Introduction</i> | 39 |
| 3.2 <i>Results</i> | 41 |
| 3.2.1 Identifying Regions of HMPV P Driving IB Formation | 41 |
| 3.2.2 Mutagenesis of HMPV P Phosphorylation Sites | 42 |
| 3.2.3 Examining P-specific Interactions of Phosphorylation Mutants..... | 45 |
| 3.2.4 Production of Recombinant HMPV Encoding P Mutations | 46 |
| 3.3 <i>Discussion</i> | 47 |
| 3.3.1 Minimal P Sequences Driving IB Formation | 48 |
| 3.3.2 The Function of HMPV P Phosphorylation | 50 |
| CHAPTER 4. DISCUSSION AND FUTURE DIRECTIONS | 64 |
| 4.1 <i>P-specific interactions driving IB formation</i> | 65 |
| 4.2 <i>The nucleoprotein, viral RNA, and other HMPV proteins within IBs</i> | 66 |
| 4.3 <i>Mechanisms controlling characteristics of IBs</i> | 69 |
| 4.4 <i>Virus-Host interactions within IBs</i> | 70 |
| 4.5 <i>Regulating HMPV P and identifying alternative function</i> | 74 |
| APPENDIX: List of Abbreviations | 78 |
| REFERENCES | 81 |
| VITA..... | 98 |

LIST OF FIGURES

| | |
|---|----|
| Figure 1.1 <i>Pneumoviridae</i> viral particles..... | 23 |
| Figure 1.2 HMPV N-RNA interactions | 24 |
| Figure 1.3 The life cycle of HMPV | 25 |
| Figure 1.4 Simplified model of an active HMPV polymerase complex..... | 26 |
| Figure 1.5 Cellular features of an HMPV infection..... | 27 |
| Figure 1.6 Sequence alignment of <i>Pneumoviridae</i> phosphoproteins..... | 28 |
| Figure 1.7 Conformational changes of HMPV N..... | 29 |
| Figure 1.8 Structure of the HMPV polymerase complex..... | 30 |
| Figure 3.1 Domains of HMPV P involved in IB formation | 53 |
| Figure 3.2 The effect of phosphorylation site mutagenesis on HMPV P function..... | 54 |
| Figure 3.3 Phosphoprotein sequence homology among strains of HMPV..... | 55 |
| Figure 3.4 The HMPV minireplicon system | 56 |
| Figure 3.5 Co-transfection of HA-P phosphorylation mutants..... | 57 |
| Figure 3.6 IB formation of HMPV HA-P phosphorylation site mutants..... | 58 |
| Figure 3.7 Co-immunoprecipitation of N and HA-P mutants..... | 59 |
| Figure 3.8 FRAP of IBs formed by mCherry-P phosphorylation site mutations .. | 61 |
| Figure 3.9 Best fit parameters of FRAP curves | 62 |
| Figure 3.10 Rescue of recombinant HMPV with HA-P mutations | 63 |

CHAPTER 1. BACKGROUND AND INTRODUCTION

1.1 Mononegavirales

Viruses within the order *Mononegavirales* contain single-stranded, nonsegmented, negative-sense RNA genomes (1). Initially divided into three families upon its creation in 1991, the continuous discovery of novel species and completion of more detailed sequence comparisons has warranted several amendments to family classifications in recent years. As of 2019 (2), there are currently eleven *Mononegavirales* families, of which four contain well-known agents of significant human disease: *Filoviridae*, *Rhabdoviridae*, *Paramyxoviridae*, and *Pneumoviridae*. Despite the biomolecular similarities grouping these viruses together, the infectivity, clinical features, and disease severity are dependent on each viral species.

Viruses in the *Filoviridae* family contain larger genomes with unique regions of overlapping genes absent in other *Mononegavirales* families (3). Among filoviruses, both Marburg virus and Ebola virus (EBOV) cause deadly hemorrhagic fever with high fatality rates and no known cure (1). Since their zoonotic emergence in the human population, outbreaks have gradually increased from sporadic cases to larger epidemics (4). *Rhabdoviridae*, such as Rabies virus, have viral particles with a distinct bullet-like morphology (1). Rabies virus is a causative agent of rabies encephalitis, which is a fatal disease that has been documented throughout human history, but is currently preventable with vaccination. Paramyxoviruses include a variety of human pathogens, such as Measles virus, Mumps virus, Nipah virus, Hendra virus, and several human parainfluenza viruses (5). Measles virus is one of the most contagious pathogens in the world and was eliminated from the US population in 2000 due to mass public vaccination efforts (6), but a recent rise in vaccine hesitancy has raised concerns for its reemergence. In contrast, the recently emerged Nipah virus (NiV) and the closely related Hendra virus can both cause viral encephalitis with high fatality rates and no treatment options (1). Although Henipavirus outbreaks have been zoonotic in origin, human-

to-human transmission observed in some NiV cases has raised concerns over its pandemic potential (7, 8).

Originally grouped as a subfamily of paramyxoviruses, the *Pneumoviridae* family was created in 2016 (9) and includes human respiratory syncytial virus (RSV) and human metapneumovirus (HMPV). These viruses are found in human populations across the globe and infection rates typically surge around the same time of the year as influenza (10-12), occasionally resulting to co-infections (1). Symptoms of pneumovirus infections range from asymptomatic to severe respiratory illness, and they are particularly dangerous to elderly, immunocompromised, and infant populations. Despite the global prevalence and human health burden of these viruses, therapeutic options are highly limited, and there are currently no vaccines available to combat pneumovirus-associated disease.

1.2 Pathogenesis and Epidemiology of Pneumoviruses

Viruses within the *Pneumoviridae* family have a range of specific hosts, including cattle (bovine RSV), mice (murine pneumonia virus), birds (avian metapneumovirus), and humans (RSV and HMPV) (13). Although RSV and HMPV are capable of infecting non-human animals in experimental studies, no animal reservoirs for either virus have been observed, making human-to-human transmission the primary source of spread (1). RSV was first isolated from humans in 1957 from infants with symptoms of respiratory infections (14), launching decades of research investigating the clinical features and pathology of RSV infection for diagnostic and therapeutic purposes. HMPV was isolated in 2001, but serological evaluation revealed HMPV had been present among humans since at least the 1950s (15). RSV and HMPV infections have similar symptoms, and it is believed that HMPV infections were previously being diagnosed as RSV infections. This, paired with limited detection methods and a poor ability to grow and propagate in cell culture, impaired the isolation of HMPV and masked its presence as a human pathogen for several decades. Today, pneumoviruses inflict a

significant burden to human health. RSV is the leading causes of hospitalizations in infants due to respiratory tract infections, and HMPV infections can occur at similar rates and severity as influenza in susceptible populations (16, 17).

1.2.1 Clinical Features and Transmission

Pneumoviruses can infect individuals of any age, but majority of the human population will have had a primary infection by RSV and HMPV by age two and five, respectively (1). Transmission occurs primarily through respiratory droplets, either from close proximity to an infected individual or direct contact with a contaminated surface. Daycares and schools are especially conducive to spread of pneumoviruses among young children, caregivers, and relatives. After infancy, asymptomatic or symptomatic reinfections can occur throughout life, but immunocompromised and elderly individuals are the most susceptible to severe reinfections. Symptomatically indistinguishable from one another, and often from other respiratory pathogens, RSV and HMPV infections require diagnosis through biochemical assays, such as antigen testing or PCR detection of viral RNA (18, 19). Detection through laboratory isolation is falling out of practice due to the instability of RSV particles and the poor ability of HMPV to be grown *in vitro*, both of which can delay diagnosis and subsequent treatment. In addition, diagnostic tests for HMPV in older adults require high sensitivity for accurate diagnosis due to decreased viral shedding compared to young children.

Symptoms of pneumovirus infections vary by age of the infected individual and location of the infection within the respiratory tract (1, 18, 20). Older children and healthy adults tend to have asymptomatic infections or mild upper respiratory tract infections (URTIs), which present with typical cold-like symptoms, such as sore throat, congestion, runny nose, and cough. Viral URTIs can also be accompanied by ear infections. Progression of RSV and HMPV infection into the lower respiratory tract (LRTI) occurs more frequently in young children and the elderly and is associated with more severe disease state. Pneumovirus LRTIs can result in pneumonia or bronchiolitis, which are characterized by wheezing, severe coughing, or difficulty breathing. Risk for developing severe RSV or HMPV

infections is increased by pre-existing conditions affecting the immune system, heart, or lungs, such as asthma, COPD, cardiovascular disease, or immunodeficiency from illness or medical treatment (20-25). RSV and HMPV infections can exacerbate symptoms of chronic health conditions, increasing disease severity and morbidity.

1.2.2 Global Impact

RSV and HMPV infections occur in countries around the world (17, 26-33). In temperate climates infections by either virus can occur throughout the year, but annual epidemics occur during the cold months (1). The peak of RSV infections frequently overlaps that of influenza in mid-to-late winter, and HMPV infections tend to peak in late winter and early spring (24, 34-39). Although children under five are highly susceptible to pneumovirus infection, infants less than 2 are the most at risk for RSV or HMPV associated hospitalizations (20, 22, 40). Surveillance studies consistently report the vast majority of young children hospitalized with detectable RSV infections are less than 6 months of age, with prematurity being an additional risk factor for severe illness (23, 41).

HMPV infections occur most frequently before age 2, but hospitalized children between ages 2-5 are more likely to have HMPV than RSV (20, 22, 40). Adults over 65 are also at risk for severe HMPV infections (20, 21, 35), and outbreaks in long term care facilities have had fatality rates ranging from 0-50% of diagnosed cases (42-44). Hospitalizations with detectable HMPV infections are commonly associated with the presence of underlying health conditions, especially among older children, adults and elderly populations (21, 22, 24, 32). Co-infections of RSV and HMPV together or with other respiratory viruses have also been reported in all age groups (20-22, 24, 45), but it is unclear what affect co-infections have on disease outcome.

While RSV is the most common virus associated with respiratory tract infections in hospitalized children, the global burden of HMPV should not be discounted. Recently, systematic reviews of over 481 RSV studies published

between 1995- 2020 (29, 46) and 119 HMPV studies published between 2001-2019 (17) illustrated the dramatic global burden for both of these viruses. In 2019 it was estimated that 33 million global RSV-associated LRTI occurred in children under 5, of which 3.6 million required hospitalization (29). Among this same age group, an estimated 1 out of every 50 total deaths was attributable to RSV infection. In 2018 there were an estimated 14.2 million HMPV associated LRTIs and 643,000 hospitalizations in children under the age of 5 worldwide (17). Of the estimated HMPV-associated deaths, 64% occurred in hospitalized infants under 6 months of age. Both studies found that majority of RSV- and HMPV-associated deaths occurred in low- or middle-income countries. These estimates reveal the significant burden RSV and HMPV have on human health and highlight the dire need for the development and global distribution of prophylactics and antivirals against these ubiquitous pathogens.

1.2.3 Treatment Options

Despite decades of research on pneumoviruses, there is currently only one treatment option available, which is specific to RSV. Palivizumab is a humanized monoclonal antibody (mAb) against the RSV fusion protein (F) developed by MedImmune (now AstraZeneca) and FDA approved in 1998 (47). It is only given to infants with the highest risk for the development of RSV infections (less than 2 years old with a history of prematurity and/or chronic lung or heart conditions) and can only be used prophylactically. High cost (around \$1000 per vial) and the requirement of monthly doses makes palivizumab a last-resort option (48). A derivative of palivizumab, called motavizumab, was later created in an attempt to improve treatment efficacy, but this mAb was ultimately abandoned due to an increased risk for allergic reaction seen during clinical trials (49). Another mAb, nirsevimab (MEDI8897), targets the pre-fusion conformation of RSV F (50). Nirsevimab was developed by AstraZeneca for single-dose administration for infants ineligible for palivizumab, and it recently completed phase 3 clinical trials (51). The FDA is currently reviewing the license application for commercialization of nirsevimab as the first single-dose RSV prophylactic (52). The mAb 54G10 was

found to neutralize both RSV and HMPV in vitro (53, 54) and act prophylactically against both viruses in mouse models (53). However, no mAb targeting both viruses is commercially available.

Ribavirin is a broad-spectrum antiviral drug that acts as a nucleoside inhibitor of viral RNA synthesis, but has been used clinically with questionable efficacy against RSV infection (55-57). Aerosolized ribavirin was approved by the FDA in 1985 for use in infants hospitalized with severe RSV infections, but subsequent studies revealed any benefits from treatment were not clinically significant (57). Despite the lack of clinical trials warranting its use, treatment of HMPV infections with ribavirin have also been reported (58-62). Due to concerns over toxicity of the drug, ribavirin treatment is generally limited to cases with a high risk for fatality and is not a viable option as an effective pneumovirus therapeutic. Excitingly, an RSV-specific drug targeting the nucleoprotein is currently in phase 2 clinical trials (Identifier: NCT05568706), with promising results as a treatment for active infections (63).

There are currently no prophylactics or therapeutics available against HMPV, and although there are several promising ongoing clinical trials, no vaccine for RSV or HMPV has ever received approval by the FDA. The first RSV vaccine that went through clinical trials met with a tragic end during the 1960's. The formalin-inactivated RSV vaccine was administered to infants and young children, but instead of protecting them from infection the vaccine increased disease severity and resulted in two infant deaths (64, 65). Similarly, a formalin-inactivated HMPV vaccine worsened disease in cotton rats and macaques after subsequent HMPV challenge (66, 67). These disastrous attempts at vaccine development permanently altered the trajectory of pneumovirus vaccine design. Instead of inactivated viruses, vaccine development for RSV and HMPV has focused on live attenuated virus, virus like particles, or viral proteins, but none have produced results warranting FDA approval (18, 68). Several clinical trials are currently investigating the use of protein-based RSV vaccines on pregnant individuals, with the goal of producing maternal antibodies that transfer to the fetus during pregnancy

and remain circulating in infants during the first months of life, when they are most susceptible to RSV (69, 70). Excitingly, an RSV vaccine for elderly adults, developed by Pfizer and BioNTech, has completed phase 3 clinical trials (Identifier: NCT05035212) and is currently under an expedited review process by the FDA (71). In addition, the recent global implementation of mRNA-based vaccines against SARS CoV2 led Moderna to develop a combined mRNA vaccine against HMPV and human parainfluenza virus type 3, which is currently undergoing phase 1 clinical trials in both young children and healthy adults (Identifier: NCT04144348).

1.3 The Viral Life Cycle

Like other members of the *Mononegavirales* order, pneumoviruses are enveloped viruses (**Fig 1.1**), meaning the viral particles consist of a lipid membrane bilayer derived from the host cell. *Pneumoviridae* virions can be either spherical or filamentous (15, 72-74), and the presence of the viral matrix protein in a lattice beneath the membrane is correlated with the filamentous form (75-78). The viral membrane is studded with three different structural glycoproteins that mediate attachment and entry of the virion to host cells (1). Packaged within the virus is a linear, single-stranded RNA genome. The viral capsid is helical, formed through oligomerization of the nucleoprotein directly on the RNA genome to form the nucleocapsid (**Fig 1.2**). In complex with the nucleocapsid is the viral RNA-dependent RNA-polymerase and its cofactor, the phosphoprotein. Also within the virion are the M2-1 and M2-2 proteins, which have roles in regulating RNA synthesis (79-81). Unique to RSV are the non-structural proteins NS1 and NS2, which are absent in the virion but expressed during infection and thought to have a role in suppression of the host interferon response (82, 83). The HMPV genome contains 8 genes, encoding 9 proteins, while RSV contains 10 genes encoding 11 proteins (1). Each protein participates in at least one step of the viral life cycle in order to facilitate infection (**Fig 1.3**).

1.3.1 Entry

The fusion protein (F), the attachment protein (G), and the small hydrophobic protein (SH) are glycosylated transmembrane proteins in the viral membrane (1). The SH protein is not necessary for entry in vitro (84, 85), but it has been proposed to act as a viroporin in the host membrane and may affect fusion efficiency (86, 87). The F and G proteins have been demonstrated to interact with a variety of host proteins during entry, but the cellular receptor for attachment of the virion to the host membrane is still under debate (88). The function of G is also somewhat dismissible in vitro, indicating F may have a basal ability to facilitate viral attachment (85, 89). Both HMPV and RSV surface glycoproteins interact with heparan sulfate on the cell surface (90, 91), but this interaction may not be physiologically relevant. Pneumoviruses primarily infect ciliated airway epithelial cells in HAE models and in vivo (54, 92-94), but the exact receptors utilized to initiate physiological infection have yet to be determined. Other potential host attachment factors include CX3CR1 and nucleolin for RSV (88) and integrins for HMPV (95).

The steps that occur in between attachment and entry are not completely understood, as they are highly complex and context dependent. Fusion of the viral membrane and the host membrane is facilitated by F, a trimeric protein that is synthesized in a precursor form that must be activated through one (HMPV) or two (RSV) proteolytic cleavage events (96, 97). Activated, pre-fusion F is in a metastable, energetically unfavorable conformation and must be triggered to initiate the fusion process (98-100). Upon triggering, F undergoes a dramatic and irreversible conformational change in which it injects a small fusion peptide into the host membrane and refolds into a highly stable, low energy, six-helix bundle. The transformation of pre-fusion F into post-fusion F merges the host and viral membranes together to create a fusion pore, allowing the packaged genome and viral proteins to enter the cell.

Whether fusion occurs at the cell surface or after internalization of the viral particle is still up for debate. For HMPV F, it has been demonstrated that low pH

can be a triggering event (96, 101), and direct fusion of viral membrane with endosomal membranes has also been reported (102), supporting the idea that HMPV could be internalized through the endocytic pathway and fuse with the cell after endosomal acidification. RSV F is not sensitive to low pH for triggering and its presence in cells through infection or transfection results in the formation of syncytia (103-105). While these results suggest RSV F is capable of facilitating fusion at the cell surface, the location and mechanism of entry is still being investigated.

1.3.2 Replication

Once the viral contents are released into the cell, the RNA genome must be copied and transcribed via RNA synthesis. Both of these processes occur in the cytosol and rely on the function of the viral polymerase complex (**Fig 1.4**), which consists of the large RNA-dependent RNA polymerase (L) and the phosphoprotein cofactor, and these proteins are associated with the nucleocapsid and the accessory protein M2-1 (1). All four of these proteins have been detected in spherical cytoplasmic inclusions that form during early infection, which have been termed inclusion bodies (IBs) (106, 107). These structures (**Fig 1.5A**) are thought to be centers for viral replication, as their formation is associated with optimal synthesis of viral RNA (108). The importance of IBs during infection is described further in section 1.4.4 and 1.5.

Mononegavirales genomes are negative sense, with the beginning of the genome at the 3' end (1). The viral polymerase directly transcribes mRNA from the genome, but it must make a positive-sense copy of the genome, called the antigenome, to use as a replication template. Unlike viral mRNA, both genome and antigenome are concurrently encapsidated by the nucleoprotein (N) during synthesis and lack a methylation cap and poly-A tail. It is presumed that N protomers are transiently displaced as L progresses along the nucleocapsid, but a mechanism for this process has not been described. The phosphoprotein (P) does not have any enzymatic activity, but it assists in RNA synthesis as a cofactor, anchoring L to the nucleocapsid through interactions with N. Without P, the highly

complex and multifunctional polymerase is rendered useless. The M2-1 protein is not required for RNA synthesis to be initiated, but it is an important processivity factor for transcription and is unique to *Pneumoviridae*.

Specific sequences within the genome itself help direct the activity of L. Located at the 3' and 5' ends of the genome are a leader region (*le*) and trailer region (*tr*) (109), which contain promoter sequences for initiating RNA synthesis in the genome and antigenome. Initiation of RNA synthesis at the first nucleotide in the *le* sequence (1U) results in antigenome production, while initiation at the third nucleotide (3C) results in mRNA (110-112). Available concentrations of ATP and GTP may act as a determining factor controlling whether L initiates transcription or replication (113). Intergenic regions between genes called gene start (GS) and gene end (GE) are recognized by L as it scans the genome during transcription (1, 114). GS sequences direct L to initiate RNA synthesis and add a methylation cap to the 5' end of nascent RNA. Once L reaches the GE sequence it polyadenylates the 3' end and releases the mRNA, then continues down the genome to scan for the next GS sequence. Basal levels of mRNA are highest for genes encoded at the 3' end of the genome and lowest for those encoded at the 5' end because L is prone to falling off the genome during transcription. The HMPV genome is organized 3'-N-P-M-F-M2-SH-G-L-5', allowing for the rapid accumulation of proteins that are in high demand during RNA synthesis (N and P) and assembly (M and F).

1.3.3 Assembly and Spread

Translation of viral mRNAs is split into two different locations (**Fig 1.3**). Synthesis of the viral membrane proteins F, G, and SH occurs in the endoplasmic reticulum (ER), where they move through the secretory pathway, undergo glycosylation and other post translational modifications, and are trafficked to the surface (1). All other viral proteins, along with the genome, are synthesized in the cytosol and must travel to the membrane and localize with the surface glycoproteins at sites of assembly. The viral matrix protein (M) can associate with lipid membranes, host factors, and viral proteins in order to facilitate assembly

(115), and oligomerization of M at the membrane is essential for production of filamentous virions (72, 78).

Although production of progeny virions to infect distant cells is the prototypical model of viral spread, the release of HMPV particles is notoriously inefficient in cell culture (15, 116), with majority of virus remaining cell-associated (117). However, a secondary method of cell-to-cell spread has been proposed. HMPV infection induces a dramatic reorganization of the actin cytoskeleton (**Fig 1.5**), resulting in formation of membrane filaments and intercellular extensions (117-119). While filaments are believed to be sites of virion assembly, intercellular extensions represent an alternative method of viral spread (120). Intercellular extensions connecting distant infected cells, or extending from an infected cell towards a non-infected cell, have been observed in cell culture and HAE tissues (54, 117). These structures act like tunnels, allowing for the transfer of cytoplasmic content between connected cells, including the transportation of IBs. Movement of viral replication centers through extensions has been observed in vitro (117, 119), allowing the infection to bypass the entry and egress steps required by production of viral particles. Extensions also act as an immune evasion technique, as circulating antibodies are primarily generated against glycoproteins on the surface of the virion. Neutralizing antibodies prevent entry of HMPV virions in cell culture and HAE tissues, but do not prevent cell-to-cell spread (54, 117), suggesting the formation of direct cellular connections is an important strategy utilized by this virus to spread infection.

1.4 Inclusion Bodies are Virus-Induced Biomolecular Condensates

The formation of spherical replication compartments containing viral protein and viral RNA (vRNA) has been observed for almost all Mononegavirales pathogens that cause human disease. The first discovery of a viral IB was made by Adelchi Negri in 1903 after observing the presence of cytoplasmic inclusions in RABV infected neurons (121). The nature of Negri bodies was unknown, but their presence in cells later became a tool for diagnosing rabies virus (RABV) infection.

IBs have since been observed during infections by members of the *Filoviridae*, *Rhabdoviridae*, *Paramyxoviridae*, and *Pneumoviridae* families. Early studies worked to characterize these viral structures, and research in the past few decades has focused on identifying the molecular interactions regulating their formation and function during infection.

1.4.1 Properties of Inclusion Bodies

IBs typically form in the cytosol during the early stages of infection. They are spherical structures containing viral proteins involved in RNA synthesis, including L, P, and N (106, 122, 123). Viral RNA, including mRNA and genomic RNA, have also been detected in IBs of some species (**Fig 1.5A**) (108, 124, 125). Multiple IBs can form per cell, and time-course studies have revealed these structures are highly dynamic and liquid-like, capable of increasing in size, fusing together, and dividing into smaller pieces (125-127). Total dissolution of IBs can occur after hypotonic shock, followed by partial reformation (127), suggesting their formation is reversible. Exchange of protein in and out of IBs is rapid, but slower than diffusion within the cytosol (126, 127). All of these observations are consistent with properties of membraneless organelles, also called liquid organelles or biomolecular condensates.

1.4.2 LLPS and Biomolecular Condensates

Biomolecular condensate is a term describing a broad category of subcellular compartments which contain high concentrations of molecules despite the absence of a membrane (128). Nucleoli, stress granules, and P granules are well-known examples (129-131). The structures are spherical and liquid-like, and condensates of the same type can fuse together (128). Instead of a physical barrier, condensates are biochemically distinct from their surrounding environment due to differences in their chemical properties. Formation of biomolecular condensates occurs through liquid-liquid phase separation (LLPS), a biophysical process where molecules within a liquid mixture undergo a liquid-to-liquid phase transition (132). LLPS is often driven by transient inter- or intramolecular

interactions such as electrostatic, polar, or hydrophobic interactions. Once a minimal threshold is reached, the combined strength of these weak interactions reduces the molecules solubility within the mixture and they spontaneously de-mix from solution into a highly concentrated liquid phase. Biomolecular condensates are sensitive to protein and/or RNA concentration, salt concentration, pH, and temperature, all factors which can influence the strength of molecular interactions driving LLPS (128, 132).

The dramatic difference in protein concentration created by LLPS is maintained by entropy, similar to the separation of oil and water (132). As a result, cells are hypothesized to utilize biomolecular condensates as a mechanism to regulate biochemical processes without the energy expenditure required to transport molecules against a concentration gradient. LLPS in cells can concentrate components of specific reactions to increase enzyme kinetics, sequester factors to inhibit certain pathways, or temporarily store or release molecules involved in signal transduction (128). Cellular phase-separated condensates, therefore, allow for the spatiotemporal compartmentalization of specific molecules to rapidly regulate biological processes in response to stimuli.

Components of biomolecular condensates are often multivalent, capable of simultaneously interacting with more than one type of molecule. Molecules such as RNA, oligomeric proteins, and intrinsically disordered proteins are common examples (128, 131). RNA provides a long and highly charged surface for electrostatic interactions with multiple copies of RNA-binding proteins. Proteins that can oligomerize increase valency by interacting with themselves and other molecules to create higher-order complexes. The intrinsically disordered regions (IDR) of proteins are domains which lack defined secondary structure, which can allow for conformational flexibility between multiple binding domains. Binding sites can also be located within IDRs, as their sequences tend to be enriched in polar or charged amino acids (133, 134) and they can be targets for phosphorylation (135). Combinations of these different types of molecules results in the formation

of a network of higher-order interactions that reach the threshold driving a phase-transition into a liquid condensate (128).

1.4.3 Regulation of Biomolecular Condensates

Because there is no membrane surrounding these structures, components within a condensate can rapidly exchange with the cytosol in an equilibrium and can recruit or exclude molecules based on binding affinities (128, 132). Post-translational modifications (PTMs) of phase separated proteins can regulate condensates by revealing or blocking binding sites (136, 137). By altering protein interaction sites, PTMs can regulate the formation of condensates, the recruitment of binding partners, and the physical properties of the condensate itself, shifting the region into a more liquid-like or more solid-like phase. Phosphorylation is a common regulator of LLPS, because the addition or removal of phosphates can influence electrostatic interactions. Methylation and acetylation have also been implicated as regulators of LLPS.

The ability of cells to regulate the formation and properties of biomolecular condensates is critical for proper cellular function. Unsurprisingly, dysregulation of LLPS is associated with human disease (138). LLPS is a spontaneous but reversible process, but defects in regulatory elements can result in aberrant phase transitions into irreversible aggregates. Examples of this can be found in neurodegenerative diseases associated with the cellular accumulation of FUS, tau, or α -synuclein. Mutations associated with ALS, Alzheimer's disease, and Parkinson's disease have been found to result in altered LLPS of these proteins, and PTMs such as phosphorylation, methylation, and acetylation can regulate their ability to phase separate. The deleterious outcomes associated with disrupted phase separation illustrate the importance of biomolecular condensates in biological processes.

1.4.4 Inclusion Bodies as a Replication Strategy

The formation of viral IBs is a replication strategy which allows for the concentration of components involved in vRNA synthesis into a subcellular compartment within the comparatively massive cell cytosol (122). It has been well established that IBs are centers of vRNA synthesis for many non-segmented, negative strand viruses (NNSVs) (108, 124, 125, 139), and recent studies support their classification as virus-induced biomolecular condensates (126, 127, 140). While vRNA can be synthesized outside these compartments or prior to their formation in early infection, formation of IBs is associated with optimal production of vRNA by the polymerase complex (108). Viral RNA has been detected within Negri bodies and pneumovirus IBs (106, 108, 127), and the coalescence of IBs is correlated with optimal replication of measles virus (MeV) and HMPV (108, 140). Viral proteins specifically involved in RNA synthesis are often required components of IBs, meaning without the presence of the protein in the cytosol, IBs will not form (123). The proteins required for IB formation can vary between species, but usually includes the RNA-binding nucleoprotein and the oligomeric phosphoprotein. Thus, IB formation and RNA synthesis are tightly correlated processes necessary for viral replication.

Due to the importance of IBs in NNSV infections, they could be ideal targets for the development of broad-spectrum antiviral strategies. Preventing formation of viral inclusions would dramatically decrease virus-specific RNA synthesis without disrupting host transcription. In later stages of infection, replication could be disrupted by altering the properties of the inclusion itself, such as hardening the compartment to a more gel-like state, which has recently been investigated for RSV (141). Another potential strategy could exploit the molecular interactions that recruit components to the inclusion. Designing vehicle molecules that specifically interact with components of the IB could allow for delivery of antivirals directly to the site of virus replication, potentially lessening off-target effects. In order for these strategies to be developed, the factors driving the formation and regulation of IBs must be understood.

1.5 Inclusion Bodies of Pneumoviruses

HMPV IBs form in the very early stages of infection and have been observed in the cytosol as early as 3 hours post inoculation (hpi), which correlates with a dramatic increase in viral RNA synthesis (108). Early stage IBs occur at a frequency of around 6-7 IBs per cell, but by 24 hpi these structures have condensed and are maintained at 1-3 per cell. The decrease in IB count over time is hypothesized to occur through coalescence of early stage IBs through an actin-dependent process. This maturation of IBs is an important step for replication, as disrupting IB coalescence with actin polymerization inhibitors is associated with a significantly reduction in both vRNA production and viral titers (108, 117).

A relationship between actin and HMPV IBs has also been observed during later stages of infection. As discussed in section 1.3.3, HMPV infection induces the formation of membrane filaments and extensions, which both contain viral proteins, vRNA, and actin (117, 119). Formation of these structures is associated with the activity of three Rho GTPases that regulate the actin cytoskeleton: CDC42, Rac1, and RhoA (117). While filaments are believed to be budding viral particles, intercellular extensions have been proposed to act as tunnels for HMPV to directly spread from an infected cell to a non-infected cell through cytosolic mixing (120). While IBs tend to remain near the nucleus (108), these structures have been observed moving around the cell and traveling between cells, sometimes through intercellular extensions (117, 119, 126). Movement of IBs through extensions to a non-infected cell may allow for direct transfer of the proteins involved in replication, bypassing the steps of attachment and fusion required by viral particles. HMPV P, an important component of IBs, interacts with actin or an actin-associated protein (117), suggesting that HMPV may utilize the actin cytoskeleton as a highway to move IBs within or between cells. Up to 50% of HMPV spread in tissue culture has been attributed to the formation of intercellular extensions. Therefore, IBs are not only important for replication during early infection but may have additional and vital roles in propagation of an HMPV infection.

1.5.1 Host Proteins Found in Inclusion Bodies

Recruitment of host factors to IBs is proposed to be another way viruses can hijack host pathways to either promote viral processes or evade the innate immune system, although these mechanisms are not clearly defined. NNSVs utilize the recruitment of host proteins to IBs to modify viral molecules to regulate their function or sequester molecules involved in an antiviral response (122). IBs formed by NNSVs have been found to contain host chaperone proteins, kinases, and phosphatases, as well as molecules involved in modifying RNA, regulating transcription, and immune signaling. Depending on the host protein, preventing the recruitment of these host factors to IBs, or inhibiting their enzymatic activity, can disrupt vRNA synthesis or even the formation of the IB itself. The identification of host proteins in HMPV IBs is severely limited, although they were recently found to contain METTL3 and METTL14, enzymes responsible for N⁶-methylation to adenosine residues (m⁶A) of host RNA (142). Recruitment of these host proteins to IBs allowed for the viral mRNA to be modified and disguised as host mRNA to avoid detection by the RIG-I pattern recognition receptor, thus subverting detection by the innate immune system.

1.5.2 The Phosphoprotein and the Nucleoprotein

As the first two proteins encoded in NNSV genomes, N and P will be among the first proteins to accumulate in the cell when IBs begin to appear during the early stages of infection (1). Accordingly, co-transfection of P and N together, in the absence of other viral proteins, is sufficient to form spherical IB-like structures in the cytosol for pneumoviruses, indicating these proteins are the minimal viral components of IBs and likely drive their formation (107, 143). The molecular features of these two proteins are consistent with the characteristics that contribute to multivalency, supporting the idea that they are important for LLPS. However, it has yet to be determined what molecular interactions involving these proteins are contributing to IB formation for HMPV. Despite both proteins being required to form IBs in cells, purified HMPV P can phase separate into droplets on its own (126).

On the other hand, purified N requires the presence of P in order to be pulled into droplets, suggesting P is an important driver of LLPS in a simplified system. It is possible that direct interactions between P and N drive LLPS in physiological conditions, but IB formation could potentially rely on a network of interactions involving P, N, and host proteins.

HMPV P is 294 amino acids in length, with large N-terminal (NTD) and C-terminal (CTD) intrinsically disordered domains on either side of a central, alpha-helical oligomerization domain (144). This protein exists as a semi-linear, parallel homo-tetramer and contains many different binding sites for other viral or host proteins (**Fig 1.6**). It is unusually enriched in charged amino acids compared to most cellular proteins, with 61 (20%) positively charged residues and 44 (15%) negatively charged residues, contributing to its disordered nature. The structures of the NTD and CTD are not resolvable, suggesting these domains are highly flexible in the absence of specific binding partners and do not maintain a specific conformation. At the NTD, a small alpha-helix interacts with monomeric HMPV N (144, 145), preventing N from non-specifically binding and oligomerizing around cellular RNAs (**Fig 1.7**) (146). Further down the NTD is a consensus sequence for protein phosphatase 1 (PP1) and a predicted binding site for M2-1 (80, 144). RSV P was shown to recruit PP1 to IBs in order to dephosphorylate M2-1 to regulate the sublocalization of M2-1 and mRNA within IBs (80), although this has yet to be investigated for HMPV P.

One of the most important roles of P is as a polymerase co-factor, and the structure of the P/L interaction for both RSV and HMPV revealed the binding site for L is at the OD and the beginning of the CTD (112, 147). Each of the four P protomers has a unique point of contact with L, with the CTDs wrapping around the polymerase asymmetrically (**Fig 1.8**). In the middle of the CTD is highly acidic patch of about 16 residues, which includes a cluster of serine and threonine residues and a glutamic acid repeat (**Fig 1.6**). This region is immediately outside the resolvable structure of the P/L interaction domain and is one of the unique sequence features differentiating it from RSV P, but its function is not known. The

terminal amino acids of HMPV P are proposed to be the location of the binding site for N that has oligomerized with RNA, allowing P to anchor L to the nucleocapsid (148, 149). Finally, P contains several phosphorylation sites (112), but the purpose of these modifications for HMPV has yet to be studied.

The P-specific interactions listed above allow for a proposed model of RNA synthesis within IBs (150). The P tetramer attaches L to the nucleocapsid and keeps it anchored as it moves along the genome (**Fig 1.4**). The M2-1 protein is recruited to IBs by P, where it acts as a processivity factor for the polymerase. The NTD of P likely interacts with monomeric N that has either been transiently displaced from the nucleocapsid or is waiting to encapsidate nascent RNA as it leaves the polymerase. This model attempts to describe a polymerase complex that is actively replicating, but it is not clear if or how these interactions change pre-replication before IBs have formed or post-replication as components must be trafficked to sites of assembly and spread. Some questions that remain regarding IBs is how does HMPV precisely regulate IB formation, protein content, RNA synthesis, exportation of nucleocapsids, and the transition between IBs involved in replication and IBs involved in spread. Answering these questions will provide important insights on a unique replication strategy utilized by HMPV and other NNSVs.

1.6 Dissertation Summary

During infection, viruses must co-opt host resources to quickly and efficiently replicate while trying to evade detection. For the virus, anything that disrupts this process is detrimental to survival. The evolution of NNSVs has resulted in a replication strategy that utilizes virus-induced biomolecular condensates as a way to compartmentalize important factors necessary to replicate and transcribe vRNAs. IBs of HMPV may also have an important role in a significant secondary mechanism of spread (120), meaning IBs are key players in the progression of an HMPV infection. Consequently, the ability to control the formation and function of these structures is likely highly regulated. In order to

better understand how this virus causes infection, it is important to identify the factors contributing to the formation and regulation of HMPV IBs.

P and N are highly concentrated within IBs and required for their formation (107), but it is not known what molecular interactions are driving this co-localization. The phosphoprotein clearly has a central role during infection, with the potential to interact with a variety of proteins to facilitate formation of higher order complexes involved in replication and assembly. The enrichment in polar and charged residues, extensive intrinsic disorder, and the ability to both oligomerize and facilitate multivalent interaction are all characteristics of HMPV P that are also found in proteins prone to phase separation, making P an ideal candidate to investigate as a driver of IB formation. P can interact with two different forms of N, and both of these interaction sites are predicted to be within the P IDRs (144). As IDRs are often prone to phase separate, a logical prediction would be that interactions between the P IDRs and N are important for driving formation of IBs. However, it is not clear if one, both, or neither of these interactions are required for both proteins to co-localize to IBs.

HMPV P is also predicted to be phosphorylated (112), a type of PTM frequently involved in the regulation of both LLPS and biological pathways. Phosphorylation of phosphoproteins has been studied for several NNSVs, with unclear results. The function of RSV P phosphorylation seen in reporter assays is not always recapitulated in an infection model (151, 152), indicating viruses may have “back-up plans” to compensate for potential interference in certain regulatory mechanisms. Additionally, many of these studies were completed before IBs were classified as biomolecular condensates, so the effect of phosphorylation on the IBs themselves was not considered. A recent study on RABV was first to illustrate a possible connection between P phosphorylation, IB size, and gene expression (127). Several phosphorylation sites of HMPV P were identified in 2020 (112), but the purpose of these phosphorylation sites has yet to be determined.

The work presented in this thesis aims to investigate the molecular interactions contributing to the formation of HMPV IBs and determine if

phosphorylation of HMPV P within these structures acts as a regulatory feature controlling RNA synthesis during infection. The hypotheses under investigation are 1) the IDRs of HMPV P are drivers of IB formation and 2) the phosphorylation state of HMPV P at specific sites is a mechanism to regulate viral RNA synthesis. Because IBs display properties of biomolecular condensates formed through LLPS, “IB formation” and “phase separation” are used interchangeably throughout this work.

Mutagenesis of HMPV P revealed that the CTD is the location of molecular interactions driving co-localization with N. One residue in the CTD, Y290, was indispensable for IB formation and was important for co-immunoprecipitation of N with P. Y290 was also required for optimal function of the polymerase complex in a reporter assay, and mutagenesis at this residue within the HMPV genome prevented rescue of recombinant virus. These results revealed the IDRs of HMPV P are not themselves drivers of IB formation, but instead a specific interaction within the disordered CTD with HMPV N is involved in this process. Either P and N directly interact to facilitate a phase transition, or their interaction allows them to form a complex with host proteins that are needed to initiate IB formation

An analysis of the HMPV P protein sequence revealed it contains many sites which are predicted to be phosphorylated by cellular kinases, some of which were previously identified through mass spectrometry analysis. Mutagenesis of both known and predicted phosphorylation sites revealed the location of four residues in the P CTD important for the function of P as a polymerase co-factor, which could be corroborated both in reporter assays and during viral infection. The four residues were located within the highly acidic patch unique to HMPV P, implicating the functional relevance may be exclusive to this specific virus. Residue S266, though not previously found to be phosphorylated, is likely a site capable of facilitating optimal levels of RNA production when phosphorylated. Interestingly, the role of phosphorylation at S271, a known phosphorylation site, was unable to be elucidated using reporter assays and requires further investigation. Mutations at the investigated residues did not prevent IB formation but did slightly alter the

diffusion dynamics of P within IBs, suggesting phosphorylation of HMPV P might alter diffusion rates by affecting P-specific molecular interactions.

This work contributes to a rapidly expanding field investigating the regulation of viral IBs. Our results indicate the CTD of HMPV P contains several molecular features that contribute to its multifaceted role during replication. This region is the location of interactions that facilitate IB formation with HMPV N and contains single residues essential for infection. Phosphorylation at several of these sites may function to regulate RNA synthesis through an unknown mechanism. Combined with past work from the Dutch lab (108, 117, 126), these results provide a framework for formation and regulation of HMPV IBs. Future mechanistic studies investigating the virus-host interactions involved in these processes are still needed in order to deepen our understanding of how this important pathogen causes disease and identify targets for therapeutic development.

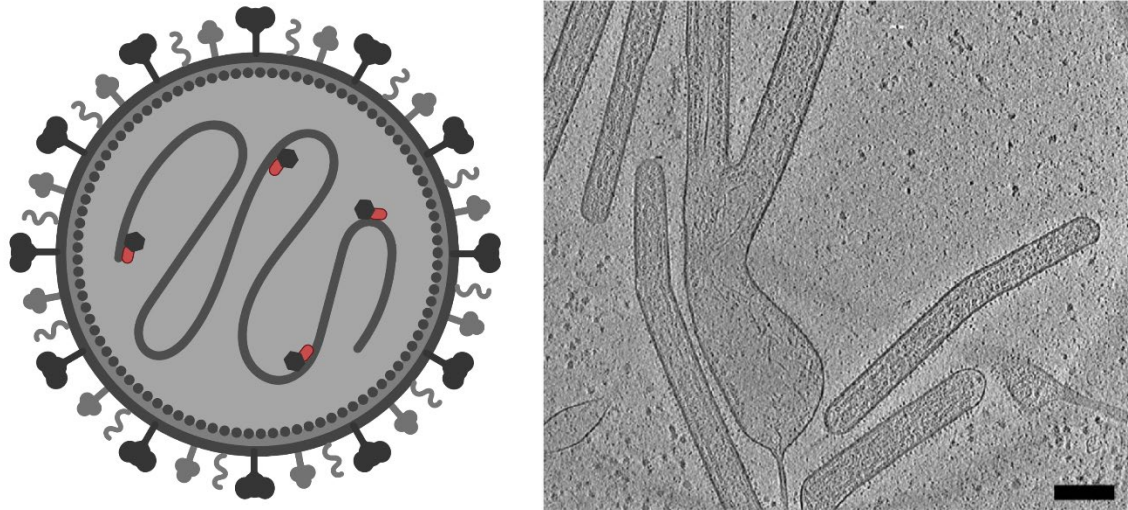


Figure 1.1 *Pneumoviridae* viral particles

The simplified schematic of a viral particle (left, created with BioRender) illustrates the location of the major structural proteins in RSV and HMPV. The glycoproteins are studded along the host-derived membrane, which surrounds the encapsidated RNA genome in complex with the polymerase complex proteins. The viral matrix protein forms a lattice along the inside of the particle. In reality, the major form of *pneumoviridae* virions produced from cell culture are filamentous in shape, not spherical. This elongated form is structurally supported by the matrix protein lattice. The right image (adapted from Ke, 2018 (74)) illustrates filamentous RSV particles produced from BEAS-2B cells, analyzed with cryo-electron tomography (scale bar, 200 nm).

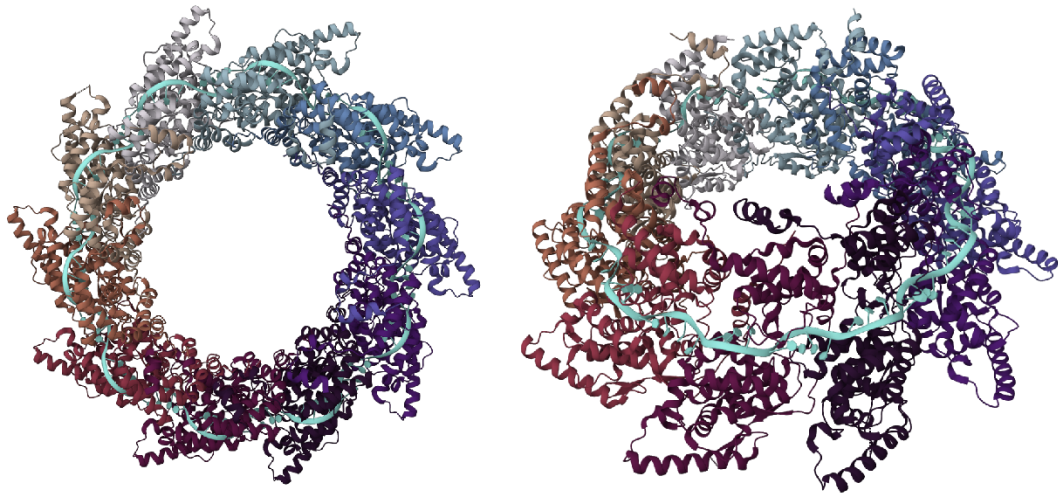


Figure 1.2 HMPV N-RNA interactions

The HMPV nucleoprotein oligomerizes to encapsidate RNA. When purified from *E. coli*, N forms decameric rings that have non-specifically interacted with cellular RNA (5FVC) (145), demonstrating its potential for helical oligomerization during genome encapsidation. The N-RNA interaction is facilitated through electrostatic interactions between the negatively charged RNA backbone and positively charged residues within the N RNA-binding pocket. Each N protomer contacts seven nucleotides and two other N subunits to form the N-RNA complex. A close up of a single N protomer interacting with RNA is depicted in Figure 1.7. Image was created using Mol* (153).

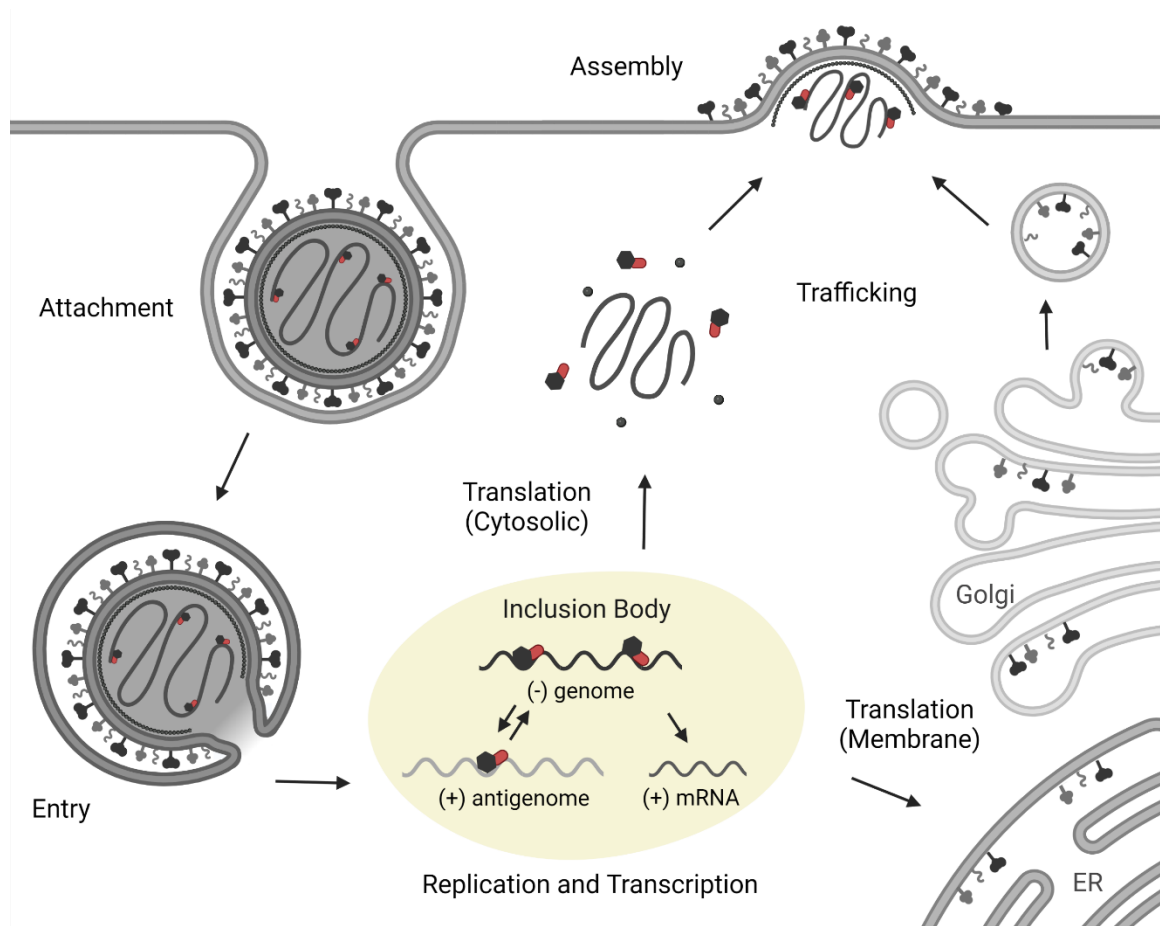


Figure 1.3 The life cycle of HMPV

Surface glycoproteins on the viral particle aid in attachment to the host membrane. HMPV is endocytosed, where acidification of the endosome triggers fusion of the viral and host membrane. The viral contents are released into the cell, where the genome is replicated and transcribed by the HMPV polymerase complex. Viral proteins localize to cytoplasmic inclusion bodies, allowing for optimal rates of RNA synthesis. Viral membrane proteins are translated in the ER and traffic through the Trans-Golgi network, where they are glycosylated and ultimately trafficked to the cell surface. Proteins to be packaged inside the virion are translated in the cytosol and are transported to assembly sites. Image was created with BioRender.

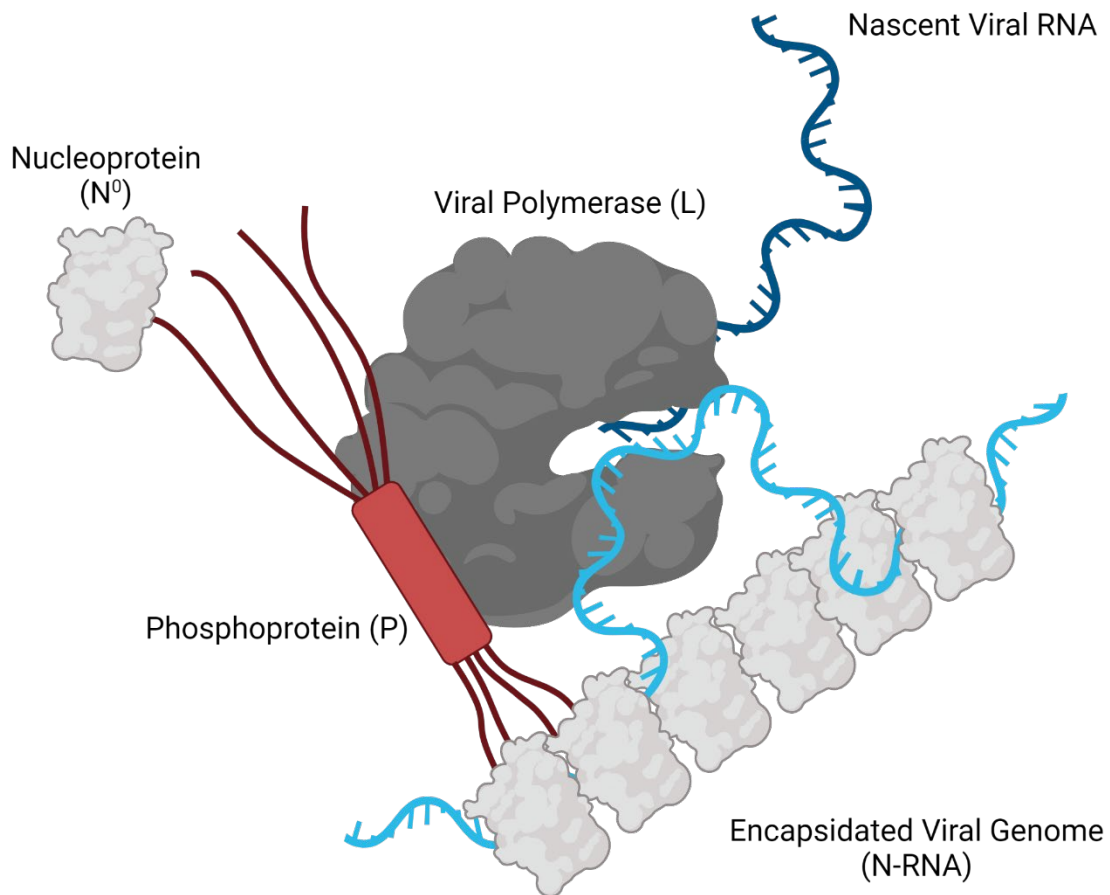


Figure 1.4 Simplified model of an active HMPV polymerase complex

The nucleocapsid (N-RNA) acts as the template for RNA synthesis, but HMPV L (dark gray, center) requires transient, localized uncoating of the nucleocapsid to expose the RNA genome (dark blue). HMPV P (red) is an essential polymerase co-factor and acts as an adaptor during RNA synthesis, facilitating interactions required for successful replication. The P tetrameric core binds to L (crystal structure shown in Figure 1.8), and the P CTD binds the nucleocapsid, anchoring L to the genome. The flexible NTD of P binds N⁰, and may be involved in temporarily displacing N from the nucleocapsid or facilitating encapsidation of nascent RNA (light blue). Figure created with BioRender.

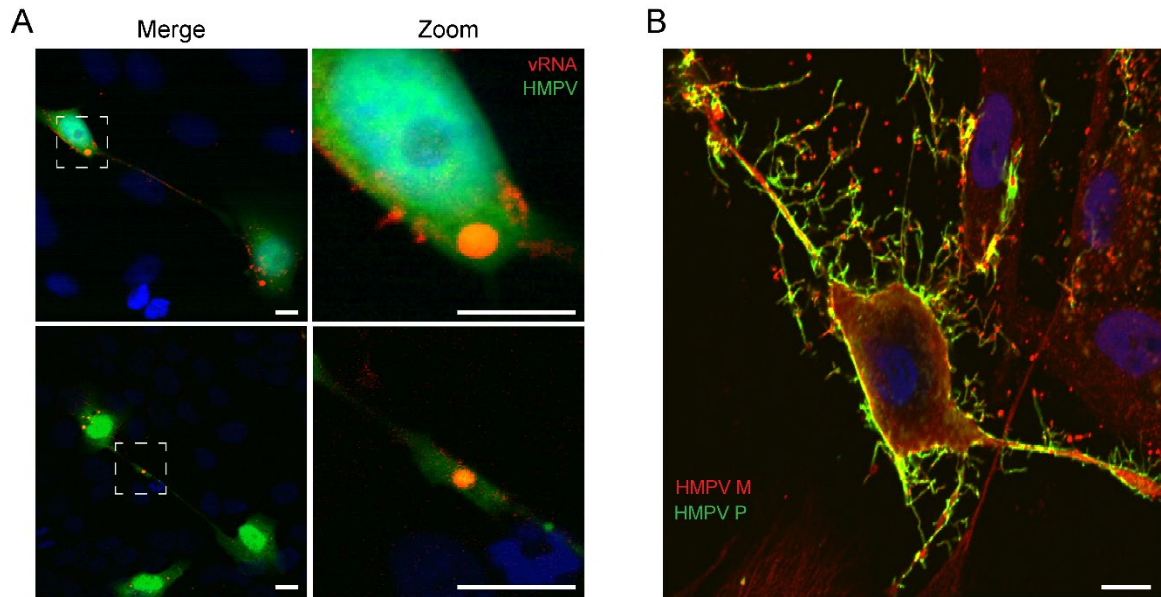


Figure 1.5 Cellular features of an HMPV infection

A) Images (adapted from el Najjar, 2016 (117)), showing HMPV infected BEAS-2B cells (green) stained with FISH probes for viral RNA (red). Scale bar represents 10 μm . Both sets of top and bottom images show two infected cells, 72 hpi, connected through intercellular extensions. Top zoom shows localization of viral RNA to spherical IBs. Bottom zoom shows an IB within the intercellular extension.

B) HMPV infected BEAS-2B cells, 24 hpi, stained for detection of HMPV M (red) and HMPV P (green). HMPV induces the formation of membrane filaments and intercellular extensions, to which viral proteins localize during late stages of infection. Scale bar represents 10 μm . Image was collected by Farah el Najjar.

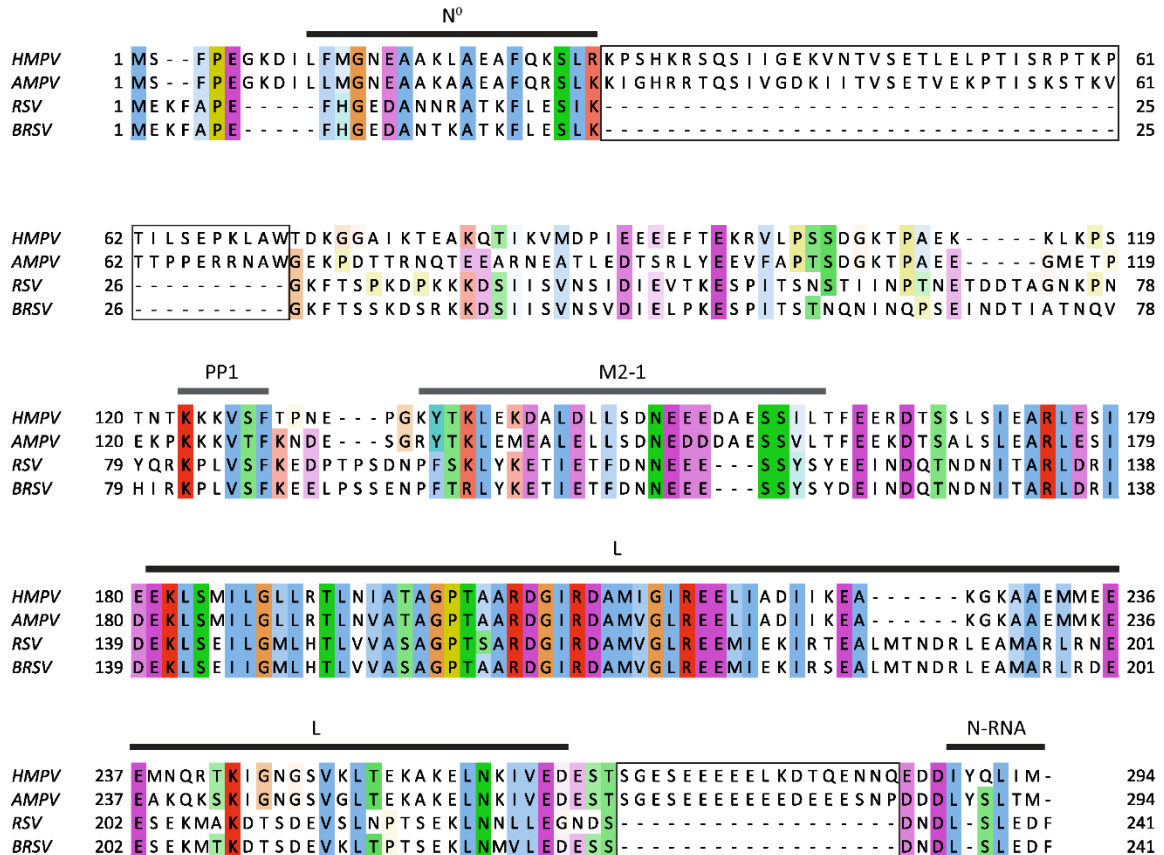


Figure 1.6 Sequence alignment of *Pneumoviridae* phosphoproteins

The sequences of the phosphoproteins for human metapneumovirus (HMPV, strain CAN97-83), avian metapneumovirus (AMPV, strain 15a), respiratory syncytial virus (RSV, strain A2), and bovine respiratory syncytial virus (BRSV, strain ATCC51908) were aligned using PROMALS3D (154) and visualized using Jalview (155). Lines indicate identified (black) or predicted (gray) binding sites for the indicated proteins on HMPV P. Boxes are used to indicate unique regions within HMPV P that are absent in RSV P. Colored residues show conserved amino acid properties, defined by the Clustal X color scheme (156). Note that regions of high homology are also critical binding domains. Figure adapted from Renner, 2017 (144).

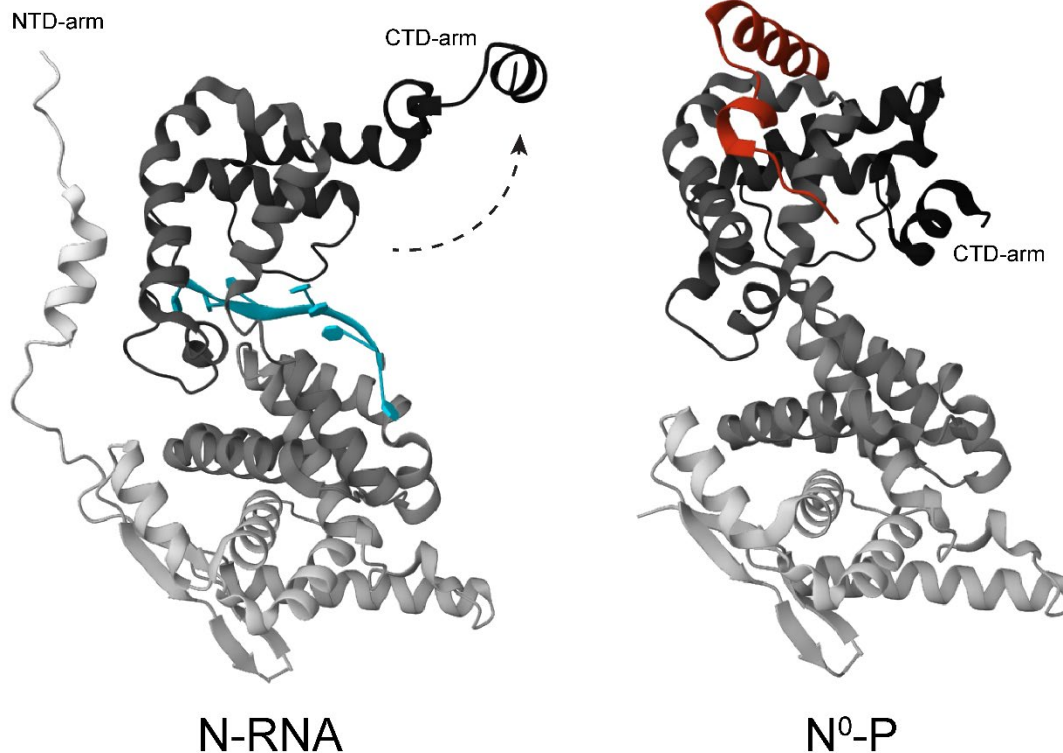


Figure 1.7 Conformational changes of HMPV N

The nucleoprotein consists of an N-terminal domain (NTD, light gray) and C-terminal domain (CTD, dark gray), separated by a flexible hinge. Depending on the binding partners, N exists in two distinct conformations. In the oligomeric state (left, 5FVC (145)), N binds RNA (light blue) in a cavity formed between the NTD and CTD. The NTD-arm (white) of one N protomer binds the preceding N protomer, and the CTD-arm (black) is flipped up to bind the succeeding N protomer. In the monomeric, RNA-free state (right, 5FVD (145)), the NTD of P (red) binds to the surface of N⁰, simultaneously overlapping both oligomerization sites utilized by the two surrounding N protomers. The CTD-arm of N has undergone a dramatic conformational change from the N-RNA state, flipping down to block the RNA-binding pocket. The viral polymerase requires transient depolymerization of the nucleocapsid to reveal the RNA genome during replication and transcription. This process likely involves a balance between P-N, N-N, and N-RNA interactions that allow N to switch between these two conformational states. Figure was generated using Mol* (153).

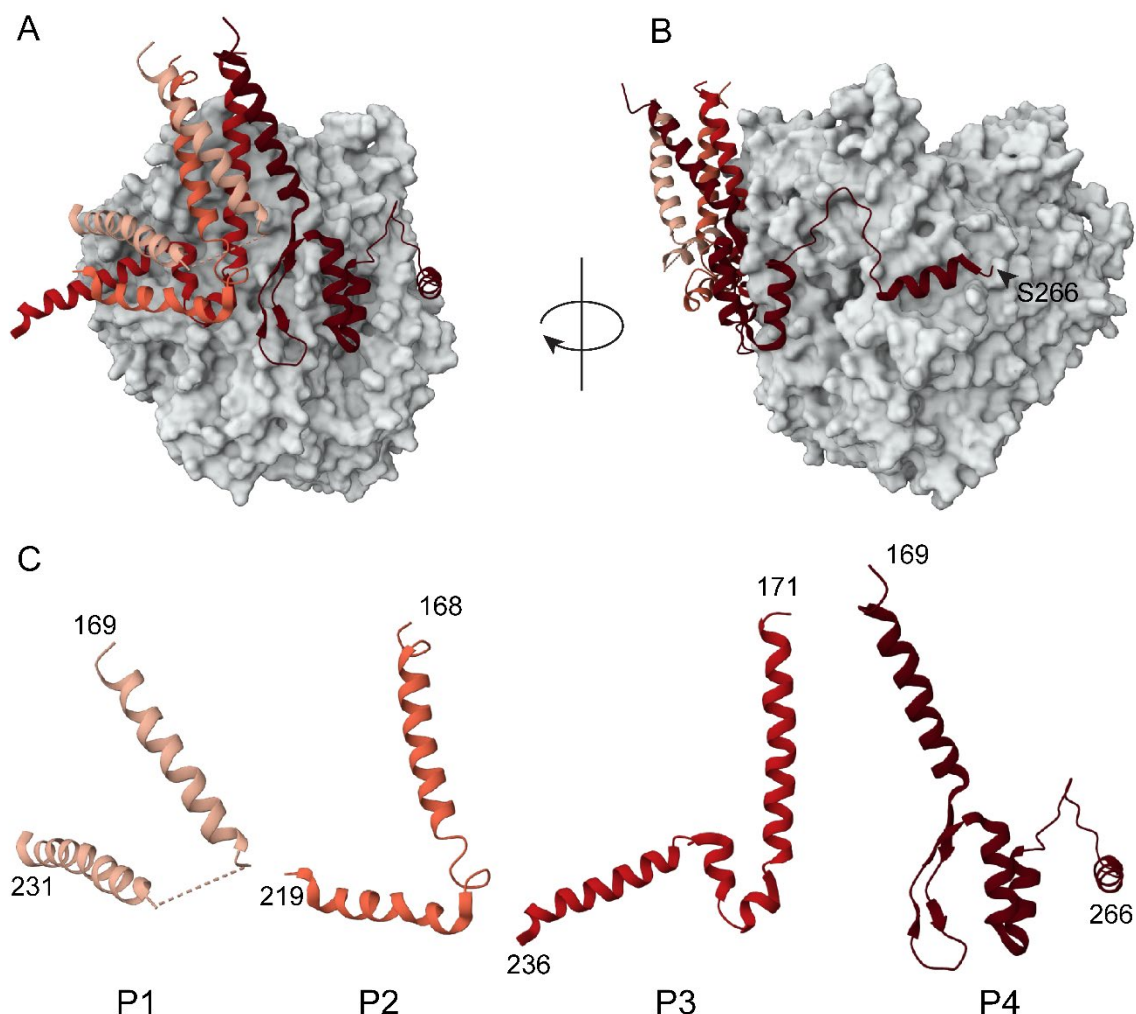


Figure 1.8 Structure of the HMPV polymerase complex

A) The crystal structure (6U5O) of tetrameric P binding to the polymerase domain of L (112). Each P subunit is colored in shades of orange and red. The molecular surface of the resolvable domains of L are depicted in gray. When purified alone, the P tetramerization domain (aa 169-194) is the only resolvable structure, and the surrounding domains are intrinsically disordered (144). Upon binding of P to the polymerase, a portion of the disordered C-terminus undergoes a disorder-to-order transition. B,C) Each P subunit adopts a unique secondary structure, interacting with L asymmetrically. Subunits P1 and P2 have the least amount of interactions with L while P3 and P4 have the most. The CTD of P4 diverges from the other three and forms a unique beta hairpin followed by 3 alpha helices. This conformation positions positively charged residues within the P sequence along an opening in L that acts as an entrance for negatively charged NTPs. P4 is resolved up to residue S266 (B, black arrowhead). The other three P subunits' CTDs form a three-helix bundle and are oriented near the entrance and exit tunnels for the genome template and likely function to facilitate proximity between L and the nucleocapsid. The P NTD are positioned near the exit tunnel for synthesized RNA, which would allow P to keep a supply of N⁰ units to encapsidate nascent RNA as it exits the polymerase. Figure was generated using Mol* (153).

CHAPTER 2. METHODS

Portions of this chapter were adapted and reprinted with permission from the American Society for Microbiology: Thompson RE, Edmonds K, Dutch RE. 2023. Specific residues in the C-terminal domain of the HMPV phosphoprotein are indispensable for formation of viral replication centers and regulation of the function of the viral polymerase complex. J Virol.

2.1 Materials and Standard Protocols

2.1.1 Cell Lines

Vero cells were obtained from ATCC (CCL-81) and grown in Dulbecco's modified Eagle's medium (DMEM; Gibco/Hyclone) supplemented with 10% fetal bovine serum (FBS; Sigma-Aldrich). BSR T7/5 cells stably expressing T7 polymerase (157), provided by Karl-Klaus Conzelmann (Pettenkofer Institute), were maintained in DMEM supplemented with 10% FBS and supplemented with 0.5 mg/ml G-418 (Invitrogen) every third passage. HEK 293T cells (kindly provided by Tony Schmitt; Pennsylvania State University) were grown in DMEM supplemented with 10% FBS. Cells were incubated at 37°C with 5% CO₂.

2.1.2 Transfections

All transfections were carried out using P3000 Reagent and Lipofectamine 3000 according to manufacturer's suggestion (Invitrogen). In one 1.5 ml tube, DNA and P3000 Reagent were combined with OptiMEM (Gibco), using 2 µl reagent for every 1 µg DNA. In a separate tube, Lipofectamine 3000 was diluted with a volume of OptiMEM equal to the DNA/P3000 mixture. The diluted Lipofectamine 3000 mixture was combined with the equal volume of DNA/P3000 mixture, and incubated at room temperature for 15 min. DNA/lipid complexes were added directly to cells on top of the DMEM growth media and incubated at 37°C with 5% CO₂.

2.1.3 Plasmids, Antibodies, and Reagents

Plasmids for WT HA-P, mCherry-P, HA-P OD, HA-P Δ CTD, and HA-P Δ NTD from the HMPV strain CAN97-83 (AY145251.1) were ordered from GenScript and subcloned into pCAGGS. All HA-P and mCherry-P mutants were created in a pUC57 cloning vector using site directed mutagenesis (below), then subcloned into pCAGGS. HMPV minireplicon plasmids pTM1-N, pTM1-L, pTM1-M2-1, and minigenome pTM1-LUC were kindly provided by Dr. Rachel Fearn (Boston University). A codon optimized version of the HMPV N gene from strain CAN97-83 was subcloned into pCAGGS. Empty pCAGGS (EV) was used for negative controls in transfection experiments and for subcloning. Rescue plasmids p(+)-JPS07E2, pCITE-P, pCITE-N, pCITE-L, and pCITE-M2-1, encoding the full-length genome and protein sequences for HMPV strain JPS02-76 (158), were graciously provided by Dr. Makoto Takeda (National Institute of Infectious Diseases, Tokyo, Japan). All DNA was prepared by transformation into chemically competent *E. coli* DH5 α grown in 2XYT media and purification using Mini and Maxi Prep kits (Macherey-Nagel). Correct sequences were confirmed after every purification through ACGT sequencing services.

Rabbit polyclonal antibody to the HA tag (ab9110) and mouse monoclonal antibody to HMPV N (hMPV 57, ab94802) were obtained from Abcam. Mouse monoclonal antibody to alpha tubulin (66031-1) was purchased from Proteintech Group. Goat anti-rabbit and goat anti-mouse secondary antibodies, conjugated to Rhodamine (TRITC) or Fluorescein (FITC), used for immunofluorescence, were obtained from Jackson ImmunoResearch. Secondary antibodies used for western blot imaging, 680RD goat anti-rabbit and 800CW goat anti-mouse, were obtained from LI-COR Biosciences. Nanobody against HMPV P was prepared and validated by the Center for Molecular Medicine Protein Core (Department of Molecular and Cellular Biochemistry, University of Kentucky) (159) using HMPV P purified from *E. coli* (126). The nanobody was coupled to magnetic beads using DynaBeads Antibody Coupling Kit (Invitrogen; method below).

2.1.4 Mutagenesis and P Domain Constructs

All HA-P and mCherry-P point mutants were generated from pUC57 plasmids using the QuikChange Site Directed Mutagenesis protocol and overlapping primers ordered from Eurofins Genomics. HA-P NTD was made by cloning in a stop codon and restriction site following residue 157, and HA-P CTD was made by cloning in a restriction site, start codon, and HA tag immediately prior to residue 238. HA-P Δ OD was created using PCR with primers linking the end of the NTD and the beginning of the CTD nucleic acid sequence. HA-P Δ 281-284 was made through mutagenesis of double stop codons at 281 and 282. After initial sequence confirmation, all constructs were subcloned into pCAGGS using EcoRI and XhoI (New England Biolabs), then sequenced again.

2.2 Methods to Analyze Inclusion Bodies

2.2.1 Inclusion Body Formation Assay

Vero cells were seeded in 8-chamber slides (Lab-Tek) to 60% confluency and transfected the next day with 200 ng EV, or 100 ng HA-P construct and 100 ng HMPV N. After 20-24 hpt, the wells were washed twice with PBS and fixed with 4% PFA in PBS for 30 min at room temperature. Wells were washed twice with PBS, then permeabilized with cold 1% Triton-x100 in PBS for 15 min at 4°C. Wells were washed once with PBS and blocked with 1% NGS in PBS for 1 h at 4°C. The blocking buffer was removed and then primary antibody diluted in 1% NGS in PBS was added (anti-HA 1:2000; anti-N 1:500), and the slides were incubated overnight at 4°C. The next day, the wells were washed seven times with 0.05% Tween-20 in PBS and incubated with secondary antibody diluted (1:300) in 1% NGS in PBS for 1 h at 4°C in the dark, then washed seven times with 0.05% Tween-20 in PBS. After all liquid was aspirated from the wells, the 8-well chamber and silicone gasket were removed. VECTASHIELD PLUS Antifade Mounting Media with DAPI (Vector Laboratories) was added on top of the cells, then a coverslip (VWR) was placed on top and sealed with black nail polish. Imaging was done using a Nikon Ti2

microscope (100x oil objective) with NIS elements software, and image processing was completed using Photoshop. Ten images were collected per well, and the experiment was completed in duplicate.

2.2.2 FRAP Acquisition

Vero cells were seeded in glass bottom Delta T heated culture dishes (Bioprotech Inc). The next day, cells were co-transfected with HMPV N and mCherry-P or mCherry-P mutant. Sixteen to twenty-four hours post transfection, FRAP was performed on live cells using a Nikon A1R confocal microscope with a Plan Fluor 40x Oil DIC objective and a heated stage set to 37°C. For each FRAP acquisition, regions of interest (ROIs) were drawn around three different IBs to be bleached and an area outside the cell for background signal. To account for permanent loss of recoverable signal due to intentional and unintentional photobleaching, a reference ROI was drawn around the entire cell. Each FRAP acquisition consisted of 5 s pre-bleaching, 8 s bleaching with a 405 nm laser at 100% power, and 4.5 min of recovery. Images were collected every 267 ms, and at least 6 FRAP acquisitions were collected per dish. Experiments were completed in triplicate.

2.2.3 FRAP Analysis

Data collection from FRAP files was completed using NIS Elements. Because IBs are not static structures in live cells, if an IB moved during recovery the ROIs were manually repositioned to keep the IB at its center. ROIs that moved out of focus, elongated outside the ROI shape, divided, or fused with another IB were excluded from analysis. IB ROI intensity was corrected for background and photobleaching at each timepoint, then normalized to a 0-1 scale, with 0 being the recovery at $t=0$ s and 1 being the average corrected pre-bleach intensity. Recovery curves were generated and analyzed in GraphPad Prism (version 7.04) by averaging corrected and normalized FRAP data of all measurable IBs collected during triplicate experiments, and each mutant was compared only to the WT FRAP data collected on the same days. Data was fit to a two-phase exponential

association model on GraphPad using a least squares fitting method. To calculate significant differences, GraphPad ran comparisons between the data sets for each mutant and corresponding WT condition and determined the likelihood that both data sets could be fit using a shared parameter. This was done for each mutant, for all four parameters used in the equation for the two-phase exponential association model: Ymax1, K1, Ymax2, and K2. A p value below 0.05 meant the best fit parameter was different between mutant and WT data sets.

2.3 Methods to Analyze HMPV P Interactions

2.3.1 Minireplicon Assay

BSR T7/5 cells were seeded in 12-well plates (Corning, 3513) to 70% confluency in 500 μ l DMEM (10% FBS) and incubated at 37°C with 5% CO₂. After 24 h, cells were transfected in duplicate with 1.2 μ g minigenome, 120 ng N, 120 ng HA-P, HA-P mutant, or EV, 100 ng M2-1, and 60 ng L, or 3.2 μ g EV in 100 μ l OptiMEM added dropwise to each well. Cells were washed twice with 1 ml PBS 22-24 hpt, on ice, then lysed in 100 μ l 1x Luciferase lysis buffer (Promega). After one freeze-thaw cycle, the cell lysate was collected and vortexed for 10 seconds. Cell debris was pelleted at 4°C, and 20 μ l of the supernatant was added to a Microlite luminescence 96-well plate (Thermo Scientific) and briefly brought to room temperature in the dark. Using either an Lmax luminometer or a SpectraMax iD3 plate reader (both Molecular Devices), 100 μ l of luciferin (Promega) was automatically injected into each well and luminescence was recorded after a 2 second delay. Average background (EV or -P control) was subtracted from each sample, duplicate wells were averaged, and all results were normalized to the WT HA-P condition of each experimental replicate. Statistical analysis was done using a one-way ANOVA, comparing the mean of each condition to the mean of HA-P. Protein expression from the remaining cell lysate was quantified using western blot analysis, described below.

2.3.2 Western Blots

Ladder (Precision Plus Protein All Blue Standards, Bio-Rad) and prepared samples were loaded into wells of a 15% SDS PAGE hand-cast gel (Bio-Rad) and run at 60 v until through the stacker, then at 80-100 v. Separated protein was transferred to a methanol-activated 0.45 µm PVDF membrane (Millipore) at 50 v for 80 min. Membranes were blocked in 5% milk in tTBS (0.2% tween-20 in tris-buffered saline), then incubated overnight with primary antibody diluted in blocking buffer (rabbit anti-HA, 1:5000 ; mouse anti-N, 1:1000-1:2000; mouse anti-tubulin, 1:10,000), rocking at 4°C. Membranes were washed three times with tTBS, then incubated with secondary antibody (1:10,000) for 1 h, rocking at room temperature. After washing three times with tTBS, then three times with deionized water, membranes were imaged on a Bio-Rad ChemiDoc and band densities were quantified using ImageQuant. The background signal was subtracted from all lanes, then the corrected signal was normalized to tubulin. For graphing and statistical analysis, all samples were additionally normalized to the WT P condition.

2.3.3 Nanobody and DynaBead Coupling

For each coupling reaction, 5 mg DynaBeads M-270 Epoxy was coupled to 100 µg HMPV P nanobody according to the manufacturers protocol. The coupling reaction was incubated for 24 h at 37°C using a rotator (Roto-Mini, Southern Labware) set to 22 rpm. All washing steps were completed by briefly vortexing tubes on a medium speed until resuspended, then spinning down the beads at 2000 rpm for 1 min at 4°C and incubating for 1 min at room temperature on a magnetic rack (DynaMag, Invitrogen). The final volume of nanobody-coupled-beads from each reaction was combined and mixed to homogenize the bead stock, then stored at 4°C to be used the following day.

2.3.4 Co-immunoprecipitation

HEK 293T cells were seeded in 6-well amine-coated plates (Corning, 356721) to approximately 70% confluency in 1.5 ml DMEM (10% FBS) and

incubated at 37°C with 5% CO₂ for 20-24 h. Using Lipofectamine 3000 in a 2:1 ratio, cells were transfected with either 1.1 µg EV, 1 µg HA-P and 100 ng EV, or 100 ng HMPV N and 1 µg EV, HA-P WT, or HA-P mutant. Approximately 20-22 hpt, cells were washed with PBS and incubated on ice with 300 µl Pierce IP lysis buffer (Thermo Scientific) supplemented with ½ a complete mini EDTA-free protease inhibitor tablet (Roche). Lysate was collected and cells were pelleted at 13,000 rpm for 10 min at 4°C, and the supernatant was transferred to a new tube. Five milligrams nanobody-coupled-beads were washed once with 1 ml PBS, then once with 500 µl lysis buffer. Beads were incubated with 260 µl cell lysate for 1 h at 4°C, rocking on a platform shaker (VWR). Beads were washed twice with PBS (0.3 M NaCl), then twice with PBS (0.15 M NaCl), and were resuspended in 50 µl 2x SDS loading buffer. Twenty-five microliters of remaining cell lysate was mixed with 25 µl 2x SDS loading buffer, and all lysate and IP samples were incubated in boiling water for 10 min, briefly set on ice, then quickly spun down. IP samples were placed on a magnetic rack for 1 min. Three microliters of ladder and 22 µl of all lysate and IP samples were loaded into a 15% SDS PAGE gel for western blot analysis.

2.3.5 Recombinant Virus Mutagenesis

To generate an mCherry expressing HMPV strain harboring HA-P mutations, a pUC57 cloning vector was designed containing the HMPV JPS02-76 sequences for N and HA-P separated by an mCherry gene and flanked by restriction sites for NheI and SexAI (GenScript). Site directed mutagenesis was performed on this cloning vector using primers specific for the JPS02-76 P sequence. Because SexAI is blocked by DNA methylation, the p(+)-JPS07E2 genome plasmid and WT and mutant constructs were grown in *E. coli* strain GM2163 (*dam-13::Tn9*, *dcm-6*), which is deficient in Dam and Dcm methylation. Using NheI and SexAI, the N-mCherry-HA-P cassettes for both WT and mutant HA-P were subcloned into the p(+)-JPS07E2 genome plasmid and grown in DH5α *E. coli* for purification. Sequencing was confirmed at each stage using whole plasmid sequencing services through Plasmidsaurus. We found our p(+)-JPS07E2

stock genome plasmid and all resulting constructs had a significant deletion in the SH gene, although this protein has been found to be completely dispensable for growth in cell culture (85).

2.3.6 Recombinant Virus Rescue

BSR T7/5 cells were seeded in DMEM+10% FBS in a 6-well plate (VWR) to 70% confluency. The next day, cells were transfected in Opti-MEM using Lipofectamine 3000 in a 2:1 ratio using the following plasmids: 1 µg pCITE-N, 1 µg pCITE-P, 0.5 µg pCITE-M2-1, 0.5 µg pCITE-L, and 2.5 µg HA-P or HA-P mutant genome. A mock well was transfected with the pCITE plasmids and 2.5 µg EV instead of genome. After 5 hpt, the transfection mixture was aspirated and replaced with 1.5 ml viral growth media (Opti-MEM GlutaMAX, supplemented with 0.3 µg/ml TPCK-Trypsin and 1% Pen/Strep). The next day, Vero cells were seeded in 60 mm dishes (TPP, 93060) to 80% confluency. The following day, 48 hpt, transfected BSRs were collected in the 1.5 ml media, and 750 µl cell suspension was overlaid on top of the Vero cells. The co-culture was grown in viral growth media and spiked every 1-2 days with 0.3 µg/ml TPCK-Trypsin for 5-6 days, or until the appearance of cytopathic effects. Infected cells and supernatant were collected, freeze-thawed once, then pelleted at 300xg for 10 min at 4°C. Passage 1 (P1) of each virus was grown by using the entire volume of supernatant to infect Vero cells seeded in a 150 mm dish (Celltreat). Cells were incubated with virus for 4-5 hours at 37°C, then infection was removed and growth media was added. Infection was spiked with 0.3 µg/ml TPCK-Trypsin every day for 10 days or until the appearance of cytopathic effects. For each virus, one random image was collected at 48 hpt and the day of co-culture collection, and 5 random images were collected the day of P1 collection using a ZOE Fluorescent Cell Imager with a 20x objective (Bio-Rad). The fluorescent images were overlaid on brightfield images at 50% opacity using ImageJ. Rescue of recombinant virus, from transfection to P1, was completed in triplicate for all strains except S268A, which was done in duplicate.

CHAPTER 3.RESULTS

Portions of this chapter were adapted and reprinted with permission from the American Society for Microbiology: Thompson RE, Edmonds K, Dutch RE. 2023. Specific residues in the C-terminal domain of the HMPV phosphoprotein are indispensable for formation of viral replication centers and regulation of the function of the viral polymerase complex. J Virol.

3.1 Introduction

Human metapneumovirus (HMPV) is a non-segmented, negative strand RNA virus (NNSV) belonging to the recently created *Pneumoviridae* family (9). Although the majority of individuals will have been exposed to HMPV by age 5, infections can still occur at any age, with symptoms of varying severity (160). Hospitalizations due to HMPV infection are most prevalent among infant, elderly, and immunocompromised populations, with symptoms ranging from a mild respiratory tract infection to bronchiolitis or pneumonia. Significant morbidity and mortality from HMPV infection occur at rates similar to influenza and respiratory syncytial virus (RSV) among infants below 1 year of age (138), but despite the prevalence and severity of HMPV infections, many mechanistic details of this virus remain unstudied. There are currently no prophylactics, therapeutics, or vaccines available to combat HMPV (161), demonstrating the need for basic research to further characterize functional and mechanistic details of the HMPV life cycle.

NNSVs utilize a common replication strategy involving the concentration of viral RNA and RNA synthesis proteins to membraneless cytoplasmic compartments termed inclusion bodies (IBs) (123), which are associated with efficient replication and transcription of the viral genome (108, 162). Studies on a variety of NNSV IBs have revealed these spherical structures display characteristics of biomolecular condensates (122, 126, 127, 140, 163). Formation of biomolecular condensates occurs through liquid-liquid phase separation (LLPS), a process where biomolecules within a homogenous mixture undergo a liquid-to-liquid phase transition to form a membraneless compartment that is biophysically distinct from the remaining mixture. Defining features of biomolecular condensates

include the ability to undergo fusion and fission, the rapid diffusion and exchange of content with the surrounding environment, and sensitivity to protein and salt concentrations, stress, and post-translational modifications (PTMs) (122, 131, 164). The dynamic and sensitive nature of these fluid compartments suggests the process of forming viral IBs and maintaining them in a replication-conducive state is likely highly regulated during infection, making viral IBs ideal targets for therapeutic development. Therefore, it is critical to determine how viral proteins control these processes.

Studies have begun to reveal factors contributing to the formation and function of NNSV IBs, although these factors can be unique to each individual virus (123). For pneumoviruses, the phosphoprotein (P) and nucleoprotein (N) are the minimal viral components necessary to induce formation of IB-like structures (107, 143), which still exhibit liquid-like properties in the absence of an active infection or other viral proteins (126, 165). P is a tetramer with N- and C-terminal intrinsically disordered regions and is a non-catalytic cofactor for the viral RNA-dependent RNA polymerase. N is an RNA-binding protein that encapsidates the single-stranded RNA genome as a helical oligomer. The N-terminal domain of P binds and maintains N in a monomeric, RNA-free state (145, 146, 166), while the C-terminal domain is believed to bind the nucleocapsid (N-RNA) (148) to anchor the viral polymerase to the genome during replication (150). Despite both proteins being required to form cellular IBs, recent works revealed purified HMPV P expressed in *E. coli* is able to undergo LLPS on its own while RSV P cannot (126, 149, 165), revealing HMPV P has a uniquely inherent ability to phase separate in the absence of PTMs or other proteins. Several HMPV P phosphorylation sites have been identified (112), but the effect of P phosphorylation on IB formation or RNA synthesis has yet to be explored. The HMPV P domains involved in driving formation of cellular IBs and the effect of P phosphorylation on IB formation, function, or regulation is largely unknown.

In this study we utilized microscopy and quantitative assays to evaluate the effect of HMPV P domain deletions and phosphorylation site mutations on IB

formation, function, and dynamics. We found the HMPV P C-terminus is the only domain indispensable for IB formation and identified an aromatic residue within this domain is critical for the formation of IBs, potentially through interaction with the nucleocapsid. Mutagenesis of both known and predicted phosphorylation sites revealed phospho-dead P mutants significantly reduced the function of the polymerase complex, and phosphomimetic mutations at only one of these sites rescue polymerase activity to WT levels, implicating its role in regulating RNA synthesis. Fluorescence recovery after photobleaching (FRAP) of IBs showed P mutations that reduced the function of the polymerase complex had altered diffusion in IBs compared to WT, but co-immunoprecipitation assays showed no change in interactions with HMPV N. Together, this data suggests the C-terminal charge of several HMPV P residues may play a role in the regulation of IB properties and function of the polymerase complex in order to control replication.

3.2 Results

3.2.1 Identifying Regions of HMPV P Driving IB Formation

The HMPV phosphoprotein has three distinct domains: an N-terminal disordered domain (NTD, residues 1-157), an alpha-helical oligomerization domain (OD, residues 158-237), and a C-terminal disordered domain (CTD, residues 238-294). In order to identify sites of molecular interactions on HMPV P that drive IB formation, HA-tagged domain constructs were made (**Fig 3.1A**) which either lacked one of the three P domains (HA-P Δ NTD, HA-P Δ OD, HA-P Δ CTD), or consisted of only one P domain (HA-P NTD, HA-P OD, HA-P CTD). These domain constructs were individually co-transfected with HMPV N to assay for the ability to co-localize into IB-like structures (**Fig 3.1B-C**). HA-P NTD and HA-P OD did not form IBs when in the presence of HMPV N, indicating these individual domains are not sufficient to drive IB formation. HA-P CTD had poor detection through IF staining, suggesting the short IDR is not stably expressed. HA-P Δ NTD and HA-P Δ OD were still able to co-localize with HMPV N in IB-like structures, suggesting the N-terminal domain and oligomerization domain are not essential for driving IB

formation. In contrast, after deleting the C-terminal domain, the HA-P Δ CTD construct and HMPV N no longer co-localized to IB-like structures and were distributed diffusely throughout the cytosol, indicating the HMPV P C-terminal domain is the site of a molecular interaction indispensable for HMPV IB formation. We also found the presence of a C-terminal HA tag disrupted IB formation (**Fig 3.1C**), further implicating the C-terminus of HMPV P as the location of critical molecular interactions driving IB formation.

To further narrow down the specific region in the HMPV P CTD driving IB formation, we truncated P from the C-terminal end, beginning with the terminal 14 amino acids. Removal of the last 14 residues from HMPV P (Δ 281-294) prevented co-localization with HMPV N upon co-transfections, identifying these residues as key determinants of IB formation. Several C-terminal residues in RSV P are important for interaction with RSV N-RNA complexes, including F241, the last residue in the protein (148). While HMPV P does not have a C-terminal aromatic residue, there is an aromatic amino acid, Y290, which is located within the last 14 amino acids and is a potential phosphorylation site identified by in silico analysis (described below). Mutagenesis of Y290 to an alanine abolished IB formation, but IB formation was restored by the mutant Y290F (**Fig 3.1C**). These results suggest an aromatic residue at position 290 could be the site of a P interaction driving co-localization with HMPV N, and phosphorylation of Y290 is not necessary for this interaction to occur.

3.2.2 Mutagenesis of HMPV P Phosphorylation Sites

Until recently, HMPV P was termed a phosphoprotein solely due to structural and functional homology to phosphorylated proteins in other NNSVs, such as RSV P, as it had not yet been shown to be phosphorylated. A 2020 study was the first to identify several P phosphorylation sites through mass spectrometry analysis of HMPV P purified from Sf9 insect cells (112), confirming P has sites that can be phosphorylated by eukaryotic kinases outside of an active HMPV infection. However, phosphorylation is often context specific, and HMPV P could have additional phosphorylation sites or changes in phosphorylation state occurring

over the course of an infection. In order to further identify potential phosphorylation sites, we performed an in-silico analysis of the HMPV P amino acid sequence using NetPhos (167), DISPHOS (135), and PhosphoSVM (168). These phosphorylation prediction tools identified the previously confirmed phosphorylation sites, as well as additional residues with high prediction scores for phosphorylation (**Fig 3.2A**). These sites are conserved among HMPV subtypes (**Fig 3.3**).

Because phosphorylation is a PTM that often regulates biological processes, we wanted to determine if phospho-dead mutations inhibited the function of P as a polymerase cofactor during RNA synthesis. We first selected a panel of serine residues which had been identified as phosphorylation sites (112) or with high phosphorylation prediction scores (**Fig 3.2A**) and eliminated the potential for phosphorylation at these sites using site-directed mutagenesis to alanine. WT or mutant HA-P constructs were co-transfected with HMPV L, HMPV M2-1, and an HMPV minireplicon containing a luciferase reporter which can only be transcribed by a functioning HMPV polymerase complex (**Fig 3.4**). Several HA-P phospho-dead mutants had significantly reduced minireplicon activity, and the majority of these mutations were located in the C-terminal domain (**Fig 3.2B**). S266A had a minor, but significant, reduction in function, showing only 68% of WT function. S268A and S271A reduced minireplicon activity to background signal observed without P. The S171A and S184A mutations were also detrimental to polymerase function as measured by the minireplicon assay, but due to the location of these residues in the P oligomerization domain we excluded them from further study to avoid possible confounding factors such as structural destabilization. Taken together, these results suggest the P C-terminal domain is not only important for IB formation but contains specific potentially phosphorylated residues which play a critical role in facilitating RNA synthesis.

In addition to serine residues, the P CTD contains a threonine (T267) and tyrosine (Y290) residue with high phosphorylation prediction scores (**Fig 3.2A**), so alanine mutations at these sites were also generated. In order to mimic a

permanently phosphorylated serine or threonine residue phosphorylation studies traditionally use glutamic acid or aspartic acid mutations, so these phosphomimetic mutants were created for S266, T267, S268, and S271. Because there is not a phosphomimetic amino acid for tyrosine, we instead used Y290F to determine if removing the phosphorylation site while retaining an aromatic amino acid would affect minireplicon activity. Strikingly, the ability of P phosphomimetic mutants to rescue minireplicon activity decreased sequentially as each residue became more C-terminal (**Fig 3.2C**). The only phosphomimetic mutant capable of rescuing minireplicon activity to WT levels was S266E, suggesting that a negative charge at this site allows HMPV P to function efficiently as a polymerase cofactor. While T267D reduces P cofactor efficiency to 30% of WT, it is still significantly higher than the negative control, suggesting a slight rescue of P function compared to T267A. Both phospho-dead and phosphomimetic mutations at S268 and S271 significantly decreased the function of the HMPV polymerase complex to levels equivalent to the negative control, suggesting permanent changes to the charge at these residues inhibits the role of P as a polymerase cofactor.

The inability of some P phosphomimetic mutants to rescue minireplicon activity may indicate a need for multiple populations of P in varying states of phosphorylation throughout the process of RNA synthesis. However, co-transfections of both the phospho-dead and phosphomimetic mutant for each phosphorylation site (ex. T267A co-transfected with T267D) failed to rescue minireplicon activity (**Fig 3.5**). The inhibition of minireplicon activity is not due to changes in protein stability or expression, as western blot analysis of cell lysates from the minireplicon assay showed all P mutants were expressed to levels that were not significantly different from WT levels (**Fig 3.2D-E**).

The cofactor function of Y290A was also significantly reduced in the minireplicon assay, but Y290F was not significantly different from WT (**Fig 3.2C**). These results parallel the ability of each mutant to form IBs (**Fig 3.1C**). Optimal HMPV RNA synthesis has been previously shown to correlate with proper formation of IBs (108), so we screened the serine and threonine P mutants for IB

formation by co-transfecting individual mutants with HMPV N. All mutants were able to co-localize with HMPV N into IB-like structures (**Fig 3.6**). This result suggests there are interactions contributing to a functional HMPV polymerase complex that are different from the interactions driving IB formation.

3.2.3 Examining P-specific Interactions of Phosphorylation Mutants

To determine if P mutations are altering P/N interactions required for replication, we utilized a nanobody specific to HMPV P to perform a co-immunoprecipitation assay. Mutant or WT HMPV P was co-transfected with HMPV N in 293T cells, then P was immunoprecipitated using DynaBeads chemically coupled to an HMPV P nanobody. P and any co-immunoprecipitated N were eluted from the beads and quantified by western blot (**Fig 3.7**). For mutations to serine or threonine residues, there was no significant difference between the WT and the P mutants in the ability to co-IP N (**Fig 3.7B**), suggesting these mutations are not significantly altering P/N interactions. There was a significant decrease in the ability of Y290A, but not Y290F, to co-IP HMPV N, which corroborates a recent report suggesting this residue is critical for HMPV P to interact with the HMPV nucleocapsid (149).

Rather than the P/N interaction, the phosphorylation site mutations could be altering interactions with other binding partners important for the HMPV polymerase complex to function. The interaction between P and other components of the polymerase complex are likely important for the function of the complex, but the P mutations being examined are outside the characterized binding domains for both L and M2-1 (80, 112, 144). Alternative to interactions with components of the polymerase complex, these P mutations could be altering the binding of P to other constituents within IBs. To test for changes in P diffusion within IBs, which would be affected by changes in P-specific interactions, mCherry-P mutants were co-transfected with HMPV N to form fluorescent IBs and fluorescence recovery after photobleaching (FRAP) of whole IBs was performed with a 4.5 min recovery period. The recovery of an mCherry signal to a bleached IB is dependent on P-

specific interactions influencing its ability to diffuse inside the IB and exchange with unbleached mCherry-P outside the IB.

For each mCherry-P construct, the average recovery of all IBs was graphed and fit to a two-phase exponential association model (**Fig 3.8**). This model is used when the overall behavior of a population is dependent on a slow component and a fast component, each with a different Y_{max} and K constant. In the context of this experiment, the slow and fast components would be subpopulations of P within an IB with varying rates of diffusion and exchange with cytosolic P. The four parameters defining the best fit non-linear regression were compared between each P mutant and its corresponding WT control (**Fig 3.9**). Remarkably, S266E was the only mutation which had no significant differences to WT parameters. All other mutants had at least one parameter that was significantly different than WT, resulting in an altered recovery. The recovery of the fast population of S266A (Y_{max2}) was lower than WT, while the recovery of the slow population (Y_{max1}) was higher. T267A recovered less (Y_{max1} and Y_{max2}) than WT but had a higher rate constant for the fast population ($K2$), while T267D had similar kinetics but altered recovery (Y_{max1} and Y_{max2}) compared to WT. The S268 and S271 mutants all had similar rates of recovery as WT, but had a higher recovery for the slow population (Y_{max1}). These results suggest phospho-dead or phosphomimetic P mutations can modulate interactions contributing to diffusion and mobility in IBs, with a phosphomimetic at S266 facilitating WT-like P dynamics. The changes in binding partners and mobility of P due to the other mutations could be a factor contributing to the reduced function of the polymerase complex in the minireplicon assay.

3.2.4 Production of Recombinant HMPV Encoding P Mutations

Mutagenesis of some RSV P phosphorylation sites has been reported to be detrimental for RNA synthesis (151) but does not significantly impact growth of a recombinant virus (152). To determine if mutating P phosphorylation sites in the HMPV genome results in a viral phenotype that parallels the minireplicon assay, we utilized an HMPV rescue system provided by Dr. Makoto Takeda (National

Institute of Infectious Diseases, Tokyo, Japan) (158). Triplicate attempts were made to rescue 10 different recombinant mutants of HMPV, each containing either a phospho-dead or phosphomimetic mutation at one potential phosphorylation site. Interestingly, the ability of each P mutant to generate an infectious recombinant virus was similar to the corresponding minireplicon activity for majority of the mutations. Out of three triplicate rescue attempts, HMPV WT and S266E were rescued three times, T267D was rescued twice, and S266A had observable infection but appeared highly attenuated (**Fig 3.10**). All other mutations could not be rescued. These results confirm that mutations to these P phosphorylation sites which severely inhibit minireplicon activity also result in a protein incapable of supporting an HMPV infection. Unexpectedly, the Y290F mutation functions similarly to WT P in the minireplicon assay, but a virus with this mutation could not be rescued, indicating HMPV P may have another critical role during infection outside its role in IB formation and function as a viral cofactor.

3.3 Discussion

Formation of cytoplasmic liquid-like replication centers is a hallmark of many NNSVs (122). NNSV phosphoproteins are oligomeric polymerase cofactors with regions of intrinsic structural disorder (169) and are repeatedly reported as a necessary component of NNSV IBs (107, 123, 127, 143, 162, 163). Despite these similarities, the size, sequence, and structural features are taxonomically divergent (170), necessitating detailed investigation at a species level to understand how these proteins promote viral infection. HMPV IBs are sites of efficient RNA synthesis which coalesce in an actin-dependent process and have been observed inside intercellular extensions, potentially acting as immune-evasive vehicles for direct cell-to-cell transmission of viral ribonucleoprotein complexes without the need for budding (108, 117, 120). However, work detailing drivers and regulators of HMPV IBs is limited. Our work expands upon this growing field, identifying the HMPV P CTD as a primary interaction site for driving the formation of HMPV IBs and revealing the role of P phosphorylation as a potential regulator of RNA synthesis and IB dynamics.

3.3.1 Minimal P Sequences Driving IB Formation

We examined three HMPV P domains and found only the CTD was absolutely required to allow co-localization with N into IB-like structures, while either the NTD or OD, but not both, were dismissible. Alanine mutagenesis of one residue within the P CTD, Y290, completely abolished IB formation, inhibited the function of the HMPV polymerase complex, and reduced P/N interactions as quantified through co-IP assays. While P is rich in charged amino acids, and phase separation often involves electrostatic interactions, we found that Y290F functioned similarly to WT P, implicating a π -interaction with HMPV N as important for HMPV IB formation. This data corroborates biochemical and molecular modeling studies showing the very C-terminal residues of RSV and HMPV P are involved in binding N-RNA, potentially through insertion of the P CTD into a pocket on N (149, 171-173). Phosphoproteins of RSV (*Pneumoviridae*), measles virus (*Paramyxoviridae*), and rabies virus (*Rhabdoviridae*) have previously been shown to require the CTD but not the NTD in order to facilitate IB formation (127, 165, 174). To our knowledge, we are the first to show that the HMPV P NTD, which binds monomeric N, was similarly dispensable for IB formation. These consistencies among P domain studies suggest the structural organization of some NNSV phosphoproteins have a functional conservation in which the interaction between the P NTD and monomeric N is not a driver of IB formation, while the ability of the P CTD to bind N-RNA is critical for this process. However, it remains unknown if, and in what capacity, alternative interactions between P, N, and/or host proteins may also contribute to the formation of these viral replication centers.

Interestingly, the reported function of P oligomerization for IB formation varies between NNSVs, even within viral families. Among the Rhabdoviridae, VSV recombinant virus with a P OD deletion was rescued and could still form IBs (175), while Rabies virus IB formation minimally requires the P dimerization domain connected through a flexible linker to the C-terminal N binding region (127). We found that removal of the HMPV P OD does not prevent co-localization with N into IB-like structures, meaning HMPV P/P interactions through tetramerization are not

a primary driver of IB formation. This is surprising, considering purified HMPV P can phase separate in the absence of N (126), presumably through P/P interactions. This data on HMPV P is in contrast to RSV P, which cannot phase separate in a purified droplet assay (126, 149) and, similarly to Rabies virus P, requires a minimum of the OD separated by a flexible linker to the C-terminal nucleocapsid binding domain in order to form cellular IBs with N (165). The stark difference in IB-driving domains between pneumovirus phosphoproteins could be linked to slight differences in their amino acid sequences. HMPV and RSV P have sequence and structural homology within conserved domains, such as the OD and the binding site for monomeric N (144). However, HMPV P is slightly longer (294 aa compared to 241 aa), containing amino acid stretches in both the N- and C-terminal IDRs that are absent in RSV P (126, 144, 170). The HMPV P C-terminal insertion contains a glutamic acid rich acidic patch, which could provide a minimal set of electrostatic interactions with other P monomers or other secondary binding partners to facilitate a phase transition in the absence of the OD.

It is important to note we could not determine if the HMPV P CTD was capable of driving IB formation in the complete absence of other P domains, as the HA-P CTD construct was poorly detected via immunofluorescence. Phase separation is sensitive to protein concentration, and the disordered CTD of HMPV P may be unstable in the absence of other components of the protein, preventing the molecular interactions driving IB formation from passing a theoretical threshold. Alternatively, like RSV P (165), HMPV P could require binding partners at the CTD and at least one additional site in order to initiate IB formation. In this scenario our data would suggest that, unlike RSV P, the secondary binding site may occur at either the P NTD or the P OD in order for molecular interactions to reach the threshold for IB formation. Importantly, these results compiled with other studies demonstrate that HMPV and RSV may have fundamental differences in the mechanisms underlying conserved processes of infection.

3.3.2 The Function of HMPV P Phosphorylation

Phosphorylation sites have been identified in many NNSV phosphoproteins, although the roles this PTM plays in IB formation and RNA synthesis has been largely contested and may not have a single conserved function (127, 140, 176-179). Mutagenesis of P phosphorylation sites which reduce the function of viral polymerase complexes in minireplicon assays does not necessarily result in reduced infection in recombinant viruses containing the same mutations. RSV P has two clusters of phosphorylation sites: an N-terminal cluster which has been reported to have a minor contribution to overall P phosphorylation state (180) but inhibits minireplicon activity upon mutagenesis to phosphomimetics (152), and a C-terminal cluster containing the major phosphorylation sites of unclear function (180). Reports of RSV P phosphorylation regulating RNA synthesis have been contradictory in purified and reporter assays (151, 152), although the C-terminal phosphorylation sites were shown to be dispensable for viral infection (152). The potential inhibitory effect of P phosphomimetic mutations on recombinant RSV infection was not investigated (152).

In contrast to RSV P, we identified serine and threonine residues in HMPV P in which alanine mutations significantly inhibit reporter assays and are indispensable for viral infection. These residues are located immediately outside the solvable structure of the recently identified HMPV P/L binding domain (112), meaning this region of P is likely uninvolved in direct P/L interactions, although mutations at these residues could affect the structure of the nearby regions which do interact with L. Importantly, the residue closest to the P/L domain, S266, behaves like WT P in our assays when mutated to a phosphomimetic, suggesting phosphorylation at this site may regulate the function of the HMPV polymerase complex. The residues sequentially following S266 become increasingly more sensitive to both phospho-dead and phosphomimetic mutations, resulting in a detrimental reduction in function in both minireplicon and viral rescue assays. Despite the location of these four examined residues in a disordered domain, the chronological effect of mutagenesis on P function might suggest they are located

in or are approaching a region which undergoes transient structural conformations upon interaction with an important binding partner. Mutagenesis could be changing binding affinities by interfering in a disorder-to-order transition (181). However, these residues are located within a highly acidic patch of amino acids, and S271 has previously been shown to be phosphorylated (112), making the dramatic reduction in function of S268E and S271E puzzling.

These intriguing results may simply reflect the imperfect nature of phosphomimetics, which cannot mimic the transience and reversibility of phosphorylation as a regulatory PTM. Our attempts to co-transfect P mutants representing both phosphorylation states failed to increase polymerase complex function to WT P levels, supporting the idea that cyclic phosphorylation and dephosphorylation may regulate P function at S268 and S271. Alternatively, given the close proximity of the examined residues, mutagenesis at one residue could be altering the affinity of kinases or phosphatases for other phosphorylation sites. For example, a phosphoprotein of hepatitis C virus, NS5A, was found to be serially phosphorylated at multiple residues by casein kinase 1 (CK1) (182, 183). This CK1 phosphorylation cascade required the priming of an upstream residue with a phosphate, and priming could not be mimicked through glutamic acid mutation, exemplifying a potential confounding factor which may interfere in proper interpretation of our results.

Additionally, how our findings relate to the unique asymmetrical conformation of P within the polymerase complex must also be considered: each P subunit adopts a different conformation within the tetramer upon contact with the polymerase (112), with the CTD of one P subunit diverging from the other three, similar to a hand holding a cup. It remains unknown if this conformational asymmetry corresponds to a delegation of functions to each P subunit, but it would be logical to hypothesize mutagenesis might individually impact each P subunit in a different way depending on its positioning within the P tetramer or the polymerase complex itself. HMPV P could also be present in multiple subpopulations with various phosphorylation states, each of which could result in

a different function during infection. This is reflected in our Y290F mutant, which functions like WT P in a minireplicon assay but, like Y290A, is unable to facilitate production of infectious viral particles. Phosphorylation of this residue may not be involved in RNA synthesis, but might impact alternative P functions in successive steps of infection such as assembly.

Viral IBs have only recently been proposed to be liquid-like condensates, so studies examining the effect of P phosphorylation on NNSV IB properties is highly limited. Phosphorylation of MeV P was found to inhibit RNA synthesis (176) while dephosphorylation was implicated in the inhibition of IB fusion (140), suggesting MeV P phosphorylation can regulate both IB properties and RNA synthesis. For HMPV, formation and maturation of IBs through an actin-dependent process is correlated with optimal transcription and replication (108). FRAP analysis of our HMPV P phosphorylation mutants have revealed a potential role for P phosphorylation in regulating P-specific interactions affecting P mobility and turnover within these IBs, which correlate to their reduced function in a minireplicon assay. The location of these mutations is outside the characterized M2-1 and L binding domains (80, 112), and we found no significant difference in their ability to interact with N, suggesting that this region of P may be important for interacting with a crucial host protein recruited to IBs during replication. Importantly, S266E was the only mutant which consistently functioned like WT in all assays and displayed WT-like behavior during FRAP analysis. This residue has not been previously identified as a phosphorylation site, but our data demonstrates altering the charge at S266 could be a regulatory mechanism to modulate P function. Thus, we have identified a novel relationship between HMPV P phosphorylation state, IB properties, RNA synthesis, and viral infection, but further mechanistic studies will be required to determine how the connection between these critical processes might regulate the progression of an HMPV infection.

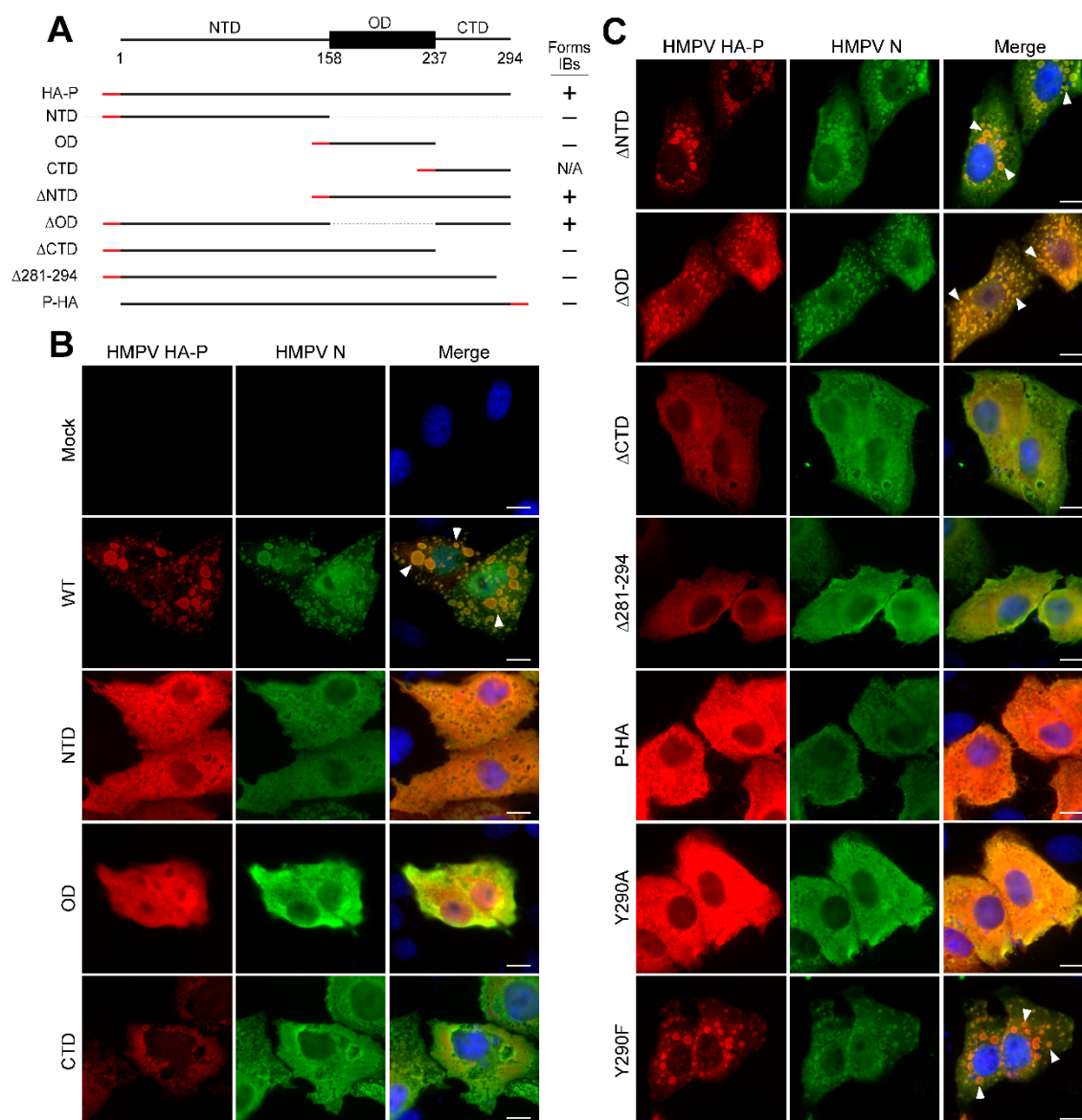


Figure 3.1 Domains of HMPV P involved in IB formation

A) Schematic of HMPV P domains (top: NTD, N-terminal domain; OD, oligomerization domain; CTD, C-terminal domain), HA-tagged domain constructs (HA tag location represented by a red line), and the constructs' ability to co-localize with HMPV N to form IBs (right column). **B,C)** HMPV HA-P WT or HA-tagged P construct were co-transfected with HMPV N in Vero cells. Cells were labeled with antibodies for anti-HA (detecting P, red) and anti-N (green), and nuclei were stained with DAPI (blue). IB formation was determined through fluorescence microscopy with a Nikon Ti2 inverted microscope with a 100x objective. Examples of IBs are indicated by white arrows. Scale bar represents 10 μ m. Representative images were selected from triplicate experiments.

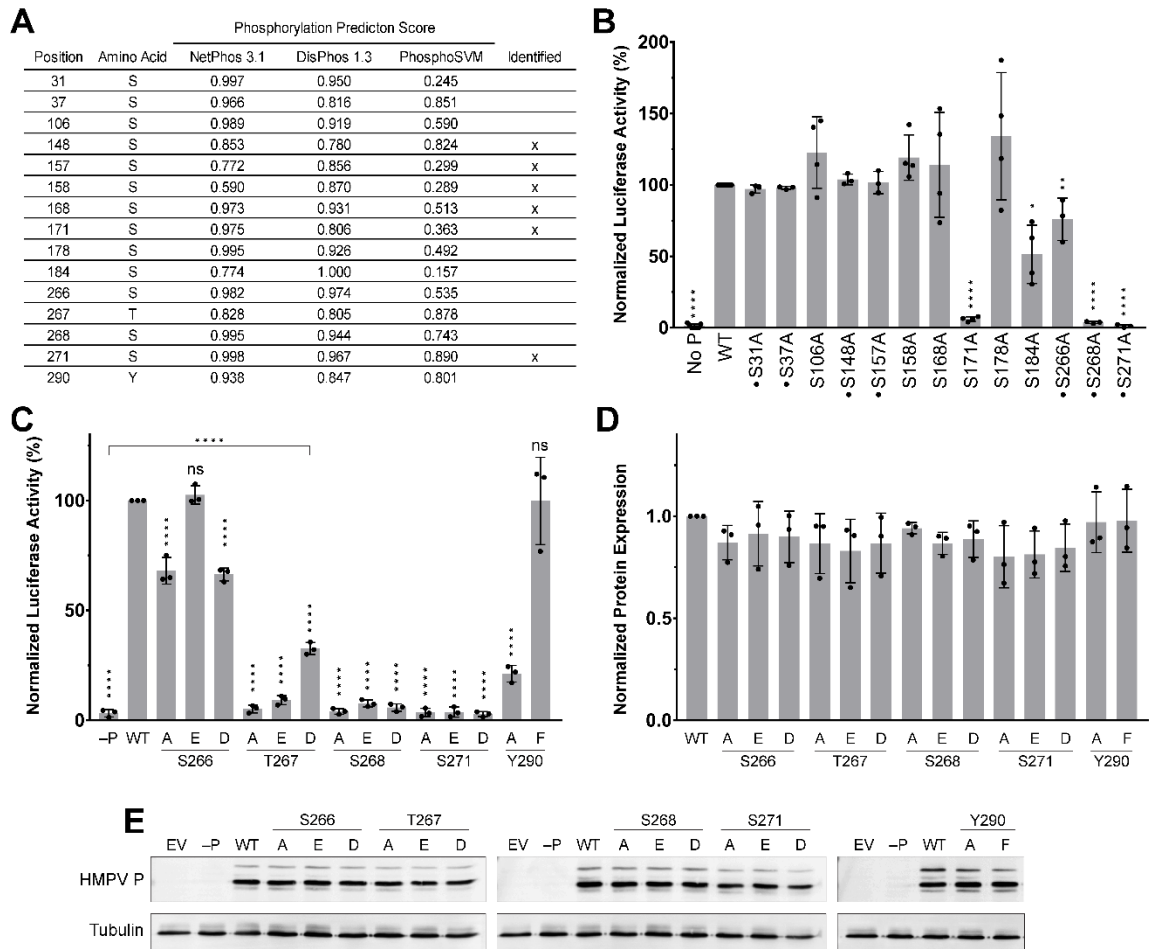


Figure 3.2 The effect of phosphorylation site mutagenesis on HMPV P function

A) Summary of investigated P phosphorylation sites. The sequence of P from strain CAN97-83 was analyzed using phosphorylation prediction sites. Prediction scores for selected residues are listed on a 0-1 scale, and phosphorylated sites that have been identified (112) are indicated in the last column. **B)** BSR T7/5 cells were transfected with an HMPV minireplicon system with WT HA-P or HA-P serine-to-alanine mutants and assayed for expression of the luciferase reporter as a measure of luminescence. **C)** The minireplicon assay was repeated using phosphodead and phosphomimetic mutations of C-terminal phosphorylation sites. P mutant expression was confirmed through western blot (**E**) and quantified (**D**). All experiments were completed in at least triplicate, and mutant values were normalized to WT. Statistical analysis for B-D was completed using one-way ANOVAs with a Dunnett's multiple comparison test. * $p < 0.05$, ** $p < 0.005$, *** $p < 0.0005$, **** $p < 0.0001$. Error bars represent one standard deviation.

| | | | |
|------------------|-----|--|-----|
| HMPV_CAN99-81_A1 | 1 | MSFPEGKDILFMGNEAAKLAEAFQKSLRKPSHKRSQSIIGEKVNTVSETL | 50 |
| HMPV_CAN97-83_A2 | 1 | MSFPEGKDILFMGNEAAKLAEAFQKSLRKPSHKRSQSIIGEKVNTVSETL | 50 |
| HMPV_CAN97-82_B1 | 1 | MSFPEGKDILFMGNEAAKIAEAFQKSLKKS GHKRTQSI VGEKVNTISETL | 50 |
| HMPV_NL_94_01_B2 | 1 | MSFPEGKDILFMGNEAAKIAEAFQKSLKKS GHKRTQSI VGEKVNTISETL | 50 |
| HMPV_JPS02-76 | 1 | MSFPEGKDILFMGNEAAKIAEAFQKSLKKS GHKRTQSI VGEKVNTISETL | 50 |
| HMPV_CAN99-81_A1 | 51 | ELPTISRPAKPTILSEPCLAWTDKGGAIKTEIKQAIKVM DPI EEEEESTEK | 100 |
| HMPV_CAN97-83_A2 | 51 | ELPTISRPTKPTILSEPCLAWTDKGGAIKTEAKQTIKVM DPI EEEEEFTEK | 100 |
| HMPV_CAN97-82_B1 | 51 | ELPTISKPARSSTLLEPKLAWADNSGITKITEK PATKT TDPV EEEEEFSEK | 100 |
| HMPV_NL_94_01_B2 | 51 | ELPTISKPARSSTLLEPKLAWADSSGATKTTEKQT TKT TDPV EEEEELNEK | 100 |
| HMPV_JPS02-76 | 51 | ELPTISKPARSSTLLEPKLAWADNSGITKITEK PATKT TDPV EEEEEFNEK | 100 |
| HMPV_CAN99-81_A1 | 101 | KVLPSSDGKTPAEKKLKPSNTNTKKKVSFTPNEPGKYTKLEKDALD LLS DN | 150 |
| HMPV_CAN97-83_A2 | 101 | RVLPSSDGKTPAEKKLKPSNTNTKKKVSFTPNEPGKYTKLEKDALD LLS DN | 150 |
| HMPV_CAN97-82_B1 | 101 | KVLPSSDGKTPAEKKSKVSTSVKKKVSFTSNEPGKYTKLEKDALD LLS DN | 150 |
| HMPV_NL_94_01_B2 | 101 | KVSPSSDGKTPAEKKSKSPNTNVKKKVSFTSNEPGKYTKLEKDALD LLS DN | 150 |
| HMPV_JPS02-76 | 101 | KVLPSSDGKTPAEKKSKFSTSVKKKVSFTSNEPGKYTKLEKDALD LLS DN | 150 |
| HMPV_CAN99-81_A1 | 151 | EEEDAESSILTFEERDTSLSIEARLESIEEKL SMILG LLRTLN IATAGP | 200 |
| HMPV_CAN97-83_A2 | 151 | EEEDAESSILTFEERDTSLSIEARLESIEEKL SMILG LLRTLN IATAGP | 200 |
| HMPV_CAN97-82_B1 | 151 | EEEDAESSILTFEERDTSLSIEARLESIEEKL SMILG LLRTLN IATAGP | 200 |
| HMPV_NL_94_01_B2 | 151 | EEEDAESSILTFEERDTSLSIEARLESIEEKL SMILG LLRTLN IATAGP | 200 |
| HMPV_JPS02-76 | 151 | EEEDAESSILTFEERDTSLSIEARLESIEEKL SMILG LLRTLN IATAGP | 200 |
| HMPV_CAN99-81_A1 | 201 | ATARDGIRDAMIGVREELIADI I KEAKGKAAEMMEEE MSQR SKI GNGSVK | 250 |
| HMPV_CAN97-83_A2 | 201 | TAARDGIRDAMIGIREELIADI I KEAKGKAAEMMEEE MNQR T KI GNGSVK | 250 |
| HMPV_CAN97-82_B1 | 201 | TAARDGIRDAMIGIREELIAEI I KEAKGKAAEMMEEE MNQR SKI GNGSVK | 250 |
| HMPV_NL_94_01_B2 | 201 | TAARDGIRDAMIGIREELIAEI I KEAKGKAAEMMEEE MNQR SKI GNGSVK | 250 |
| HMPV_JPS02-76 | 201 | TAARDGIRDAMIGIREELIAEI I KEAKGKAAEMMEEE MNQR SKI GNGSVK | 250 |
| HMPV_CAN99-81_A1 | 251 | LTEKAKELNKIVEDESTSGESEEEEEEPKD IQD NSQ EDDIYQLIM | 294 |
| HMPV_CAN97-83_A2 | 251 | LTEKAKELNKIVEDESTSGESEEEEEELKDTQENNQ EDDIYQLIM | 294 |
| HMPV_CAN97-82_B1 | 251 | LTEKAKELNKIVEDESTSGESEEEEEEPKETQD NSQ GED IYQLIM | 294 |
| HMPV_NL_94_01_B2 | 251 | LTEKAKELNKIVEDESTSGESEEEEEEPKETQD NNQ GED IYQLIM | 294 |
| HMPV_JPS02-76 | 251 | LTEKAKELNKIVEDESTSGESEEEEEEPKETQD NNQ GED IYQLIM | 294 |

Figure 3.3 Phosphoprotein sequence homology among strains of HMPV

A representative strain was selected for each subtype of HMPV: A1, CAN99-81; A2, CAN97-83 (used in our study); B1, CAN97-82; B2, NL/94/01. The strain used in our recombinant virus rescue system, JPS02-76, was also included. All chosen phosphoprotein sequences were aligned using PROMALS3D (154) and visualized using Jalview (155). Residues are colored by percent conservation among all five sequences, although some non-conserved residues may be conserved among subfamilies A or B. The blue box indicates the alpha helical tetramerization domain, and blue dashed lines indicate the boundary of the oligomerization domain utilized in our study, containing additional residues that may stabilize the tetrameric core (144). Red boxes are located around the disordered sequences unique to HMPV P (see Figure 1.6), and the presence of conserved runs within these domains may hint at an unknown conserved function. Black lines are located above single residues that were mutated in our study. While S31 appears to be subtype specific, all other investigated residues are highly conserved among HMPV strains.

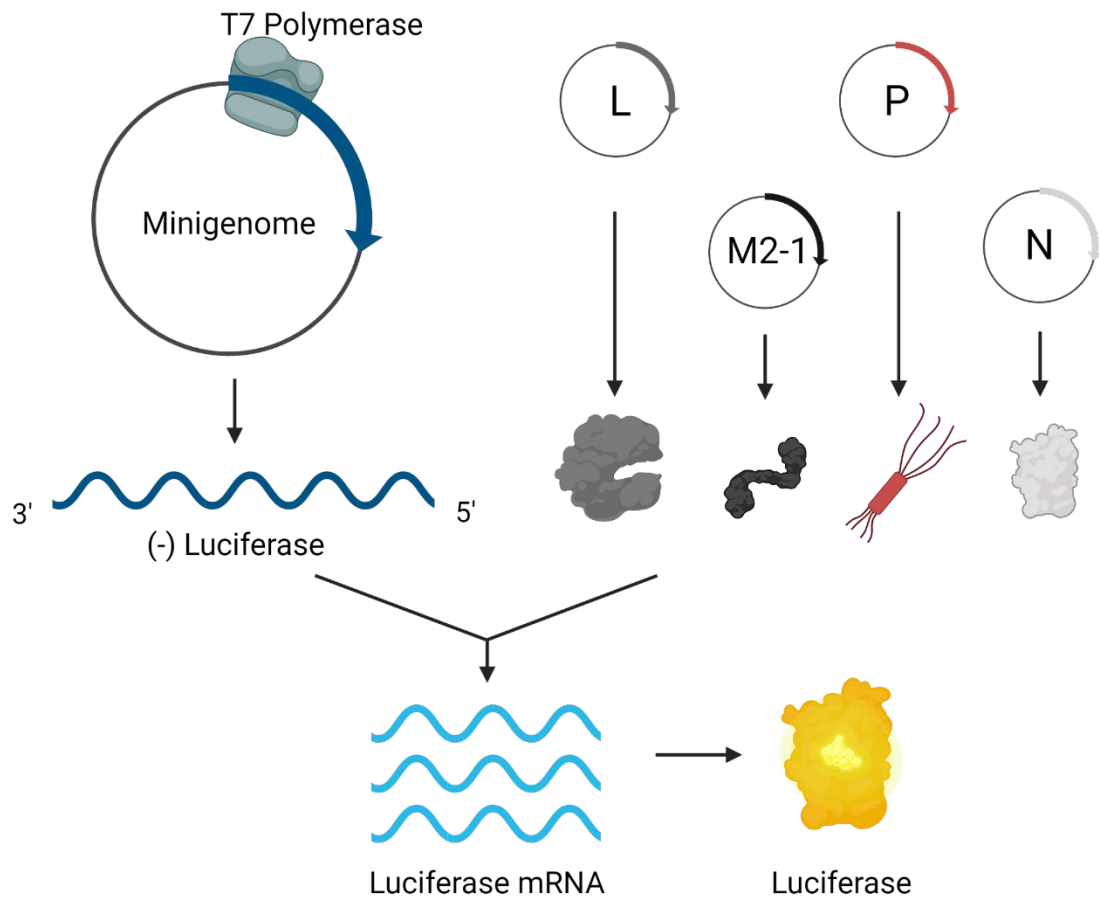


Figure 3.4 The HMPV minireplicon system

This assay relies on the ability of HMPV L to utilize a negative-sense RNA template to synthesize RNA. Cellular transcription of the minigenome plasmid is under the control of a T7 polymerase promoter, and transfection of the plasmid in BSR T7/5 cells results in a negative-sense RNA transcript that cannot be translated. This RNA transcript contains an antisense luciferase gene flanked by non-coding HMPV genomic sequences that can be recognized by HMPV L. Upon co-transfection of the minigenome with plasmids encoding the viral RNA synthesis machinery, the expressed HMPV polymerase complex will both replicate and transcribe the negative-sense minigenome transcript, resulting in luciferase mRNA. Inhibition or disruption of the polymerase complex is reported as a decrease in luciferase expression, measured through quantification of luciferase activity. Image was created with BioRender.

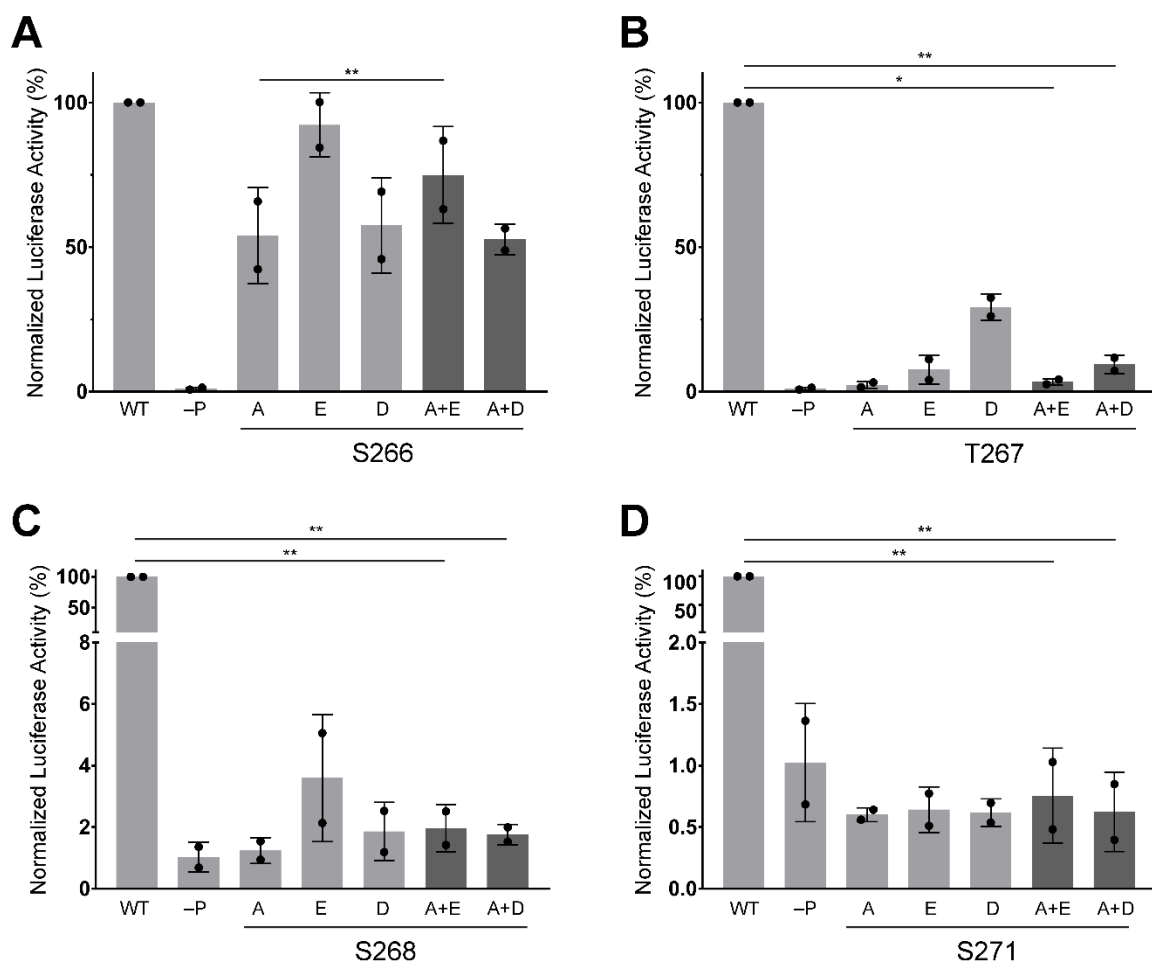


Figure 3.5 Co-transfection of HA-P phosphorylation mutants

A phosphomimetic and a phospho-dead P mutant for residues S266 (**A**), T267 (**B**), S268 (**C**), or S271 (**D**) were transfected alone or co-transfected together, along with the minireplicon system. All data is normalized to WT P. Co-transfections are in dark gray. Breaks were made in the Y axis in **C** and **D** to increase visibility of the data. Experiment was done in duplicate and analyzed using a paired T-test. * $p < 0.05$, ** $p < 0.01$. Error bars represent standard error.

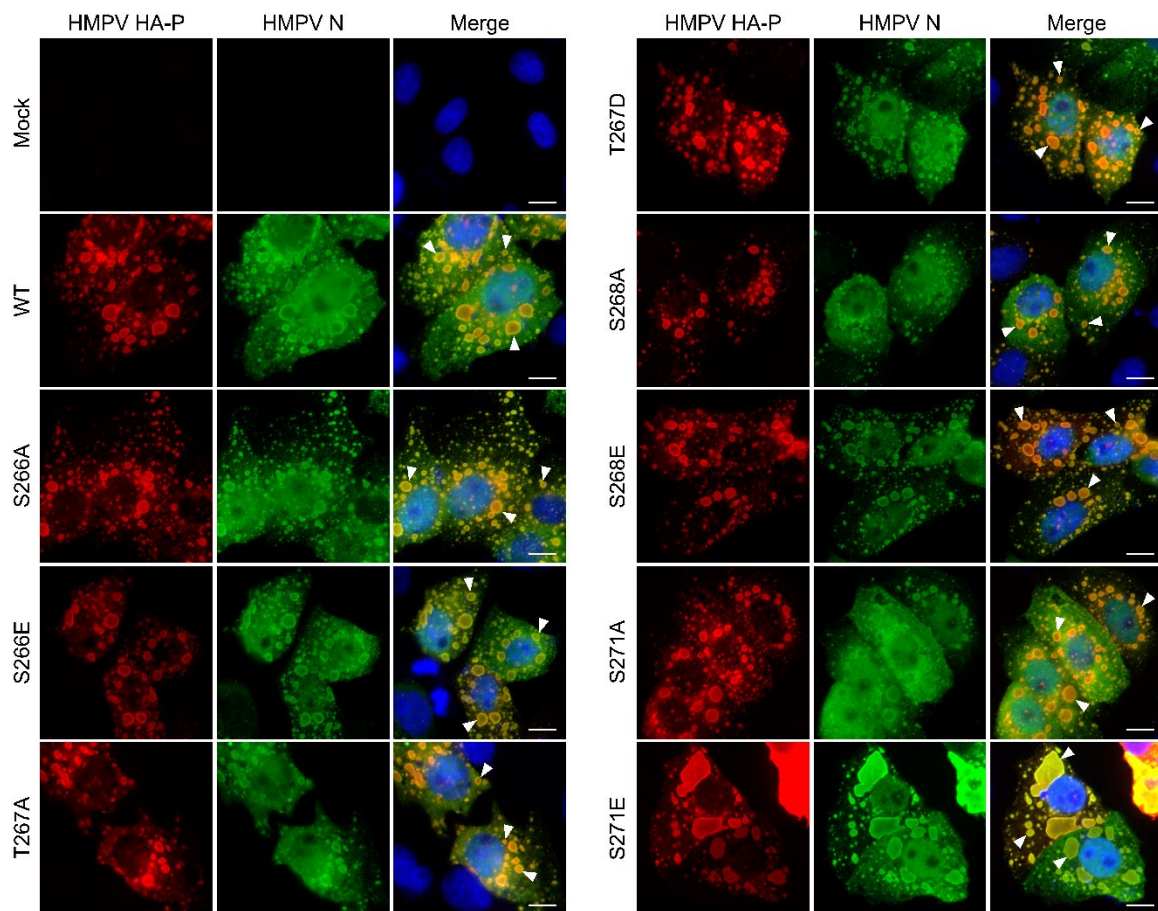


Figure 3.6 IB formation of HMPV HA-P phosphorylation site mutants

Vero cells were co-transfected with HMPV N and HMPV HA-P WT or HA-P mutant. IBs were detected using antibodies for anti-HA (red) and anti-N (green), and nuclei were stained using DAPI (blue). IB formation was determined through fluorescence microscopy with a Nikon Ti2 inverted microscope with a 100x objective. Examples of IBs are indicated by white arrows. Scale bar represents 10 μ m. Representative images were selected from duplicate experiments.

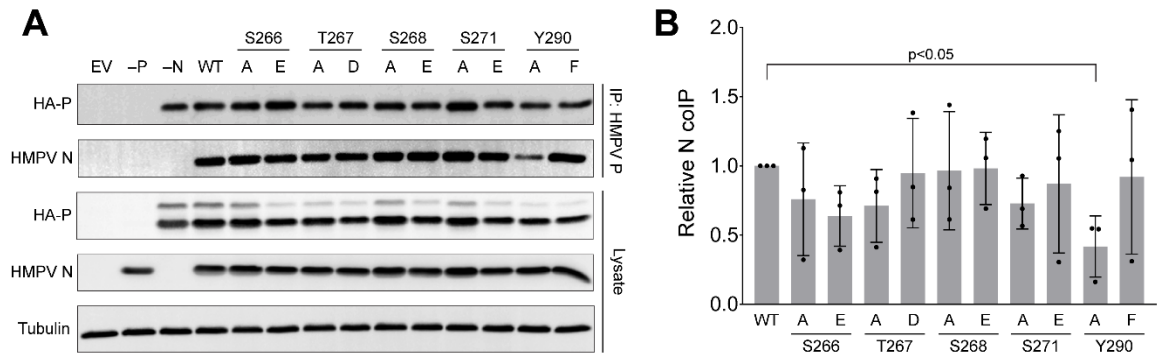


Figure 3.7 Co-immunoprecipitation of N and HA-P mutants

A) HEK 293T cells were co-transfected with HMPV N and HA-P construct. HA-P WT and mutants were immunoprecipitated using DynaBeads chemically coupled to a nanobody specific to HMPV P. HA-P constructs and co-immunoprecipitates were eluted from the beads and separated by western blot. **B)** Western blot band intensities were quantified and normalized. N co-IP was calculated by normalizing data to both the N expression (lysate) and the immunoprecipitation of the corresponding HA-P construct. Statistical significance was determined using paired t-tests between WT and mutant conditions from triplicate experiments. Error bars represent one standard deviation.

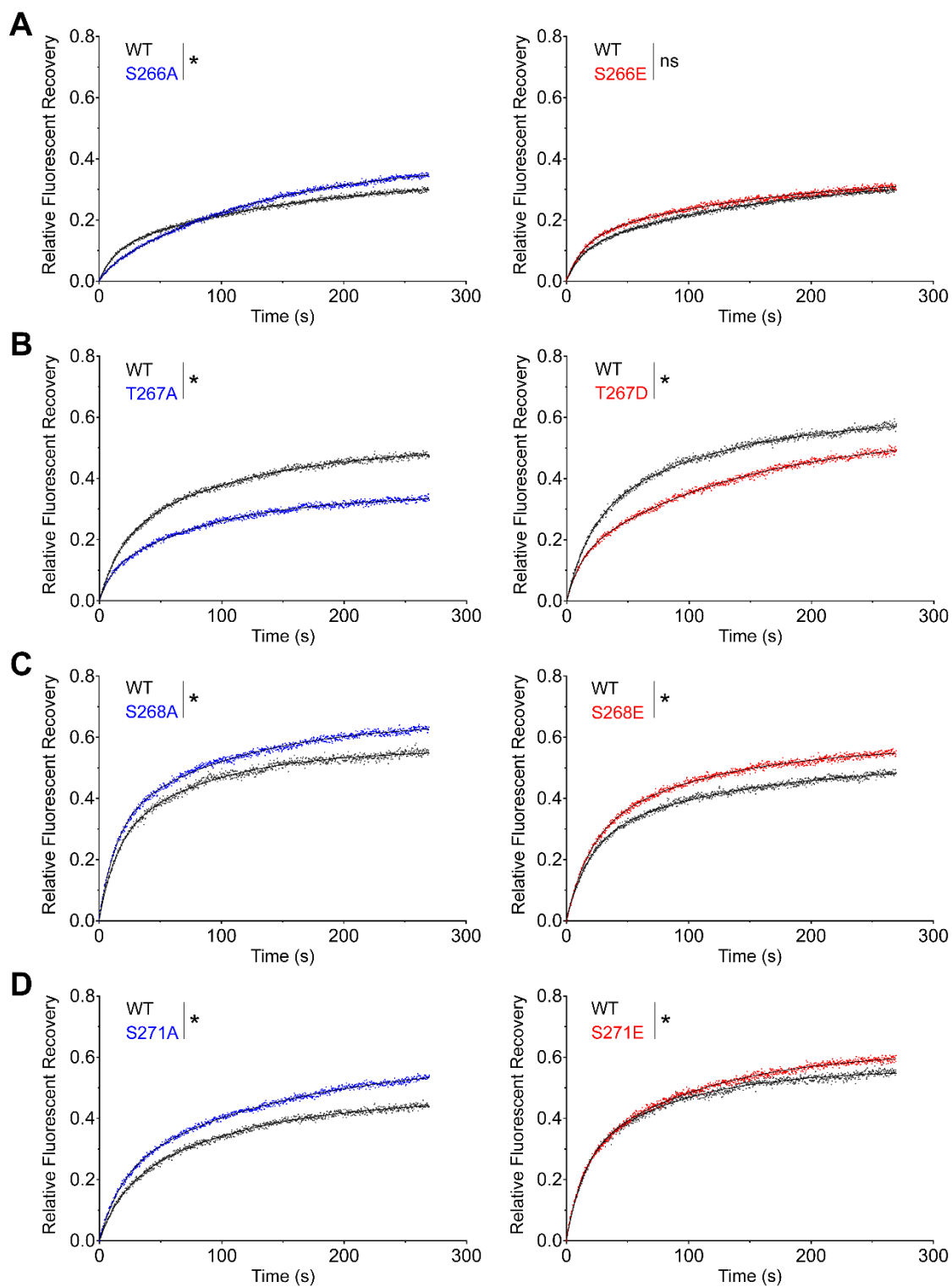


Figure 3.8 FRAP of IBs formed by mCherry-P phosphorylation site mutations

Vero cells were co-transfected with HMPV N and an mCherry-P construct to form fluorescent IBs. Individual IBs were bleached and the fluorescence recovery within the IB was followed for 4.5 min. The recovery phase of IBs formed by WT (gray), phosphodead (blue) or phosphomimetic (red) mCherry-P constructs from triplicate experiments are shown. **A)** S266 mutants; **B)** T267 mutants; **C)** S268 mutants; **D)** S271 mutants. Dots represent the average recovery at each time point, and solid lines indicate the best fit line generated by a two-phase exponential association model. Significant differences in the best fit line between WT and mutant are indicated by an asterisk. Parameters defining the best fit line for each data set can be found in Figure 3.9. Acquisition of FRAP data was completed by Kearstin Edmonds.

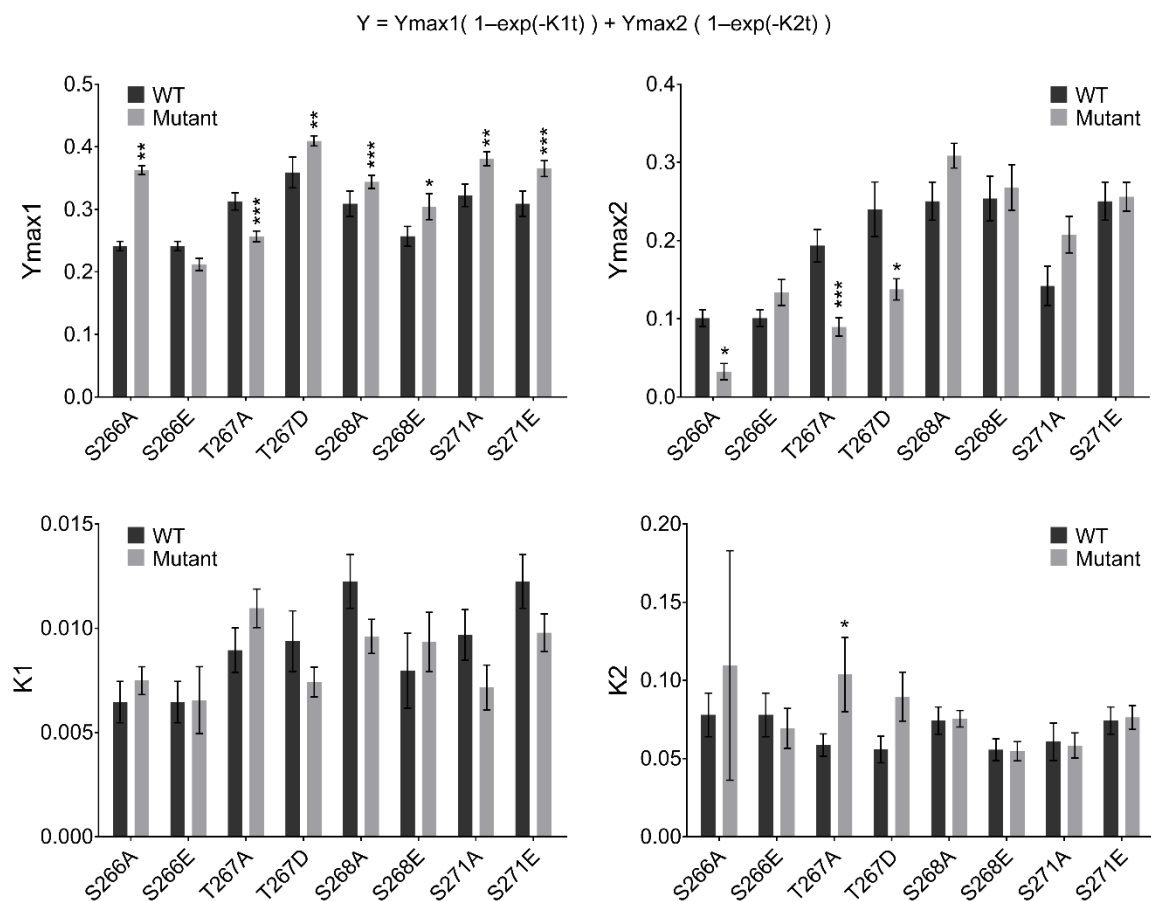


Figure 3.9 Best fit parameters of FRAP curves

Data sets from Figure 5 were fit to a two-phase exponential association model (equation; top) and analyzed for statistically significant differences in equation parameters using GraphPad Prism. Each graph shows the values of one parameter, indicated on the Y axis, for WT (dark gray) and mutant (light gray) best fit equations. Asterisks above a mutant indicate significant difference to the corresponding WT control. *p<0.05, **p<0.001, ***p<0.0001. Error bars represent standard error.

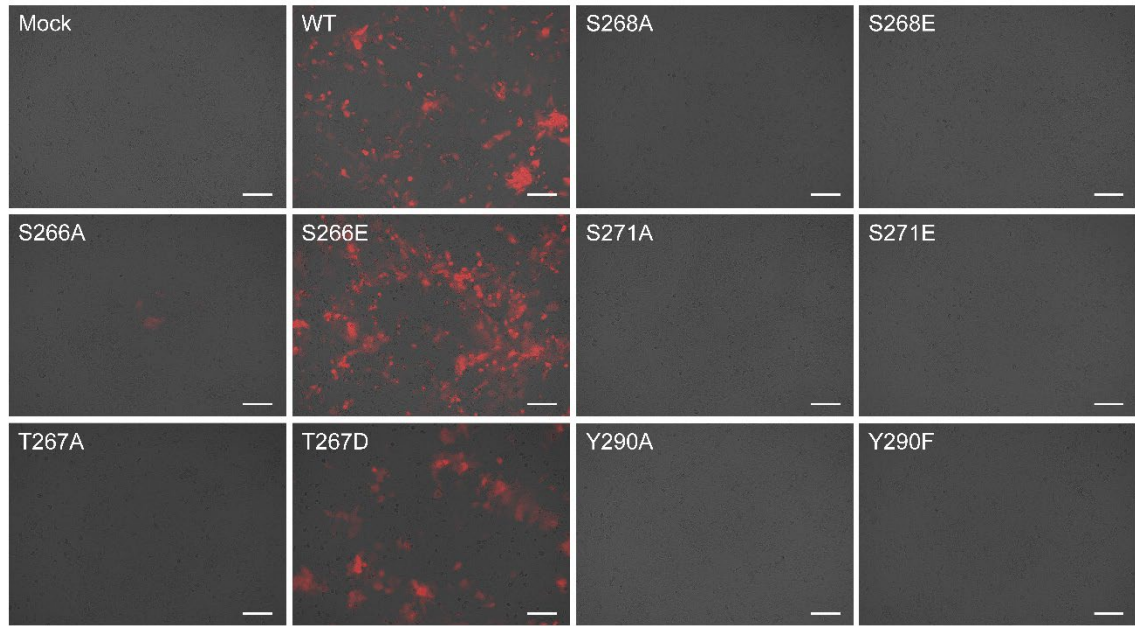


Figure 3.10 Rescue of recombinant HMPV with HA-P mutations

Genes for mCherry and the indicated HA-P constructs were cloned into the cDNA genome of HMPV JPS02-76. BSR T7/5 cells were transfected with EV, WT genome, or mutant genome along with L, N, M2-1, and WT P rescue plasmids to ensure initial production of recombinant mutants regardless of mutant P function. After 48h, cells and supernatant were collected and overlaid on Vero cells and grown until cytopathic effects began. Virus was collected and passaged once in Vero cells (P1). Shown are representative images from P1 after 10 dpi, taken using a ZOE Fluorescent Cell Imager with a 20x objective. Fluorescent images were overlaid on brightfield images using ImageJ. Scale bar represents 100 μ m.

CHAPTER 4. DISCUSSION AND FUTURE DIRECTIONS

In the past decade there has been a rapidly growing body of research investigating the role of virus-induced biomolecular condensates during infection (122, 123). Viral components of IBs have been identified for many NNSVs, and formation of these structures is closely tied to vRNA replication and successful infection. However, the viral and cellular mechanisms that connect IB formation and viral replication remain largely undefined. In this work, “inclusion body” has been used to broadly refer to NNSV replication centers with properties of biomolecular condensates, but some features of IBs have been found to be unique to specific viruses.

For example, when RABV Negri bodies first form they have properties of biomolecular condensates (127), but around 16-24 hpi they become engulfed by an ER-derived double membrane and lose their spherical shape (124). NiV infection induces two different types of IBs, and unlike most NNSVs discussed thus far, neither are associated with RNA synthesis: IBs near the nucleus non-specifically recruit over-expressed cytosolic proteins and may function as an aggresome, and square-shaped IBs near the plasma membrane contain M protein and are thought to function in assembly (184). RSV IBs have liquid-like subcompartments that temporarily store nascent mRNAs with M2-1 and host translation initiation factors (80, 106), and similar structures have been observed within Negri bodies (185). Viral IBs are often observed fusing, dividing, or moving around the cell, but the portion of the cytoskeleton utilized for this dynamic behavior varies between species. Movement of EBOV and HMPV IBs is dependent on actin polymerization (108, 186), but MeV and RABV IBs are transported using microtubules (124, 127, 140).

Many of these differences in IBs are likely a result of the unique evolutionary paths that have allowed each virus to survive as a human pathogen. Understanding and identifying which aspects of NNSV IBs are shared and which are diverged will be necessary in order to develop both broad-spectrum and specific anti-viral therapies. The work presented in Chapter 3, along with other

published studies (107, 108, 117, 119, 126, 149), have revealed important information in characterizing HMPV IBs, but there are still many questions about these structures that remain unanswered.

4.1 P-specific interactions driving IB formation

Phosphoproteins of other NNSVs appear to require multiple interactions for IBs to form, including P/N-RNA interactions at the P CTD and P/P interactions through an oligomerization domain (127, 165, 174). It is also important for these two binding domains to be separated with a flexible or disordered linker in order to provide the minimal P-specific components facilitating IB formation. We found that HMPV P has a unique set of interactions contributing to phase separation. Only the CTD of HMPV P was indispensable for the formation of IBs while tetramerization through the OD was completely dispensable *if* the NTD was still present. We were unable to determine if the CTD alone is capable of providing the minimal interactions driving phase separation with HMPV N. Attachment of mCherry or other larger tags to the CTD could help stabilize the short, disordered fragment and increase expression. Co-expression with HMPV N would then confirm if a stabilized CTD can drive IB formation in the absence of all other P domains. The same experiment could be done with just the 14 C-terminal residues (281-294), with or without a random disordered sequence separating the tag from the P fragment. This would help determine if there are multiple locations within the CTD that facilitate IB formation, if the presence of a flexible linker is required, or if the sole P determinant for phase separation are among the last 14 residues at the C-terminus.

Once the minimal P fragment driving IB formation has been identified, use of that fragment as an inhibitor could be investigated. A study on RSV found that treatment of cells with a purified P fragment could significantly inhibit infection (187). The fragment consisted of a portion of the P OD and the N-RNA binding domain, which are important for RSV IB formation. Although IBs were not investigated in the study, the RSV P fragment was likely pulled into viral IBs,

competing with full-length P for interactions between the nucleocapsid and disrupting the polymerase complex. HMPV P fragments could also be investigated as inhibitors of infection, and could have several potential mechanisms of action. A fragment containing the HMPV P NTD and the OD would not form IBs, but it has N and P binding domains that might allow the fragment to interact with IB components and dissolve the IB. Similar to RSV, a fragment of HMPV P containing the minimal domains for IB formation would likely be recruited to IBs but be replication defective. Alternatively, the same fragment containing a Y290A mutation could be tested for the ability to completely dissolve IBs if N-terminal P fragments are not effective. Stably expressing the HMPV P nanobody in cells could also be done to determine if targeting IBs with a protein that binds P would be disruptive to IB properties or viral infection. The ability to disrupt IBs or viral replication could be tested through microscopy, minireplicon assays, or during HMPV infection.

4.2 The nucleoprotein, viral RNA, and other HMPV proteins within IBs

While HMPV P can undergo LLPS when purified from *E. coli* (126) phase separation in cells is dependent on co-expression with HMPV N (107). Given the ability of N to oligomerize, bind RNA, and interact with other viral proteins, the contribution of N to IB formation must also be examined. WT N can exist in a monomeric, RNA-free form (N^0) and an oligomeric, RNA-bound form (N-RNA or the nucleocapsid) (145). N^0 interacts with the NTD of P, and our data on the P CTD corroborates a recent publication proposing the last 6 amino acids of HMPV P, including Y290 and the surrounding residues, are the binding site for N-RNA (149). Molecular modeling of the RSV and HMPV P/N-RNA interaction suggests that the P C-terminal end may insert into a pocket on the surface of the nucleocapsid to facilitate binding (149, 150, 172, 173). The RSV model was used to perform an *in silico* screen of small molecule inhibitors, and a compound was identified that competed with P for N binding and specifically inhibited RSV infection (172). Our data also suggests the P/N-RNA interaction, not P/ N^0 , is required for HMPV IB

formation, indicating the P/N-RNA binding sites could be an ideal target for developing HMPV antiviral strategies.

Presumably, N⁰ must either be present within IBs at a high amount or must be constantly recruited to IBs to encapsidate nascent genomic RNA. The effect of N⁰ on HMPV IBs has not been investigated. To differentiate the role of N⁰ and N-RNA in HMPV IBs, a permanent N⁰ mutant defective for RNA binding (126) could be co-transfected with P and analyzed via microscopy to assay for IB formation, size, and frequency. A homologous N⁰ mutant was found to be unable to form IBs in RSV (165) but was able to form WT-like IBs in MeV (140). Based on our P domain data, it would be expected that an HMPV N⁰ mutant would function similarly to RSV and not be competent for IB formation, so a tagged N⁰ construct could also be co-transfected with WT N and P. This would determine if monomeric N has the capacity to modulate IB properties or if N⁰ can still be recruited to WT IBs if it cannot oligomerize. Investigating the recruitment of N⁰ to IBs could provide interesting insights on additional mechanisms regulating IB formation and nucleocapsid assembly.

It is not known how the transition from N⁰ to N-RNA, or the presence of different viral RNAs, affect the formation or behavior of HMPV IBs. The N⁰-binding NTD of P is dispensable for phase separation for RSV (165), RABV (127), and MeV (174). We found the N⁰-binding NTD of P is also dispensable for HMPV IB formation. However, a purified HMPV N⁰ mutant defective for RNA binding was still able to be pulled into phase separated droplets by HMPV P (126), indicating N-RNA is not required for phase separation in a purified system. These conflicting results suggest the interaction between HMPV N and RNA may have an important role facilitating phase separation with P in the highly congested cellular environment. It is widely accepted that NNSV N proteins encapsidate viral genomic RNAs and do not encapsidate viral mRNA, yet N is found to non-specifically bind and oligomerize around cellular RNAs when purified from bacteria (1, 145), and the P binding site for N-RNA is critical for IB formation in our transfection studies where genomic RNA is absent. This suggests there may be a viral mechanism

directing the oligomerization of N preferentially towards genomic RNA and away from mRNAs during infection.

Although IBs produced through co-transfections of P and N are still liquid-like and dynamic, the microscopic analysis of IBs presented in Chapter 3 were not facilitating synthesis of RNA. The effect of vRNA on IB formation could be examined in several ways. Transfection of the minireplicon system with or without L, followed by immunofluorescence and FRAP, would reveal if IBs have altered size, frequency, or diffusion rates when facilitating RNA synthesis. FISH probes designed to detect the HMPV-specific sequences within the minigenome would confirm if these pseudo-vRNAs are preferentially localized to IBs. A time course analysis of each of these methods could be done in parallel to qRT-PCR analysis measuring levels of minigenome RNAs to determine if the concentration of RNA is correlated with any observable or measurable changes to the IBs. These experiments would be repeated during an HMPV infection to confirm physiological relevance. IBs that form during transfection are often highly abundant in the cell by 24 hpt, while the frequency of IBs that form during infection are maintained at lower numbers that fluctuate over time (108). The average number of IBs decreases between 3-24 hpi, then slowly increases to an average of 3 IBs per cell by 72 hpi. Comparing data from transfected and infected conditions could help identify additional factors that regulate formation of HMPV IBs.

Finally, although HMPV IBs are proposed viral replication centers, P and N are the only components of the viral polymerase complex that have been attempted to be detected within IBs. HMPV L and M2-1 lack specific antibodies that would allow easy detection through immunofluorescence, and to our knowledge no tagged versions of these proteins have been made for use in cell culture. However, tagged versions of RSV L and M2-1 localize to IBs (106), and inserting tags in the homologous locations in the HMPV proteins would easily allow their cellular location to be detected. Using these tagged proteins with the minireplicon system would determine if L or M2-1 are excluded from IBs in the presence of P mutations or during RNA synthesis.

RSV IBs were found to have even smaller liquid-like compartments inside them that contained M2-1 and nascent mRNA and excluded P, N, and L (106). Called IB-associated granules (IBAGs), these structures only formed if mRNA was being synthesized by the viral polymerase, and the dissolution of IBAGs over time was proposed to correspond to the release of stored RNA from the IB. If HMPV IBs contain IBAGs, it would be important to determine if P mutations disrupt the temporary storage or exportation of mRNA from the inclusion. Rather than disrupting RNA synthesis, P mutations may disrupt IBAG formation or behavior, preventing mRNAs from entering the cytosol and resulting in decreased expression of the minigenome reporter.

4.3 Mechanisms controlling characteristics of IBs

FRAP analysis of MeV infection found that the liquid-like properties of IBs depended on size, with smaller IBs recovering faster than larger IBs after photobleaching (140). Negri bodies of RABV coalesce over time into larger IBs, but then eject smaller IBs that have been observed trafficking along microtubules (127). A proposed model for RABV infection involves coalescence of early Negri bodies into larger ones that act as centers for viral replication. They then eject smaller IBs to transport viral components to sites of assembly. HMPV IBs that form from transfections appear to vary greatly in size and frequency, while during infection early HMPV IBs coalesce over time into larger structures that are kept at low numbers by 24-72 hpi (108). What are the factors regulating the size and frequency of HMPV IBs, do early and late IBs differ from one another, and do any differences between IBs have a functional purpose during infection?

The high frequency of IBs seen during transfections may simply be due to the overexpression of P and N to levels that are not reached during infection. This can be examined by titering the amount of DNA being transfected or using a weak promoter in order to determine a P:N stoichiometry that mimics IBs during infection. The initial formation of IBs could be observed at early times post-transfection, and a time course analysis could track the development and behavior

of IBs as expression of P and N increases over time. Examining the effect of active vRNA production on IBs using the minireplicon system or infections, as proposed in earlier sections, may also reveal if viral processes have a role limiting IBs to an optimal size.

FRAP analysis on HMPV IBs of different sizes in both transfected and infected conditions would reveal if fluidity correlates with size, which could point to any functional differences between small and large IBs. In addition to bleaching entire IBs to measure exchange with cytosolic protein, a portion of the IB could be bleached to analyze how quickly the fluorescent signal is redistributed throughout the IB due to the rate of internal diffusion. The movement of different sized IBs within the cytosol could also be recorded to determine if there is a relationship between size, fluidity, and spatial mobility of IBs. The timing of any significant changes in IB appearance or behavior could be compared to corresponding levels of RNA and protein production. The resulting data could be used to identify features of IBs that may be controlled by viral processes in order to promote infection. Screening for compounds that disrupt IB properties or dynamics could be an important method for identifying antivirals. For example, cyclopamine and a cyclopamine analogue (188), drugs originally investigated in cancer therapy, were found to inhibit RSV infection in vitro and in vivo by hardening viral IBs through an M2-1-specific mechanism (141, 189). Similar screens could be done for HMPV to identify compounds that specifically target IBs to inhibit RNA synthesis or viral spread. However, due to the similar properties between viral IBs and cellular biomolecular condensates, extensive studies would need to be done to ensure the investigated compounds are only targeting viral mechanisms.

4.4 Virus-Host interactions within IBs

Our data supports the hypothesis that interactions between P and the nucleocapsid are necessary for IBs to form, but the requirement of unidentified host proteins cannot be ruled out. Purification of biomolecular condensates from cell lysate has been achieved for FUS droplets (190, 191), so a similar protocol

could be followed in order to isolate IBs that form under both transfected and infected conditions. Mass spectrometry could be used to identify host components that are recruited to all IBs or those which are only recruited to IBs during infection. Proximity labeling assays could also be used to confirm if specific host proteins are closely associated with P or N. After confirming the presence of these host factors in or near IBs using microscopy, proteins present in both conditions could be investigated through knockdown studies to determine if any are involved in driving IB formation. Alternatively, proteins recruited to IBs during infection may be involved in vRNA synthesis, and use of inhibitors or knockdown techniques would reveal if these proteins are recruited to IBs in order to replicate and transcribe the HMPV genome.

If any kinases or phosphatases are found to be located within IBs, these could be investigated further as potential regulators of the phosphorylation state of P or other viral proteins. The effect of kinase or phosphatase inhibitors on IB behavior or RNA synthesis could reveal if phosphorylation is a regulator for those processes. Protein phosphatase 1 (PP1) and casein kinase 2 (CK2) have been shown to act on RSV M2-1 and P, respectively (80, 151, 180). RSV P recruits PP1 to IBs and also interacts with M2-1, resulting in M2-1 dephosphorylation and re-localization to IBAGs. HMPV P has a consensus binding site for interaction with PP1 upstream of the predicted M2-1 binding site (80), so recruitment of PP1 to IBs is expected and could be confirmed using immunofluorescence. Determining if HMPV M2-1 is regulated by the same mechanism as RSV could be important for investigating broad-spectrum pneumovirus inhibitors.

The major phosphorylation sites of RSV P are S232 and S237, located at the P C-terminus and phosphorylated by CK2 (151, 180). The purpose of phosphorylation at these sites has been disputed, but they may be involved in regulating RNA synthesis (151, 152). There is poor sequence homology between the HMPV and RSV P C-terminal domains, and HMPV P residues S266, T267, S268, and S271 are located in a highly acidic patch that is not found in RSV P. However, S271 has been demonstrated to be phosphorylated (112) and is located

in a consensus sequence for CK2 and the acidophilic Polo like kinases PLK2 and PLK3 (192). We found that these residues are important for proper functioning of P during RNA synthesis, so determining if specific kinases localize to HMPV IBs, phosphorylate P, or have kinase activity required for RNA synthesis could reveal potential antiviral targets.

Unpublished data from our lab suggests host enzymes involved in the rate limiting steps of purine biosynthesis pathways may be localized within, or in close proximity to, HMPV IBs, and HMPV infection induces a localized increase in cellular GTP between 6-12 hpi. Ribavirin, a drug that has been inconsistently used to treat RSV and HMPV, is a guanosine analogue proposed to be an inhibitor of the GTP biosynthesis enzyme IMPDH (193). An abundance of ribonucleotides is required for viral replication and transcription, and the availability of purines, specifically, may be involved in initiation events by the pneumoviral polymerase complex (113). Thus, localization of host enzymes that produce purines to sites of viral replication could be beneficial for optimal infection. Because recruitment of molecules to biomolecular condensates depends on their ability to interact with the core components, it would be interesting to see if localization of purine biosynthesis enzymes during infection is dependent on HMPV P. The cellular localization of these enzymes in the presence of IBs formed by P domain constructs or P phosphorylation mutants would reveal if certain P domains or phosphorylation sites are involved in the recruitment of these enzymes to IBs. Speculatively, disrupting a potential interaction between these enzymes and P mutants would provide an explanation for their defect in RNA synthesis that is alternative to the function of P as a polymerase co-factor. Proximity ligation or co-immunoprecipitation assays could be used to test for an interaction between HMPV P and purine biosynthesis enzymes.

Rac1, CDC42, and RhoA are Rho GTPases in the signaling pathway regulating actin polymerization. All three of these proteins were recently demonstrated to localize to RSV IBs during infection, and Rac1 was also found to localize with F at sites of assembly (194). The dramatic reorganization of actin

filaments during HMPV infection is disrupted through the inhibition of these same three GTPases (117). HMPV P has also been shown to interact with an actin-associated protein (117), and HMPV IBs coalesce as a result of actin polymerization (108), potentially as a result of IBs moving through the cytosol along the cytoskeleton. The cellular location of Rac1, CDC42, and RhoA during HMPV infection is not known, but determining if these proteins are located within HMPV IBs could provide a missing link connecting IB maturation with the rearrangement of the actin cytoskeleton. Similar to the above studies, various P mutants could be used to determine if P facilitates recruitment of these host proteins to IBs.

Another host-virus interaction to consider is the innate immune response to components of HMPV IBs. A previous study found cellular METTL proteins are pulled into HMPV IBs in order to modify and mask nascent RNA as “self”, preventing detection of vRNA by host pattern recognition receptors (142). Other immune signaling molecules have been found localized to other NNSV IBs or interact with IB components, including NF κ B, RIG-I, MDA5, and MAVS in RSV (195, 196) and TLR3, STAT1, and STAT2 in RABV (197-199). Interestingly, P and N transfections were enough to localize MDA5 and MAVS to RSV IBs and inhibit production of IFN β , suggesting these innate immune molecules are sequestered into IBs to evade the host immune response (195). RABV Negri bodies were unable to form in the absence of TLR3, and TLR3 knockout mice had less severe disease, indicating this innate immune protein may actually be coopted for optimal RABV infection (197). Our imaging and FRAP analysis of HMPV IBs, along with our recombinant virus infection, were done in Vero cells (African green monkey, kidney), which are unable to induce a type I interferon antiviral response. Using more physiologically relevant cell lines, such as A549 cells (human lung epithelial, carcinoma) or BEAS-2B cells (human lung epithelial, non-cancerous), would allow for the examination of innate immune signaling in response to HMPV IBs and determine how these processes interact.

4.5 Regulating HMPV P and identifying alternative function

The HMPV phosphoprotein is multifunctional and likely has many additional roles during infection that have not yet been determined. P acts as a co-factor for L, but the viral polymerase gene is transcribed at low levels compared to P, meaning the P/L interaction is likely saturated, with L being the limiting factor. Excess P may simply function in maintaining the structure of the IB, or certain subpopulations of P may assist in recruiting other viral and host proteins to the inclusion that are necessary for replication. Close proximity between P and actin (117) warrants speculation that P may have roles in trafficking of IBs or nucleocapsids through intercellular extensions or to sites of assembly. The potential to interact with so many different proteins over the course of an infection means these interactions must be regulated, ensuring P functions as required during each step of the viral life cycle. Identifying some of the molecular features that determine the function of HMPV P has been the focus of this dissertation. While our work revealed some new information, there are still many unanswered questions regarding the regulation of this complex protein.

Although not discussed in Chapter 3, when detecting HMPV P in western blots we regularly observed low levels of a higher molecular weight species. The difference in size between the major and minor P bands is approximately the size of a ubiquitin or SUMO moiety. This modification could represent an additional PTM with an unknown viral function. If the identity and location of this modification can be determined, mutagenesis would reveal if the PTM has a functional role in our established assays. Negative results using these methods would suggest the modification may be involved in viral processes outside the IB. Determining a function for this secondary modification and the timing of its appearance during infection will be important for discovering additional roles of HMPV P.

The function of P within IBs and the polymerase complex is paramount, but P likely has secondary functions that are just as important for the survival of the virus. Somehow, viral components must exit IBs, traffic to the host membrane, and assemble into budding virions. The flexibility and multivalency afforded to P as a

disordered tetramer allows it to act as a scaffold for higher order complexes, which can then be transported as a unit. Expression of HMPV P alone can induce formation of membrane filaments and cellular extensions (117), and expression of RSV P with F and M is required for M to localize with F at sites of assembly (200, 201). M was also pulled into RSV IBs but was unable to localize with F in the absence of P, indicating the interaction between P and M is critical for recruitment of viral components to sites of assembly. HMPV IBs can also move between cells, potentially through interaction with the actin cytoskeleton (117, 119). Transfection of HMPV P mutants, N, M, and F would reveal if any of the examined phosphorylation sites influence M localization or trafficking of viral proteins to filaments. Proximity ligation assays could be performed to quantify any potential changes in the frequency of interaction between P mutants and actin.

HMPV P has many potential phosphorylation sites, one of which we found phosphorylation was likely involved in promoting optimal RNA synthesis. The function of phosphorylation at other investigated sites remains unclear, and we did not examine the effect of phosphomimetic mutations to sites within the NTD or OD. Several RSV studies have utilized radiolabeling to analyze the P phosphorylation state and identify sites that contribute the most to the protein's phosphate content (151, 152, 180). Similar use of radioactive phosphate with HMPV P phospho-dead mutants could be used to determine if P has major phosphorylation sites that are constitutively phosphorylated. If S266 is indeed phosphorylated to promote optimal RNA synthesis, mutations at this site might result in a measurable drop in phosphate content. The extent of P phosphorylation at different stages of infection could also be determined using a time course analysis, which would help identify key times during infection where an increase or decrease in P phosphorylation might correspond to regulatory mechanisms.

The role of phosphorylation at T267, S268, and S271 may be difficult to determine. If transient or cyclic phosphorylation is required at these sites, typical mutagenesis techniques for studying phosphorylation would be ineffective. There is also the potential for phosphorylation to differentially regulate interactions with

binding partners based on the location of each of the four P protomers within the tetramer or their asymmetrical spatial orientation within a higher order complex. Attempting to measure a single function of a highly multifunctional and interactive protein will require stringent assays that can isolate individual processes. For example, the minireplicon system we used was a general reporter for successful RNA synthesis by the HMPV polymerase complex, but it does not differentiate replication of the minireplicon from transcription of the luciferase reporter. Disruption of either one of these processes would result in a defective system. Minireplicons have been modified for other viruses to report only transcription, which have revealed instances where variables affect one process and not the other (125, 202, 203). Use of a more definitive reporter could reveal if any phospho-dead or phosphomimetic mutations specifically affect replication or transcription. If such a result is found it would provide insight on additional mechanisms that determine which type of RNA synthesis is performed by the polymerase.

While phosphorylation site mutations control the charge at a single residue, the phosphorylation state of the surrounding residues cannot be known or controlled. Mutations to one site may inadvertently alter the affinity of kinases or phosphatases for the surrounding sites. Variations in the total phosphorylation state may have contributed to some of the variability seen in our data. To account for these possibilities, mutants could be made which contain different combinations of phospho-dead and phosphomimetic mutations at S266, T267, S268, and S271. This would allow us to determine how these sites function in relation to one another and might increase the precision of cellular assays for the production of more conclusive data. Additionally, phosphorylation of P mutants or P isolated from infected cells could be analyzed using 2D gel electrophoresis in order to identify potential P isoforms representing different phosphorylation states.

The majority of the P mutations failed to rescue infectious virus, including the Y290F mutant which functioned at WT levels in the minireplicon assay. The S266E and T267D mutants were rescued but were not tested for attenuation in comparison to WT HMPV. To further explore the effect of these mutations during

infection the rescue protocol could be repeated, but instead of propagating rescued virus in Vero cells, all recombinant HMPV mutants could be passaged in a cell line stably expressing WT P until enough virus has been collected to measure the viral titer. Collected virus will then be used to infect standard cell lines at a measurable MOI, where growth will now be dependent on the mutant P encoded in the genome. A variety of analyses could be achieved with this method, including quantification of growth kinetics, vRNA, and protein expression, as well as time course studies to monitor IBs and trafficking of viral proteins. Ideally, this would allow us to identify the steps in the viral life cycle being disrupted by each P mutation that failed to rescue infectious virus. If use of a WT P stable cell line still does not rescue infection, that would indicate the P mutation has a severe dominant negative effect over WT P. Identifying how that mutation is disrupting infection would be even more critical for understanding how P coordinates viral processes.

In summary, HMPV is a global respiratory pathogen with high morbidity among infants, the elderly, and the immunocompromised. While over two decades have passed since this virus was first isolated in 2001, the mechanistic details of an HMPV infection have only recently begun to be revealed. In this work, the systematic investigation into HMPV P resulted in identification of specific residues within the disordered C-terminal domain which significantly contribute to the function of this viral protein. Not only is this domain indispensable for the formation of liquid-like viral replication centers, but it also contains several serine, threonine, and tyrosine residues that are required for infection. Through the use of mutagenesis, reporter systems, and recombinant virus infection studies, this work revealed these sites contribute significantly to the function of P as a co-factor for successful RNA synthesis during viral replication. The results of this study have provided critical insights to the field, increasing our understanding of the function of HMPV P during infection.

APPENDIX: List of Abbreviations

| | |
|-------------|--|
| ALS | Amyotrophic Lateral Sclerosis |
| CDC42 | Cell Division Control protein 42 |
| CK1/CK2 | Casein Kinase 1 and 2 |
| COPD | Chronic Obstructive Pulmonary Disease |
| CTD | C-Terminal Domain |
| CX3CR1 | C-X3-C Motif Chemokine Receptor 1 |
| EBOV | Ebola Virus |
| ER | Endoplasmic Reticulum |
| EV | Empty Vector |
| F | Fusion glycoprotein |
| FISH | Fluorescence in situ Hybridization |
| FRAP | Fluorescence Recovery After Photobleaching |
| FUS | Fused in Sarcoma |
| G | Attachment Glycoprotein |
| GE | Gene End |
| GS | Gene Start |
| HAE | Human Airway Epithelial tissue |
| HMPV | Human metapneumovirus |
| IB | Inclusion Body |
| IBAG | Inclusion Body-Associated Granule |
| IDR | Intrinsically Disordered Region |
| IFN β | Interferon beta |

| | |
|------------------|---|
| IMPDH | Inosine Monophosphate Dehydrogenase |
| L | Large polymerase protein |
| <i>le</i> | Leader sequence |
| LLPS | Liquid-Liquid Phase Separation |
| LRTI | Lower Respiratory Tract Infection |
| M | Matrix protein |
| M2-1/M2-2 | Matrix-2 proteins 1 and 2 |
| m ⁶ A | Adenosine N ⁶ -methylation |
| mAb | Monoclonal Antibody |
| MAVS | Mitochondrial Antiviral-Signaling protein |
| MDA5 | Melanoma Differentiation-Associated protein 5 |
| METTL3/METTL4 | Methyltransferase-Like protein 3 and 4 |
| MeV | Measles Virus |
| N ⁰ | Monomeric RNA-free nucleoprotein |
| NGS | Normal Goat Serum |
| NiV | Nipah Virus |
| NNSV | Non-segmented Negative Strand RNA Virus |
| N-RNA | RNA-bound N or the nucleocapsid |
| NS1/NS2 | Non-Structural proteins 1 and 2 |
| NS5A | Phosphoprotein of hepatitis C virus |
| NTD | N-Terminal Domain |
| OD | Oligomerization Domain |
| P | Phosphoprotein |

| | |
|-------------|--|
| PLK2/PLK3 | Polo-Like Kinase 2 and 3 |
| PP1 | Protein phosphatase 1 |
| PTM | Post-Translational Modification |
| RABV | Rabies Virus |
| Rac1 | RAS-related C3 botulinum toxin substrate 1 |
| RhoA | Ras Homolog family member A |
| RIG-I | Retinoic acid-Inducible Gene 1 |
| ROI | Region of Interest |
| RSV | Respiratory Syncytial Virus |
| SARS CoV2 | Severe acute respiratory syndrome coronavirus 2 |
| SH | Small Hydrophobic protein |
| STAT1/STAT2 | Signal Transducer and Activator of Transcription 1 and 2 |
| TLR3 | Toll-Like Receptor 3 |
| <i>tr</i> | Trailer sequence |
| URTI | Upper Respiratory Tract Infection |
| vRNA | Virus-derived RNA |
| VSV | Vesicular Stomatitis Virus |
| WT | Wild Type |

REFERENCES

1. Fields BN, Knipe DM, Howley PM, Cohen JL. 2013. Fields virology, Sixth edition. ed, vol 1. Wolters Kluwer/Lippincott Williams & Wilkins Health, Philadelphia.
2. Amarasinghe GK, Ayllón MA, Bào Y, Basler CF, Bavari S, Blasdel KR, Briese T, Brown PA, Bukreyev A, Balkema-Buschmann A, Buchholz UJ, Chabi-Jesus C, Chandran K, Chiapponi C, Crozier I, de Swart RL, Dietzgen RG, Dolnik O, Drexler JF, Dürrwald R, Dundon WG, Duprex WP, Dye JM, Easton AJ, Fooks AR, Formenty PBH, Fouchier RAM, Freitas-Astúa J, Griffiths A, Hewson R, Horie M, Hyndman TH, Jiāng D, Kitajima EW, Kobinger GP, Kondō H, Kurath G, Kuzmin IV, Lamb RA, Lavazza A, Lee B, Lelli D, Leroy EM, Lǐ J, Maes P, Marzano SL, Moreno A, Mühlberger E, Netesov SV, Nowotny N, et al. 2019. Taxonomy of the order Mononegavirales: update 2019. Arch Virol 164:1967-1980.
3. Beer B, Kurth R, Bukreyev A. 1999. Characteristics of Filoviridae: Marburg and Ebola viruses. Naturwissenschaften 86:8-17.
4. Suschak JJ, Schmaljohn CS. 2019. Vaccines against Ebola virus and Marburg virus: recent advances and promising candidates. Hum Vaccin Immunother 15:2359-2377.
5. Rima B, Balkema-Buschmann A, Dundon WG, Duprex P, Easton A, Fouchier R, Kurath G, Lamb R, Lee B, Rota P, Wang L, Ictv Report C. 2019. ICTV Virus Taxonomy Profile: Paramyxoviridae. J Gen Virol 100:1593-1594.
6. Katz SL, Hinman AR. 2004. Summary and conclusions: measles elimination meeting, 16-17 March 2000. J Infect Dis 189 Suppl 1:S43-7.
7. Gurley ES, Montgomery JM, Hossain MJ, Bell M, Azad AK, Islam MR, Molla MA, Carroll DS, Ksiazek TG, Rota PA, Lowe L, Comer JA, Rollin P, Czub M, Grolla A, Feldmann H, Luby SP, Woodward JL, Breiman RF. 2007. Person-to-person transmission of Nipah virus in a Bangladeshi community. Emerg Infect Dis 13:1031-7.
8. Devnath P, Masud H. 2021. Nipah virus: a potential pandemic agent in the context of the current severe acute respiratory syndrome coronavirus 2 pandemic. New Microbes New Infect 41:100873.
9. Afonso CL, Amarasinghe GK, Bányai K, Bào Y, Basler CF, Bavari S, Bejerman N, Blasdel KR, Briand FX, Briese T, Bukreyev A, Calisher CH, Chandran K, Chéng J, Clawson AN, Collins PL, Dietzgen RG, Dolnik O, Domier LL, Dürrwald R, Dye JM, Easton AJ, Ebihara H, Farkas SL, Freitas-Astúa J, Formenty P, Fouchier RA, Fù Y, Ghedin E, Goodin MM, Hewson R, Horie M, Hyndman TH, Jiāng D, Kitajima EW, Kobinger GP, Kondo H, Kurath G, Lamb RA, Lenardon S, Leroy EM, Li CX, Lin XD, Liú L, Longdon B, Marton S, Maisner A, Mühlberger E, Netesov SV, Nowotny N, et al. 2016. Taxonomy of the order Mononegavirales: update 2016. Arch Virol 161:2351-60.
10. Zanolini P, Bonaccorsi G, Lorini C, Haag M, McGovern I, Paget J, Caini S. 2022. Global patterns of seasonal influenza activity, duration of activity and

- virus (sub)type circulation from 2010 to 2020. *Influenza Other Respir Viruses* 16:696-706.
11. Obando-Pacheco P, Justicia-Grande AJ, Rivero-Calle I, Rodríguez-Tenreiro C, Sly P, Ramilo O, Mejías A, Baraldi E, Papadopoulos NG, Nair H, Nunes MC, Kragten-Tabatabaie L, Heikkinen T, Greenough A, Stein RT, Manzoni P, Bont L, Martínón-Torres F. 2018. Respiratory Syncytial Virus Seasonality: A Global Overview. *J Infect Dis* 217:1356-1364.
 12. Haynes AK, Fowlkes AL, Schneider E, Mutuc JD, Armstrong GL, Gerber SI. 2016. Human Metapneumovirus Circulation in the United States, 2008 to 2014. *Pediatrics* 137.
 13. Rima B, Collins P, Easton A, Fouchier R, Kurath G, Lamb RA, Lee B, Maisner A, Rota P, Wang L, Ictv Report C. 2017. ICTV Virus Taxonomy Profile: Pneumoviridae. *J Gen Virol* 98:2912-2913.
 14. Chanock R, Roizman B, Myers R. 1957. Recovery from infants with respiratory illness of a virus related to chimpanzee coryza agent (CCA). I. Isolation, properties and characterization. *Am J Hyg* 66:281-90.
 15. van den Hoogen BG, de Jong JC, Groen J, Kuiken T, de Groot R, Fouchier RA, Osterhaus AD. 2001. A newly discovered human pneumovirus isolated from young children with respiratory tract disease. *Nat Med* 7:719-24.
 16. Group PERfCHPS. 2019. Causes of severe pneumonia requiring hospital admission in children without HIV infection from Africa and Asia: the PERCH multi-country case-control study. *Lancet* 394:757-779.
 17. Wang X, Li Y, Deloria-Knoll M, Madhi SA, Cohen C, Ali A, Basnet S, Bassat Q, Brooks WA, Chittaganpitch M, Echavarria M, Fasce RA, Goswami D, Hirve S, Homaira N, Howie SRC, Kotloff KL, Khuri-Bulos N, Krishnan A, Lucero MG, Lupisan S, Mira-Iglesias A, Moore DP, Moraleda C, Nunes M, Oshitani H, Owor BE, Polack FP, O'Brien KL, Rasmussen ZA, Rath BA, Salimi V, Scott JAG, Simões EAF, Strand TA, Thea DM, Treurnicht FK, Vaccari LC, Yoshida L-M, Zar HJ, Campbell H, Nair H, Libster R, Otieno G, Joundi I, Broor S, Nicol M, Amarchand R, Shi T, López-Labrador FX, et al. 2021. Global burden of acute lower respiratory infection associated with human metapneumovirus in children under 5 years in 2018: a systematic review and modelling study. *The Lancet Global Health* 9:e33-e43.
 18. Borchers AT, Chang C, Gershwin ME, Gershwin LJ. 2013. Respiratory syncytial virus--a comprehensive review. *Clin Rev Allergy Immunol* 45:331-79.
 19. Feuillet F, Lina B, Rosa-Calatrava M, Boivin G. 2012. Ten years of human metapneumovirus research. *J Clin Virol* 53:97-105.
 20. van den Hoogen BG, van Doornum GJ, Fockens JC, Cornelissen JJ, Beyer WE, de Groot R, Osterhaus AD, Fouchier RA. 2003. Prevalence and clinical symptoms of human metapneumovirus infection in hospitalized patients. *J Infect Dis* 188:1571-7.
 21. Falsey AR, Erdman D, Anderson LJ, Walsh EE. 2003. Human metapneumovirus infections in young and elderly adults. *J Infect Dis* 187:785-90.

22. Edwards KM, Zhu Y, Griffin MR, Weinberg GA, Hall CB, Szilagyi PG, Staat MA, Iwane M, Prill MM, Williams JV. 2013. Burden of human metapneumovirus infection in young children. *N Engl J Med* 368:633-43.
23. Hall CB, Weinberg GA, Iwane MK, Blumkin AK, Edwards KM, Staat MA, Auinger P, Griffin MR, Poehling KA, Erdman D, Grijalva CG, Zhu Y, Szilagyi P. 2009. The burden of respiratory syncytial virus infection in young children. *N Engl J Med* 360:588-98.
24. Loubet P, Mathieu P, Lenzi N, Galtier F, Lainé F, Lesieur Z, Vanhems P, Duval X, Postil D, Amour S, Rogez S, Lagathu G, L'Honneur AS, Foulongne V, Houhou N, Lina B, Carrat F, Launay O. 2021. Characteristics of human metapneumovirus infection in adults hospitalized for community-acquired influenza-like illness in France, 2012-2018: a retrospective observational study. *Clin Microbiol Infect* 27:127.e1-127.e6.
25. Martinello RA, Esper F, Weibel C, Ferguson D, Landry ML, Kahn JS. 2006. Human metapneumovirus and exacerbations of chronic obstructive pulmonary disease. *J Infect* 53:248-54.
26. Yu J, Liu C, Xiao Y, Xiang Z, Zhou H, Chen L, Shen K, Xie Z, Ren L, Wang J. 2019. Respiratory Syncytial Virus Seasonality, Beijing, China, 2007-2015. *Emerg Infect Dis* 25:1127-1135.
27. Salimi V, Tavakoli-Yaraki M, Yavarian J, Bont L, Mokhtari-Azad T. 2016. Prevalence of human respiratory syncytial virus circulating in Iran. *J Infect Public Health* 9:125-35.
28. Vardas E, Blaauw D, McAnerney J. 1999. The epidemiology of respiratory syncytial virus (RSV) infections in South African children. *S Afr Med J* 89:1079-84.
29. Li Y, Wang X, Blau DM, Caballero MT, Feikin DR, Gill CJ, Madhi SA, Omer SB, Simões EAF, Campbell H, Pariente AB, Bardach D, Bassat Q, Casalegno JS, Chakhunashvili G, Crawford N, Danilenko D, Do LAH, Echavarria M, Gentile A, Gordon A, Heikkinen T, Huang QS, Jullien S, Krishnan A, Lopez EL, Markić J, Mira-Iglesias A, Moore HC, Moyes J, Mwananyanda L, Nokes DJ, Noordeen F, Obodai E, Palani N, Romero C, Salimi V, Satav A, Seo E, Shchomak Z, Singleton R, Stolyarov K, Stoszek SK, von Gottberg A, Wurzel D, Yoshida LM, Yung CF, Zar HJ, Nair H. 2022. Global, regional, and national disease burden estimates of acute lower respiratory infections due to respiratory syncytial virus in children younger than 5 years in 2019: a systematic analysis. *Lancet* 399:2047-2064.
30. Maggi F, Pifferi M, Vatteroni M, Fornai C, Tempestini E, Anzilotti S, Lanini L, Andreoli E, Ragazzo V, Pistello M, Specter S, Bendinelli M. 2003. Human metapneumovirus associated with respiratory tract infections in a 3-year study of nasal swabs from infants in Italy. *J Clin Microbiol* 41:2987-91.
31. Nissen MD, Siebert DJ, Mackay IM, Sloots TP, Withers SJ. 2002. Evidence of human metapneumovirus in Australian children. *Med J Aust* 176:188.
32. Hahn A, Wang W, Jaggi P, Dvorchik I, Ramilo O, Koranyi K, Mejias A. 2013. Human metapneumovirus infections are associated with severe morbidity in hospitalized children of all ages. *Epidemiol Infect* 141:2213-23.

33. FF IJ, Beekhuis D, Cotton MF, Pieper CH, Kimpen JL, van den Hoogen BG, van Doornum GJ, Osterhaus DM. 2004. Human metapneumovirus infection in hospital referred South African children. *J Med Virol* 73:486-93.
34. Fowlkes A, Giorgi A, Erdman D, Temte J, Goodin K, Di Lonardo S, Sun Y, Martin K, Feist M, Linz R, Boulton R, Bancroft E, McHugh L, Lojo J, Filbert K, Finelli L. 2014. Viruses associated with acute respiratory infections and influenza-like illness among outpatients from the Influenza Incidence Surveillance Project, 2010-2011. *J Infect Dis* 209:1715-25.
35. Boivin G, Abed Y, Pelletier G, Ruel L, Moisan D, Côté S, Peret TC, Erdman DD, Anderson LJ. 2002. Virological features and clinical manifestations associated with human metapneumovirus: a new paramyxovirus responsible for acute respiratory-tract infections in all age groups. *J Infect Dis* 186:1330-4.
36. Peret TC, Boivin G, Li Y, Couillard M, Humphrey C, Osterhaus AD, Erdman DD, Anderson LJ. 2002. Characterization of human metapneumoviruses isolated from patients in North America. *J Infect Dis* 185:1660-3.
37. Sloots TP, Mackay IM, Bialasiewicz S, Jacob KC, McQueen E, Harnett GB, Siebert DJ, Masters BI, Young PR, Nissen MD. 2006. Human metapneumovirus, Australia, 2001-2004. *Emerg Infect Dis* 12:1263-6.
38. van den Hoogen BG, Osterhaus DM, Fouchier RA. 2004. Clinical impact and diagnosis of human metapneumovirus infection. *Pediatr Infect Dis J* 23:S25-32.
39. Davis CR, Stockmann C, Pavia AT, Byington CL, Blaschke AJ, Hersh AL, Thorell EA, Korgenski K, Daly J, Ampofo K. 2016. Incidence, Morbidity, and Costs of Human Metapneumovirus Infection in Hospitalized Children. *J Pediatric Infect Dis Soc* 5:303-11.
40. Heikkinen T, Osterback R, Peltola V, Jartti T, Vainionpää R. 2008. Human metapneumovirus infections in children. *Emerg Infect Dis* 14:101-6.
41. Stockman LJ, Curns AT, Anderson LJ, Fischer-Langley G. 2012. Respiratory syncytial virus-associated hospitalizations among infants and young children in the United States, 1997-2006. *Pediatr Infect Dis J* 31:5-9.
42. Boivin G, De Serres G, Hamelin ME, Côté S, Argouin M, Tremblay G, Maranda-Aubut R, Sauvageau C, Ouakki M, Boulianne N, Couture C. 2007. An outbreak of severe respiratory tract infection due to human metapneumovirus in a long-term care facility. *Clin Infect Dis* 44:1152-8.
43. Louie JK, Schnurr DP, Pan CY, Kiang D, Carter C, Tougaw S, Ventura J, Norman A, Belmusto V, Rosenberg J, Trochet G. 2007. A summer outbreak of human metapneumovirus infection in a long-term-care facility. *J Infect Dis* 196:705-8.
44. Liao RS, Appelgate DM, Pelz RK. 2012. An outbreak of severe respiratory tract infection due to human metapneumovirus in a long-term care facility for the elderly in Oregon. *J Clin Virol* 53:171-3.
45. Touzard-Romo F, Tapé C, Lonks JR. 2020. Co-infection with SARS-CoV-2 and Human Metapneumovirus. *R I Med J* (2013) 103:75-76.
46. Shi T, McAllister DA, O'Brien KL, Simoes EAF, Madhi SA, Gessner BD, Polack FP, Balsells E, Acacio S, Aguayo C, Alassani I, Ali A, Antonio M,

- Awasthi S, Awori JO, Azziz-Baumgartner E, Baggett HC, Baillie VL, Balmaseda A, Barahona A, Basnet S, Bassat Q, Basualdo W, Bigogo G, Bont L, Breiman RF, Brooks WA, Broor S, Bruce N, Bruden D, Buchy P, Campbell S, Carosone-Link P, Chadha M, Chipeta J, Chou M, Clara W, Cohen C, de Cuellar E, Dang DA, Dash-Yandag B, Deloria-Knoll M, Dherani M, Eap T, Ebruke BE, Echavarria M, de Freitas Lázaro Emediato CC, Fasce RA, Feikin DR, Feng L, et al. 2017. Global, regional, and national disease burden estimates of acute lower respiratory infections due to respiratory syncytial virus in young children in 2015: a systematic review and modelling study. *Lancet* 390:946-958.
47. Simoes EA, Groothuis JR. 2002. Respiratory syncytial virus prophylaxis--the story so far. *Respir Med* 96 Suppl B:S15-24.
 48. Elhassan NO, Sorbero ME, Hall CB, Stevens TP, Dick AW. 2006. Cost-effectiveness analysis of palivizumab in premature infants without chronic lung disease. *Arch Pediatr Adolesc Med* 160:1070-6.
 49. O'Brien KL, Chandran A, Weatherholtz R, Jafri HS, Griffin MP, Bellamy T, Millar EV, Jensen KM, Harris BS, Reid R, Moulton LH, Losonsky GA, Karron RA, Santosham M. 2015. Efficacy of motavizumab for the prevention of respiratory syncytial virus disease in healthy Native American infants: a phase 3 randomised double-blind placebo-controlled trial. *Lancet Infect Dis* 15:1398-408.
 50. McLellan JS, Chen M, Leung S, Graepel KW, Du X, Yang Y, Zhou T, Baxa U, Yasuda E, Beaumont T, Kumar A, Modjarrad K, Zheng Z, Zhao M, Xia N, Kwong PD, Graham BS. 2013. Structure of RSV fusion glycoprotein trimer bound to a prefusion-specific neutralizing antibody. *Science* 340:1113-7.
 51. Hammitt LL, Dagan R, Yuan Y, Baca Cots M, Bosheva M, Madhi SA, Muller WJ, Zar HJ, Brooks D, Grenham A, Wählby Hamrén U, Mankad VS, Ren P, Takas T, Abram ME, Leach A, Griffin MP, Villafana T. 2022. Nirsevimab for Prevention of RSV in Healthy Late-Preterm and Term Infants. *N Engl J Med* 386:837-846.
 52. Anonymous. 2023. Nirsevimab US regulatory submission accepted for the prevention of RSV lower respiratory tract disease in infants and children up to age 24 months, AstraZeneca.
 53. Schuster JE, Cox RG, Hastings AK, Boyd KL, Wadia J, Chen Z, Burton DR, Williamson RA, Williams JV. 2015. A broadly neutralizing human monoclonal antibody exhibits in vivo efficacy against both human metapneumovirus and respiratory syncytial virus. *J Infect Dis* 211:216-25.
 54. Kinder JT, Moncman CL, Barrett C, Jin H, Kallewaard N, Dutch RE. 2020. Respiratory Syncytial Virus and Human Metapneumovirus Infections in Three-Dimensional Human Airway Tissues Expose an Interesting Dichotomy in Viral Replication, Spread, and Inhibition by Neutralizing Antibodies. *J Virol* 94.
 55. Tejada S, Martinez-Reviejo R, Karakoc HN, Peña-López Y, Manuel O, Rello J. 2022. Ribavirin for Treatment of Subjects with Respiratory Syncytial

- Virus-Related Infection: A Systematic Review and Meta-Analysis. *Adv Ther* 39:4037-4051.
56. de Zwart A, Riezebos-Brilman A, Lunter G, Vonk J, Glanville AR, Gottlieb J, Permpalung N, Kerstjens H, Alffenaar JW, Verschuuren E. 2022. Respiratory Syncytial Virus, Human Metapneumovirus, and Parainfluenza Virus Infections in Lung Transplant Recipients: A Systematic Review of Outcomes and Treatment Strategies. *Clin Infect Dis* 74:2252-2260.
 57. Randolph AG, Wang EE. 1996. Ribavirin for respiratory syncytial virus lower respiratory tract infection. A systematic overview. *Arch Pediatr Adolesc Med* 150:942-7.
 58. Raza K, Ismailjee SB, Crespo M, Studer SM, Sanghavi S, Paterson DL, Kwak EJ, Rinaldo CR, Jr., Pilewski JM, McCurry KR, Husain S. 2007. Successful outcome of human metapneumovirus (hMPV) pneumonia in a lung transplant recipient treated with intravenous ribavirin. *J Heart Lung Transplant* 26:862-4.
 59. Kitanovski L, Kopriva S, Pokorn M, Dolničar MB, Rajić V, Stefanović M, Jazbec J. 2013. Treatment of severe human metapneumovirus (hMPV) pneumonia in an immunocompromised child with oral ribavirin and IVIG. *J Pediatr Hematol Oncol* 35:e311-3.
 60. Bonney D, Razali H, Turner A, Will A. 2009. Successful treatment of human metapneumovirus pneumonia using combination therapy with intravenous ribavirin and immune globulin. *Br J Haematol* 145:667-9.
 61. Shachor-Meyouhas Y, Ben-Barak A, Kassis I. 2011. Treatment with oral ribavirin and IVIG of severe human metapneumovirus pneumonia (HMPV) in immune compromised child. *Pediatr Blood Cancer* 57:350-1.
 62. Akhmedov M, Wais V, Sala E, Neagoie A, Nguyen TM, Gantner A, von Harsdorf S, Kuchenbauer F, Schubert A, Michel D, Döhner H, Bunjes D. 2020. Respiratory syncytial virus and human metapneumovirus after allogeneic hematopoietic stem cell transplantation: Impact of the immunodeficiency scoring index, viral load, and ribavirin treatment on the outcomes. *Transpl Infect Dis* 22:e13276.
 63. Ahmad A, Eze K, Noulin N, Horvathova V, Murray B, Baillet M, Grey L, Mori J, Adda N. 2022. EDP-938, a Respiratory Syncytial Virus Inhibitor, in a Human Virus Challenge. *N Engl J Med* 386:655-666.
 64. Chin J, Magoffin RL, Shearer LA, Schieble JH, Lennette EH. 1969. Field evaluation of a respiratory syncytial virus vaccine and a trivalent parainfluenza virus vaccine in a pediatric population. *Am J Epidemiol* 89:449-63.
 65. Kim HW, Canchola JG, Brandt CD, Pyles G, Chanock RM, Jensen K, Parrott RH. 1969. Respiratory syncytial virus disease in infants despite prior administration of antigenic inactivated vaccine. *Am J Epidemiol* 89:422-34.
 66. Yim KC, Cragin RP, Boukhvalova MS, Blanco JC, Hamlin ME, Boivin G, Porter DD, Prince GA. 2007. Human metapneumovirus: enhanced pulmonary disease in cotton rats immunized with formalin-inactivated virus vaccine and challenged. *Vaccine* 25:5034-40.

67. de Swart RL, van den Hoogen BG, Kuiken T, Herfst S, van Amerongen G, Yüksel S, Sprong L, Osterhaus AD. 2007. Immunization of macaques with formalin-inactivated human metapneumovirus induces hypersensitivity to hMPV infection. *Vaccine* 25:8518-28.
68. Principi N, Esposito S. 2014. Paediatric human metapneumovirus infection: epidemiology, prevention and therapy. *J Clin Virol* 59:141-7.
69. Simões EAF, Center KJ, Tita ATN, Swanson KA, Radley D, Houghton J, McGrory SB, Gomme E, Anderson M, Roberts JP, Scott DA, Jansen KU, Gruber WC, Dormitzer PR, Gurtman AC. 2022. Prefusion F Protein-Based Respiratory Syncytial Virus Immunization in Pregnancy. *N Engl J Med* 386:1615-1626.
70. Madhi SA, Polack FP, Piedra PA, Munoz FM, Trenholme AA, Simões EAF, Swamy GK, Agrawal S, Ahmed K, August A, Baqui AH, Calvert A, Chen J, Cho I, Cotton MF, Cutland CL, Englund JA, Fix A, Gonik B, Hammitt L, Heath PT, de Jesus JN, Jones CE, Khalil A, Kimberlin DW, Libster R, Llapur CJ, Lucero M, Pérez Marc G, Marshall HS, Masenya MS, Martínón-Torres F, Meece JK, Nolan TM, Osman A, Perrett KP, Plested JS, Richmond PC, Snape MD, Shakib JH, Shinde V, Stoney T, Thomas DN, Tita AT, Varner MW, Vatish M, Vrbicky K, Wen J, Zaman K, Zar HJ, et al. 2020. Respiratory Syncytial Virus Vaccination during Pregnancy and Effects in Infants. *N Engl J Med* 383:426-439.
71. Anonymous. 2022. Pfizer and BioNTech Submit Application to U.S. FDA for Emergency Use Authorization of Omicron BA.4/BA.5-Adapted Bivalent COVID-19 Vaccine in Children Under 5 Years, Pfizer.
72. Kuppen JP, Mitrovich MD, Vahey MD. 2021. A morphological transformation in respiratory syncytial virus leads to enhanced complement deposition. *Elife* 10.
73. Bächli T, Howe C. 1973. Morphogenesis and ultrastructure of respiratory syncytial virus. *J Virol* 12:1173-80.
74. Ke Z, Dillard RS, Chirkova T, Leon F, Stobart CC, Hampton CM, Strauss JD, Rajan D, Rostad CA, Taylor JV, Yi H, Shah R, Jin M, Hartert TV, Peebles RS, Jr., Graham BS, Moore ML, Anderson LJ, Wright ER. 2018. The Morphology and Assembly of Respiratory Syncytial Virus Revealed by Cryo-Electron Tomography. *Viruses* 10.
75. Mitra R, Baviskar P, Duncan-Decocq RR, Patel D, Oomens AG. 2012. The human respiratory syncytial virus matrix protein is required for maturation of viral filaments. *J Virol* 86:4432-43.
76. Kiss G, Holl JM, Williams GM, Alonas E, Vanover D, Lifland AW, Gudheti M, Guerrero-Ferreira RC, Nair V, Yi H, Graham BS, Santangelo PJ, Wright ER. 2014. Structural analysis of respiratory syncytial virus reveals the position of M2-1 between the matrix protein and the ribonucleoprotein complex. *J Virol* 88:7602-17.
77. Liljeroos L, Krzyzaniak MA, Helenius A, Butcher SJ. 2013. Architecture of respiratory syncytial virus revealed by electron cryotomography. *Proc Natl Acad Sci U S A* 110:11133-8.

78. Conley MJ, Short JM, Burns AM, Streetley J, Hutchings J, Bakker SE, Power BJ, Jaffery H, Haney J, Zanetti G, Murcia PR, Stewart M, Fearn R, Vijayakrishnan S, Bhella D. 2022. Helical ordering of envelope-associated proteins and glycoproteins in respiratory syncytial virus. *Embo j* 41:e109728.
79. Buchholz UJ, Biacchesi S, Pham QN, Tran KC, Yang L, Luongo CL, Skiadopoulou MH, Murphy BR, Collins PL. 2005. Deletion of M2 gene open reading frames 1 and 2 of human metapneumovirus: effects on RNA synthesis, attenuation, and immunogenicity. *J Virol* 79:6588-97.
80. Richard CA, Rincheval V, Lassoued S, Fix J, Cardone C, Esneau C, Nekhai S, Galloux M, Rameix-Welti MA, Sizun C, Eléouët JF. 2018. RSV hijacks cellular protein phosphatase 1 to regulate M2-1 phosphorylation and viral transcription. *PLoS Pathog* 14:e1006920.
81. Cheng X, Park H, Zhou H, Jin H. 2005. Overexpression of the M2-2 protein of respiratory syncytial virus inhibits viral replication. *J Virol* 79:13943-52.
82. Spann KM, Tran KC, Chi B, Rabin RL, Collins PL. 2004. Suppression of the induction of alpha, beta, and lambda interferons by the NS1 and NS2 proteins of human respiratory syncytial virus in human epithelial cells and macrophages [corrected]. *J Virol* 78:4363-9.
83. Ren J, Liu T, Pang L, Li K, Garofalo RP, Casola A, Bao X. 2011. A novel mechanism for the inhibition of interferon regulatory factor-3-dependent gene expression by human respiratory syncytial virus NS1 protein. *J Gen Virol* 92:2153-2159.
84. Bukreyev A, Whitehead SS, Murphy BR, Collins PL. 1997. Recombinant respiratory syncytial virus from which the entire SH gene has been deleted grows efficiently in cell culture and exhibits site-specific attenuation in the respiratory tract of the mouse. *J Virol* 71:8973-82.
85. Biacchesi S, Skiadopoulou MH, Yang L, Lamirande EW, Tran KC, Murphy BR, Collins PL, Buchholz UJ. 2004. Recombinant human Metapneumovirus lacking the small hydrophobic SH and/or attachment G glycoprotein: deletion of G yields a promising vaccine candidate. *J Virol* 78:12877-87.
86. Gan SW, Tan E, Lin X, Yu D, Wang J, Tan GM, Vararattanavech A, Yeo CY, Soon CH, Soong TW, Pervushin K, Torres J. 2012. The small hydrophobic protein of the human respiratory syncytial virus forms pentameric ion channels. *J Biol Chem* 287:24671-89.
87. Masante C, El Najjar F, Chang A, Jones A, Moncman CL, Dutch RE. 2014. The human metapneumovirus small hydrophobic protein has properties consistent with those of a viroporin and can modulate viral fusogenic activity. *J Virol* 88:6423-33.
88. Feng Z, Xu L, Xie Z. 2022. Receptors for Respiratory Syncytial Virus Infection and Host Factors Regulating the Life Cycle of Respiratory Syncytial Virus. *Front Cell Infect Microbiol* 12:858629.
89. Karron RA, Buonagurio DA, Georgiu AF, Whitehead SS, Adamus JE, Clements-Mann ML, Harris DO, Randolph VB, Udem SA, Murphy BR, Sidhu MS. 1997. Respiratory syncytial virus (RSV) SH and G proteins are not essential for viral replication in vitro: clinical evaluation and molecular

- characterization of a cold-passaged, attenuated RSV subgroup B mutant. *Proc Natl Acad Sci U S A* 94:13961-6.
90. Chang A, Masante C, Buchholz UJ, Dutch RE. 2012. Human metapneumovirus (HMPV) binding and infection are mediated by interactions between the HMPV fusion protein and heparan sulfate. *J Virol* 86:3230-43.
 91. Krusat T, Streckert HJ. 1997. Heparin-dependent attachment of respiratory syncytial virus (RSV) to host cells. *Arch Virol* 142:1247-54.
 92. Wright C, Oliver KC, Fenwick FI, Smith NM, Toms GL. 1997. A monoclonal antibody pool for routine immunohistochemical detection of human respiratory syncytial virus antigens in formalin-fixed, paraffin-embedded tissue. *J Pathol* 182:238-44.
 93. Villenave R, Thavagnanam S, Sarlang S, Parker J, Douglas I, Skibinski G, Heaney LG, McKaigue JP, Coyle PV, Shields MD, Power UF. 2012. In vitro modeling of respiratory syncytial virus infection of pediatric bronchial epithelium, the primary target of infection in vivo. *Proc Natl Acad Sci U S A* 109:5040-5.
 94. Kuiken T, van den Hoogen BG, van Riel DA, Laman JD, van Amerongen G, Sprong L, Fouchier RA, Osterhaus AD. 2004. Experimental human metapneumovirus infection of cynomolgus macaques (*Macaca fascicularis*) results in virus replication in ciliated epithelial cells and pneumocytes with associated lesions throughout the respiratory tract. *Am J Pathol* 164:1893-900.
 95. Cox RG, Livesay SB, Johnson M, Ohi MD, Williams JV. 2012. The human metapneumovirus fusion protein mediates entry via an interaction with RGD-binding integrins. *J Virol* 86:12148-60.
 96. Schowalter RM, Smith SE, Dutch RE. 2006. Characterization of human metapneumovirus F protein-promoted membrane fusion: critical roles for proteolytic processing and low pH. *J Virol* 80:10931-41.
 97. González-Reyes L, Ruiz-Argüello MB, García-Barreno B, Calder L, López JA, Albar JP, Skehel JJ, Wiley DC, Melero JA. 2001. Cleavage of the human respiratory syncytial virus fusion protein at two distinct sites is required for activation of membrane fusion. *Proc Natl Acad Sci U S A* 98:9859-64.
 98. Lamb RA, Jardetzky TS. 2007. Structural basis of viral invasion: lessons from paramyxovirus F. *Curr Opin Struct Biol* 17:427-36.
 99. Cox RG, Williams JV. 2013. Breaking in: human metapneumovirus fusion and entry. *Viruses* 5:192-210.
 100. Russell CJ, Jardetzky TS, Lamb RA. 2001. Membrane fusion machines of paramyxoviruses: capture of intermediates of fusion. *Embo j* 20:4024-34.
 101. Herfst S, Mas V, Ver LS, Wierda RJ, Osterhaus AD, Fouchier RA, Melero JA. 2008. Low-pH-induced membrane fusion mediated by human metapneumovirus F protein is a rare, strain-dependent phenomenon. *J Virol* 82:8891-5.
 102. Cox RG, Mainou BA, Johnson M, Hastings AK, Schuster JE, Dermody TS, Williams JV. 2015. Human Metapneumovirus Is Capable of Entering Cells by Fusion with Endosomal Membranes. *PLoS Pathog* 11:e1005303.

103. Srinivasakumar N, Ogra PL, Flanagan TD. 1991. Characteristics of fusion of respiratory syncytial virus with HEp-2 cells as measured by R18 fluorescence dequenching assay. *J Virol* 65:4063-9.
104. Kahn JS, Schnell MJ, Buonocore L, Rose JK. 1999. Recombinant vesicular stomatitis virus expressing respiratory syncytial virus (RSV) glycoproteins: RSV fusion protein can mediate infection and cell fusion. *Virology* 254:81-91.
105. Battles MB, McLellan JS. 2019. Respiratory syncytial virus entry and how to block it. *Nat Rev Microbiol* 17:233-245.
106. Rincheval V, Lelek M, Gault E, Bouillier C, Sitterlin D, Blouquit-Laye S, Galloux M, Zimmer C, Eleouet JF, Rameix-Welti MA. 2017. Functional organization of cytoplasmic inclusion bodies in cells infected by respiratory syncytial virus. *Nat Commun* 8:563.
107. Derdowski A, Peters TR, Glover N, Qian R, Utley TJ, Burnett A, Williams JV, Spearman P, Crowe JE. 2008. Human metapneumovirus nucleoprotein and phosphoprotein interact and provide the minimal requirements for inclusion body formation. *J Gen Virol* 89:2698-2708.
108. Cifuentes-Muñoz N, Brantje J, Slaughter KB, Dutch RE. 2017. Human Metapneumovirus Induces Formation of Inclusion Bodies for Efficient Genome Replication and Transcription. *J Virol* 91:e01282-17.
109. Mink MA, Stec DS, Collins PL. 1991. Nucleotide sequences of the 3' leader and 5' trailer regions of human respiratory syncytial virus genomic RNA. *Virology* 185:615-24.
110. Noton SL, Cowton VM, Zack CR, McGivern DR, Fearn R. 2010. Evidence that the polymerase of respiratory syncytial virus initiates RNA replication in a nontemplated fashion. *Proc Natl Acad Sci U S A* 107:10226-31.
111. Tremaglio CZ, Noton SL, Deflubé LR, Fearn R. 2013. Respiratory syncytial virus polymerase can initiate transcription from position 3 of the leader promoter. *J Virol* 87:3196-207.
112. Pan J, Qian X, Lattmann S, El Sahili A, Yeo TH, Jia H, Cressey T, Ludeke B, Noton S, Kalocsay M, Fearn R, Lescar J. 2020. Structure of the human metapneumovirus polymerase phosphoprotein complex. *Nature* 577:275-279.
113. Cressey TN, Noton SL, Nagendra K, Braun MR, Fearn R. 2018. Mechanism for de novo initiation at two sites in the respiratory syncytial virus promoter. *Nucleic Acids Res* 46:6785-6796.
114. Fearn R, Plemper RK. 2017. Polymerases of paramyxoviruses and pneumoviruses. *Virus Res* 234:87-102.
115. Sabo Y, Ehrlich M, Bacharach E. 2011. The conserved YAGL motif in human metapneumovirus is required for higher-order cellular assemblies of the matrix protein and for virion production. *J Virol* 85:6594-609.
116. Deffrasnes C, Côté S, Boivin G. 2005. Analysis of replication kinetics of the human metapneumovirus in different cell lines by real-time PCR. *J Clin Microbiol* 43:488-90.
117. El Najjar F, Cifuentes-Muñoz N, Chen J, Zhu H, Buchholz UJ, Moncman CL, Dutch RE. 2016. Human metapneumovirus Induces Reorganization of

- the Actin Cytoskeleton for Direct Cell-to-Cell Spread. *PLoS Pathog* 12:e1005922.
118. Loo LH, Jumat MR, Fu Y, Ayi TC, Wong PS, Tee NW, Tan BH, Sugrue RJ. 2013. Evidence for the interaction of the human metapneumovirus G and F proteins during virus-like particle formation. *Virol J* 10:294.
 119. El Najjar F, Castillo SR, Moncman CL, Wu C, Isla E, Ortega ACV, Frolenkov GI, Cifuentes-Munoz N, Dutch RE. 2023. Imaging analysis reveals budding of filamentous human metapneumovirus virions and direct transfer of inclusion bodies through intercellular extensions. *mBio*, In Review
 120. Cifuentes-Muñoz N, Ellis Dutch R. 2019. To assemble or not to assemble: The changing rules of pneumovirus transmission. *Virus Res* 265:68-73.
 121. Kristensson K, Dastur DK, Manghani DK, Tsiang H, Bentivoglio M. 1996. Rabies: interactions between neurons and viruses. A review of the history of Negri inclusion bodies. *Neuropathol Appl Neurobiol* 22:179-87.
 122. Wu C, Holehouse AS, Leung DW, Amarasinghe GK, Dutch RE. 2022. Liquid Phase Partitioning in Virus Replication: Observations and Opportunities. *Annu Rev Virol* 9:285-306.
 123. Dolnik O, Gerresheim GK, Biedenkopf N. 2021. New Perspectives on the Biogenesis of Viral Inclusion Bodies in Negative-Sense RNA Virus Infections. *Cells* 10:1460.
 124. Lahaye X, Vidy A, Pomier C, Obiang L, Harper F, Gaudin Y, Blondel D. 2009. Functional characterization of Negri bodies (NBs) in rabies virus-infected cells: Evidence that NBs are sites of viral transcription and replication. *J Virol* 83:7948-58.
 125. Hoenen T, Shabman RS, Groseth A, Herwig A, Weber M, Schudt G, Dolnik O, Basler CF, Becker S, Feldmann H. 2012. Inclusion bodies are a site of ebolavirus replication. *J Virol* 86:11779-88.
 126. Boggs KB, Edmonds K, Cifuentes-Munoz N, El Najjar F, Ossandón C, Roe M, Wu C, Moncman CL, Creamer TP, Amarasinghe GK, Leung DW, Dutch RE. 2022. Human Metapneumovirus Phosphoprotein Independently Drives Phase Separation and Recruits Nucleoprotein to Liquid-Like Bodies. *mBio* 13:e0109922.
 127. Nikolic J, Le Bars R, Lama Z, Scrima N, Lagaudrière-Gesbert C, Gaudin Y, Blondel D. 2017. Negri bodies are viral factories with properties of liquid organelles. *Nat Commun* 8:58.
 128. Banani SF, Lee HO, Hyman AA, Rosen MK. 2017. Biomolecular condensates: organizers of cellular biochemistry. *Nat Rev Mol Cell Biol* 18:285-298.
 129. Molliex A, Temirov J, Lee J, Coughlin M, Kanagaraj AP, Kim HJ, Mittag T, Taylor JP. 2015. Phase separation by low complexity domains promotes stress granule assembly and drives pathological fibrillization. *Cell* 163:123-33.
 130. Brangwynne CP, Eckmann CR, Courson DS, Rybarska A, Hoege C, Gharakhani J, Jülicher F, Hyman AA. 2009. Germline P granules are liquid droplets that localize by controlled dissolution/condensation. *Science* 324:1729-32.

131. Gomes E, Shorter J. 2019. The molecular language of membraneless organelles. *J Biol Chem* 294:7115-7127.
132. Hyman AA, Weber CA, Jülicher F. 2014. Liquid-liquid phase separation in biology. *Annu Rev Cell Dev Biol* 30:39-58.
133. Zhao B, Kurgan L. 2022. Compositional Bias of Intrinsically Disordered Proteins and Regions and Their Predictions. *Biomolecules* 12.
134. Romero P, Obradovic Z, Li X, Garner EC, Brown CJ, Dunker AK. 2001. Sequence complexity of disordered protein. *Proteins* 42:38-48.
135. Iakoucheva LM, Radivojac P, Brown CJ, O'Connor TR, Sikes JG, Obradovic Z, Dunker AK. 2004. The importance of intrinsic disorder for protein phosphorylation. *Nucleic Acids Res* 32:1037-49.
136. Li J, Zhang M, Ma W, Yang B, Lu H, Zhou F, Zhang L. 2022. Post-translational modifications in liquid-liquid phase separation: a comprehensive review. *Mol Biomed* 3:13.
137. Hofweber M, Dormann D. 2019. Friend or foe-Post-translational modifications as regulators of phase separation and RNP granule dynamics. *J Biol Chem* 294:7137-7150.
138. Wang B, Zhang L, Dai T, Qin Z, Lu H, Zhang L, Zhou F. 2021. Liquid-liquid phase separation in human health and diseases. *Signal Transduct Target Ther* 6:290.
139. Zhang S, Jiang Y, Cheng Q, Zhong Y, Qin Y, Chen M. 2017. Inclusion Body Fusion of Human Parainfluenza Virus Type 3 Regulated by Acetylated α -Tubulin Enhances Viral Replication. *J Virol* 91.
140. Zhou Y, Su JM, Samuel CE, Ma D. 2019. Measles Virus Forms Inclusion Bodies with Properties of Liquid Organelles. *J Virol* 93:e00948-19.
141. Risso-Ballester J, Galloux M, Cao J, Le Goffic R, Hontonnou F, Jobart-Malfait A, Desquesnes A, Sake SM, Haid S, Du M, Zhang X, Zhang H, Wang Z, Rincheval V, Zhang Y, Pietschmann T, Eléouët JF, Rameix-Welti MA, Altmeyer R. 2021. A condensate-hardening drug blocks RSV replication in vivo. *Nature* 595:596-599.
142. Lu M, Zhang Z, Xue M, Zhao BS, Harder O, Li A, Liang X, Gao TZ, Xu Y, Zhou J, Feng Z, Niewiesk S, Peeples ME, He C, Li J. 2020. N(6)-methyladenosine modification enables viral RNA to escape recognition by RNA sensor RIG-I. *Nat Microbiol* 5:584-598.
143. García-Barreno B, Delgado T, Melero JA. 1996. Identification of protein regions involved in the interaction of human respiratory syncytial virus phosphoprotein and nucleoprotein: significance for nucleocapsid assembly and formation of cytoplasmic inclusions. *J Virol* 70:801-8.
144. Renner M, Paesen GC, Grison CM, Granier S, Grimes JM, Leyrat C. 2017. Structural dissection of human metapneumovirus phosphoprotein using small angle x-ray scattering. *Sci Rep* 7:14865.
145. Renner M, Bertinelli M, Leyrat C, Paesen GC, Saraiva de Oliveira LF, Huiskonen JT, Grimes JM. 2016. Nucleocapsid assembly in pneumoviruses is regulated by conformational switching of the N protein. *Elife* 5:e12627.
146. Galloux M, Gabiane G, Sourimant J, Richard CA, England P, Moudjou M, Aumont-Nicaise M, Fix J, Rameix-Welti MA, Eléouët JF. 2015. Identification

- and characterization of the binding site of the respiratory syncytial virus phosphoprotein to RNA-free nucleoprotein. *J Virol* 89:3484-96.
147. Gilman MSA, Liu C, Fung A, Behera I, Jordan P, Rigaux P, Ysebaert N, Tcherniuk S, Sourimant J, Eléouët JF, Sutto-Ortiz P, Decroly E, Roymans D, Jin Z, McLellan JS. 2019. Structure of the Respiratory Syncytial Virus Polymerase Complex. *Cell* 179:193-204.e14.
 148. Tran TL, Castagné N, Bhella D, Varela PF, Bernard J, Chilmonczyk S, Berkenkamp S, Benhamo V, Grznarova K, Grosclaude J, Nespoulos C, Rey FA, Eléouët JF. 2007. The nine C-terminal amino acids of the respiratory syncytial virus protein P are necessary and sufficient for binding to ribonucleoprotein complexes in which six ribonucleotides are contacted per N protein protomer. *J Gen Virol* 88:196-206.
 149. Decool H, Bardiaux B, Checa Ruano L, Sperandio O, Fix J, Gutsche I, Richard CA, Bajorek M, Eléouët JF, Galloux M. 2022. Characterization of the Interaction Domains between the Phosphoprotein and the Nucleoprotein of Human Metapneumovirus. *J Virol* 96:e0090921.
 150. Decool H, Gonnin L, Gutsche I, Sizun C, Eléouët JF, Galloux M. 2021. Interactions between the Nucleoprotein and the Phosphoprotein of Pneumoviruses: Structural Insight for Rational Design of Antivirals. *Viruses* 13:2449.
 151. Barik S, McLean T, Dupuy LC. 1995. Phosphorylation of Ser232 directly regulates the transcriptional activity of the P protein of human respiratory syncytial virus: phosphorylation of Ser237 may play an accessory role. *Virology* 213:405-12.
 152. Lu B, Ma CH, Brazas R, Jin H. 2002. The major phosphorylation sites of the respiratory syncytial virus phosphoprotein are dispensable for virus replication in vitro. *J Virol* 76:10776-84.
 153. Sehnal D, Bittrich S, Deshpande M, Svobodová R, Berka K, Bazgier V, Velankar S, Burley SK, Koča J, Rose AS. 2021. Mol* Viewer: modern web app for 3D visualization and analysis of large biomolecular structures. *Nucleic Acids Research* 49:W431-W437.
 154. Pei J, Kim BH, Grishin NV. 2008. PROMALS3D: a tool for multiple protein sequence and structure alignments. *Nucleic Acids Res* 36:2295-300.
 155. Clamp M, Cuff J, Searle SM, Barton GJ. 2004. The Jalview Java alignment editor. *Bioinformatics* 20:426-7.
 156. Thompson JD, Gibson TJ, Plewniak F, Jeanmougin F, Higgins DG. 1997. The CLUSTAL_X windows interface: flexible strategies for multiple sequence alignment aided by quality analysis tools. *Nucleic Acids Res* 25:4876-82.
 157. Buchholz UJ, Finke S, Conzelmann KK. 1999. Generation of bovine respiratory syncytial virus (BRSV) from cDNA: BRSV NS2 is not essential for virus replication in tissue culture, and the human RSV leader region acts as a functional BRSV genome promoter. *J Virol* 73:251-9.
 158. Shirogane Y, Takeda M, Iwasaki M, Ishiguro N, Takeuchi H, Nakatsu Y, Tahara M, Kikuta H, Yanagi Y. 2008. Efficient multiplication of human

- metapneumovirus in Vero cells expressing the transmembrane serine protease TMPRSS2. *J Virol* 82:8942-6.
159. Chow KM, Whiteheart SW, Smiley JR, Sharma S, Boaz K, Coleman MJ, Maynard A, Hersh LB, Vander Kooi CW. 2019. Immunization of Alpacas (*Lama pacos*) with Protein Antigens and Production of Antigen-specific Single Domain Antibodies. *J Vis Exp* doi:10.3791/58471:e58471.
 160. Schildgen V, van den Hoogen B, Fouchier R, Tripp RA, Alvarez R, Manoha C, Williams J, Schildgen O. 2011. Human Metapneumovirus: lessons learned over the first decade. *Clin Microbiol Rev* 24:734-54.
 161. Shafagati N, Williams J. 2018. Human metapneumovirus - what we know now. *F1000Res* 7:135.
 162. Nevers Q, Albertini AA, Lagaudrière-Gesbert C, Gaudin Y. 2020. Negri bodies and other virus membrane-less replication compartments. *Biochim Biophys Acta Mol Cell Res* 1867:118831.
 163. Heinrich BS, Maliga Z, Stein DA, Hyman AA, Whelan SPJ. 2018. Phase Transitions Drive the Formation of Vesicular Stomatitis Virus Replication Compartments. *mBio* 9:e02290-17.
 164. Feng Z, Chen X, Wu X, Zhang M. 2019. Formation of biological condensates via phase separation: Characteristics, analytical methods, and physiological implications. *J Biol Chem* 294:14823-14835.
 165. Galloux M, Risso-Ballester J, Richard CA, Fix J, Rameix-Welti MA, Eléouët JF. 2020. Minimal Elements Required for the Formation of Respiratory Syncytial Virus Cytoplasmic Inclusion Bodies In Vivo and In Vitro. *mBio* 11:e01202-20.
 166. Esneau C, Raynal B, Roblin P, Brûlé S, Richard CA, Fix J, Eléouët JF, Galloux M. 2019. Biochemical characterization of the respiratory syncytial virus N(0)-P complex in solution. *J Biol Chem* 294:3647-3660.
 167. Blom N, Gammeltoft S, Brunak S. 1999. Sequence and structure-based prediction of eukaryotic protein phosphorylation sites. *J Mol Biol* 294:1351-62.
 168. Dou Y, Yao B, Zhang C. 2014. PhosphoSVM: prediction of phosphorylation sites by integrating various protein sequence attributes with a support vector machine. *Amino Acids* 46:1459-69.
 169. Longhi S, Bloyet LM, Gianni S, Gerlier D. 2017. How order and disorder within paramyxoviral nucleoproteins and phosphoproteins orchestrate the molecular interplay of transcription and replication. *Cell Mol Life Sci* 74:3091-3118.
 170. Cardone C, Caseau CM, Pereira N, Sizun C. 2021. Pneumoviral Phosphoprotein, a Multidomain Adaptor-Like Protein of Apparent Low Structural Complexity and High Conformational Versatility. *Int J Mol Sci* 22:1537.
 171. Galloux M, Tarus B, Blazevic I, Fix J, Duquerroy S, Eléouët JF. 2012. Characterization of a viral phosphoprotein binding site on the surface of the respiratory syncytial nucleoprotein. *J Virol* 86:8375-87.
 172. Ouizougoun-Oubari M, Pereira N, Tarus B, Galloux M, Lassoued S, Fix J, Tortorici MA, Hoos S, Baron B, England P, Desmaële D, Cuvreur P,

- Bontems F, Rey FA, Eléouët JF, Sizun C, Slama-Schwok A, Duquerroy S. 2015. A Druggable Pocket at the Nucleocapsid/Phosphoprotein Interaction Site of Human Respiratory Syncytial Virus. *J Virol* 89:11129-43.
173. Liu H, Shen L, Pan C, Huang W. 2023. Structural modeling, energetic analysis and molecular design of a π -stacking system at the complex interface of pediatric respiratory syncytial virus nucleocapsid with the C-terminal peptide of phosphoprotein. *Biophys Chem* 292:106916.
 174. Guseva S, Milles S, Jensen MR, Salvi N, Kleman JP, Maurin D, Ruigrok RWH, Blackledge M. 2020. Measles virus nucleo- and phosphoproteins form liquid-like phase-separated compartments that promote nucleocapsid assembly. *Sci Adv* 6:eaaz7095.
 175. Bloyet LM, Morin B, Brusica V, Gardner E, Ross RA, Vadakkan T, Kirchhausen T, Whelan SPJ. 2020. Oligomerization of the Vesicular Stomatitis Virus Phosphoprotein Is Dispensable for mRNA Synthesis but Facilitates RNA Replication. *J Virol* 94:e00115-20.
 176. Sugai A, Sato H, Yoneda M, Kai C. 2012. Phosphorylation of measles virus phosphoprotein at S86 and/or S151 downregulates viral transcriptional activity. *FEBS Lett* 586:3900-7.
 177. Hwang LN, Englund N, Das T, Banerjee AK, Pattnaik AK. 1999. Optimal replication activity of vesicular stomatitis virus RNA polymerase requires phosphorylation of a residue(s) at carboxy-terminal domain II of its accessory subunit, phosphoprotein P. *J Virol* 73:5613-20.
 178. Das SC, Pattnaik AK. 2004. Phosphorylation of vesicular stomatitis virus phosphoprotein P is indispensable for virus growth. *J Virol* 78:6420-30.
 179. Fuentes SM, Sun D, Schmitt AP, He B. 2010. Phosphorylation of paramyxovirus phosphoprotein and its role in viral gene expression. *Future Microbiol* 5:9-13.
 180. Sánchez-Seco MP, Navarro J, Martínez R, Villanueva N. 1995. C-terminal phosphorylation of human respiratory syncytial virus P protein occurs mainly at serine residue 232. *J Gen Virol* 76 (Pt 2):425-30.
 181. Fuxreiter M. 2020. Fuzzy protein theory for disordered proteins. *Biochem Soc Trans* 48:2557-2564.
 182. Chiang CH, Lai YL, Huang YN, Yu CC, Lu CC, Yu GY, Yu MJ. 2020. Sequential Phosphorylation of the Hepatitis C Virus NS5A Protein Depends on NS3-Mediated Autocleavage between NS3 and NS4A. *J Virol* 94:e00420-20.
 183. Yu CC, Lin PC, Chiang CH, Jen ST, Lai YL, Hsu SC, Lo LC, Lin JJ, Chan NL, Yu MJ. 2022. Sequential Phosphorylation of Hepatitis C Virus NS5A Protein Requires the ATP-Binding Domain of NS3 Helicase. *J Virol* 96:e0010722.
 184. Ringel M, Heiner A, Behner L, Halwe S, Sauerhering L, Becker N, Dietzel E, Sawatsky B, Kolesnikova L, Maisner A. 2019. Nipah virus induces two inclusion body populations: Identification of novel inclusions at the plasma membrane. *PLOS Pathogens* 15:e1007733.

185. Nikolic J, Civas A, Lama Z, Lagaudrière-Gesbert C, Blondel D. 2016. Rabies Virus Infection Induces the Formation of Stress Granules Closely Connected to the Viral Factories. *PLoS Pathog* 12:e1005942.
186. Takamatsu Y, Kolesnikova L, Becker S. 2018. Ebola virus proteins NP, VP35, and VP24 are essential and sufficient to mediate nucleocapsid transport. *Proc Natl Acad Sci U S A* 115:1075-1080.
187. Hara K, Yaita K, Khamrin P, Kumthip K, Kashiwagi T, Eléouët JF, Rameix-Welti MA, Watanabe H. 2020. A small fragmented P protein of respiratory syncytial virus inhibits virus infection by targeting P protein. *J Gen Virol* 101:21-32.
188. Lee ST, Welch KD, Panter KE, Gardner DR, Garrossian M, Chang CW. 2014. Cyclopamine: from cyclops lambs to cancer treatment. *J Agric Food Chem* 62:7355-62.
189. Bailly B, Richard CA, Sharma G, Wang L, Johansen L, Cao J, Pendharkar V, Sharma DC, Galloux M, Wang Y, Cui R, Zou G, Guillon P, von Itzstein M, Eléouët JF, Altmeyer R. 2016. Targeting human respiratory syncytial virus transcription anti-termination factor M2-1 to inhibit in vivo viral replication. *Sci Rep* 6:25806.
190. Reber S, Jutzi D, Lindsay H, Devoy A, Mechtersheimer J, Levone BR, Domanski M, Bentmann E, Dormann D, Mühlemann O, Barabino SML, Ruepp MD. 2021. The phase separation-dependent FUS interactome reveals nuclear and cytoplasmic function of liquid-liquid phase separation. *Nucleic Acids Res* 49:7713-7731.
191. Kamelgarn M, Chen J, Kuang L, Jin H, Kasarskis EJ, Zhu H. 2018. ALS mutations of FUS suppress protein translation and disrupt the regulation of nonsense-mediated decay. *Proc Natl Acad Sci U S A* 115:E11904-e11913.
192. Salvi M, Trashi E, Cozza G, Franchin C, Arrigoni G, Pinna LA. 2012. Investigation on PLK2 and PLK3 substrate recognition. *Biochim Biophys Acta* 1824:1366-73.
193. Leyssen P, Balzarini J, De Clercq E, Neyts J. 2005. The predominant mechanism by which ribavirin exerts its antiviral activity in vitro against flaviviruses and paramyxoviruses is mediated by inhibition of IMP dehydrogenase. *J Virol* 79:1943-7.
194. Ravi LI, Tan TJ, Tan BH, Sugrue RJ. 2021. Virus-induced activation of the rac1 protein at the site of respiratory syncytial virus assembly is a requirement for virus particle assembly on infected cells. *Virology* 557:86-99.
195. Lifland AW, Jung J, Alonas E, Zurla C, Crowe JE, Jr., Santangelo PJ. 2012. Human respiratory syncytial virus nucleoprotein and inclusion bodies antagonize the innate immune response mediated by MDA5 and MAVS. *J Virol* 86:8245-58.
196. Jobe F, Simpson J, Hawes P, Guzman E, Bailey D. 2020. Respiratory Syncytial Virus Sequesters NF- κ B Subunit p65 to Cytoplasmic Inclusion Bodies To Inhibit Innate Immune Signaling. *J Virol* 94.
197. Ménager P, Roux P, Mégret F, Bourgeois JP, Le Sourd AM, Danckaert A, Lafage M, Préhaud C, Lafon M. 2009. Toll-like receptor 3 (TLR3) plays a

- major role in the formation of rabies virus Negri Bodies. PLoS Pathog 5:e1000315.
198. Manokaran G, Audsley MD, Funakoda H, David CT, Garnham KA, Rawlinson SM, Deffrasnes C, Ito N, Moseley GW. 2022. Deactivation of the antiviral state by rabies virus through targeting and accumulation of persistently phosphorylated STAT1. PLoS Pathog 18:e1010533.
 199. Brzózka K, Finke S, Conzelmann KK. 2006. Inhibition of interferon signaling by rabies virus phosphoprotein P: activation-dependent binding of STAT1 and STAT2. J Virol 80:2675-83.
 200. Meshram CD, Baviskar PS, Ognibene CM, Oomens AGP. 2016. The Respiratory Syncytial Virus Phosphoprotein, Matrix Protein, and Fusion Protein Carboxy-Terminal Domain Drive Efficient Filamentous Virus-Like Particle Formation. J Virol 90:10612-10628.
 201. Bajorek M, Galloux M, Richard CA, Szekely O, Rosenzweig R, Sizun C, Eleouet JF. 2021. Tetramerization of Phosphoprotein is Essential for Respiratory Syncytial Virus Budding while its N Terminal Region Mediates Direct Interactions with the Matrix Protein. J Virol 95.
 202. Fearn R, Peeples ME, Collins PL. 1997. Increased expression of the N protein of respiratory syncytial virus stimulates minigenome replication but does not alter the balance between the synthesis of mRNA and antigenome. Virology 236:188-201.
 203. Fearn R, Peeples ME, Collins PL. 2002. Mapping the transcription and replication promoters of respiratory syncytial virus. J Virol 76:1663-72.

VITA

Rachel Erin Thompson

Education

University of Kentucky: Lexington, Kentucky 2017-2023
Expected PhD in Molecular and Cellular Biochemistry

University of Louisville: Louisville, Kentucky 2013-2017
B.S. in Biology (Subcellular Biology and Genetics)

Professional Positions

Graduate Teaching Assistant, Biochemistry 2021
University of Kentucky

Awards and Honors

Data Club Travel Grant 2019
University of Kentucky

ASV Student Travel Award 2019
American Society for Virology

ASBMB Graduate Travel Award 2019
American Society for Biochemistry and Molecular Biology

Publications

Thompson RE, Edmonds K, Dutch RE. Specific residues in the C-terminal domain of the HMPV phosphoprotein are indispensable for formation of viral replication centers and regulation of the function of the viral polymerase complex. April 2023 J. Virol.

Barrett CT, Neal HE, Edmonds K, Moncman CL, Thompson R, Branttie JM, Boggs KB, Wu CY, Leung DW and Dutch RE. Effect of mutations in the SARS-CoV-2 spike protein on protein stability, cleavage, and cell-cell fusion function. July 2021 J. Biol. Chem. 297(1).